



République Algérienne Démocratique Et Populaire
Ministère De L'enseignement Supérieur Et De La Recherche Scientifique
Université Mohamed Khider De Biskra



Faculté des Sciences Exactes et Sciences de la Nature et de la Vie
Département de Sciences de la matière

Ref :

Thèse présentée en vue de l'obtention du diplôme de :

Doctorat

Option : **Physique des matériaux**

Thème:

Contribution à l'étude de couches minces d'oxydes transparents conducteurs à base de zinc et de titan par spray pneumatique pour applications catalytiques et photovoltaïques

Présentée par:

Attouche Hafida

Soutenue le: / / 2023

Devant le jury :

Hachemi BEN TEMAM	Professeur	Université de Biskra	Président
Saâd RAHMANE	Professeur	Université de Biskra	Rapporteur
Abdelouahad CHALA	Professeur	Université de Khenchela	Examineur
Abdallah ATTAF	Professeur	Université de Biskra	Examineur
Abdelouahab OUAHAB	Professeur	Université de Biskra	Examineur



Democratic and Popular Republic of Algeria
Ministry of Higher Education and Scientific Research
University Mohamed Khider of Biskra



Faculty of Exact Sciences and Science of Nature and Life
Department of Material Sciences

Ref :

Thesis Presented to obtain the degree of

Doctorate in Physics

Option: **Physics of thin films**

Entitled:

**Contribution to the study of thin films of transparent conductive oxides
based on zinc and titanium by pneumatic spray for catalytic and
photovoltaic applications**

Presented by:
Attouche Hafida

Publicly defended on: / / 2023

In front of the Jury committee composed of:

Mr. Hachemi Ben Temam	Professor	University of Biskra	President
Mr. Saâd RAHMANE	Professor	University of Biskra	Supervisor
Mr. Abdelouahad CHALA	Professor	University of Khenchela	Examiner
Mr. Abdallah ATTAF	Professor	University of Biskra	Examiner
Mr. Abdelouahab Ouahab	Professor	University of Biskra	Examiner

DEDICATION

To everyone who contributed in this humble work

From near or far

With a lot or a little

In openly or in secretly

I mentioned him or not

I knew him or not

I dedicate this thesis

May Allah reward you with all goodness

ACKNOWLEDGMENT

Firstly, I thank GOD the whole powerful for having agreed his infinite kindness, courage, the force and patience to complete this modest work.

I want to express my sincere gratitude to, professor Saad Rahmane at the Department of Sciences of Matter at the Faculty of exact sciences and Sciences of Nature and Life at the University Mohamed Khider of Biskra, for coming up with the problem and for his unwavering guidance and supervision throughout this work.

I should thank from the bottom of my heart to Hachemi Ben Temam. Professor at the Department of Industrial Chemistry at Faculty of Sciences and Technolgy in University Mohamed Khider of Biskra, who agreed to be the president of the doctoral committee and for his constant encouragement and kind help extended to my work.

I am also thankful to Attaf Abdallah. Professor and Head, of the Department of Sciences of Matter at Faculty of Exact Sciences and Sciences of Nature and Life in University Mohamed Khider of Biskra, who agreed to accept to belong to the jury and to examine my work.

I make a point of deeply thanking to Abdelouahab Ouahab, Professor at the Department of sciences of matter at Faculty of Exact Sciences and Sciences of Nature and Life in Mohamed Khider University of Biskra, who agreed to accept to belong to the jury and to examine my work.

I owe my heartfelt thanks to Prof. Chala Abdelouahed. Rector of Khenchela University, Algeria, who showed great interest in my research work and accepted to belong to the jury and to examine my work.

I am indebted to Prof.Tibermacine Toufik and dr. Elhachmi Guettaf Temam for their help during the progress of my work.

I would like to express my gratitude to Mr. Gasmi Brahim and Mrs. Touhami Hanane, two engineers working in the LPCMA laboratory at Biskra University, for their availability, assistance, and SEM and XRD measurements.

I express my sincere thanks to my colleague researchers MCS Kater Aicha, Dr. Kouidri nabila, Dr. Yahia Anouar, Dr. Dahnoune Mohamed, Dr. Allag Abdelkrim, Dr Mekkaoui Amer, Souhila Hettal, Warda Ben Messaoud,saadi bouthaina without forgetting all the members of thin films laboratory and its application.

I am grateful for the love, support, and encouragement from my cherished Parents. I also want to thank my brothers for their never-ending support and encouragement while I worked to finish my research project.

Lastly, I offer my regards to many people who have helped me at various stages of my work then and there needed. This work would not be possible without their help.

Table of contents

Dedication	I
Acknowledgement	II
Table of contents	IV
Figures liste	VII
Tables liste	X
General introduction	01
ChapterI:Material system.....	05
I.1. Titanium Dioxide.....	06
I.1.2. Titania polymorphs.....	06
I.2.1. A. Rutile.....	07
I.1.2. B. Anatase.....	08
I.1.2. C. Brookite.....	09
I.1.3. Electronic properties.....	10
I.1.4. Electrical and optical properties	11
I.1.5. Doping of TiO ₂	11
I.2. Zinc oxide	13
I.2.1. Brief Historical Review of Research and Development on ZnO	13
I.2.2. Basic Properties of ZnO and Related Alloys	14
I.2.2.1. ZnO Surfaces	15
I.2.2.2. Optical Properties of ZnO	15
I.2.2.3. ZnO Electrical Properties.....	16
I.2.2.4. Dopants in ZnO.....	17
I.2.3. ZnO thin films applications.....	19
I.2. References.....	19
Chapter II: Thin films Preparation and characterization techniques.....	23
II.1 Introduction.....	24
II.2. Thin films depositions techniques	25
II.2.1. Physical vapor deposition (PVD) process.....	25
II.2.2. Chemical Methods	26
II.2.2.1. Chemical vapor deposition (CVD) process.....	26
II.2.2.2. Chemical solution deposition techniques (CSD)	27
II.2.2.2.1. Sol–Gel.....	29
II.2.2.2.2. Spray Pyrolysis (SP)	29
II.2.2.2.2.1. Models for Film Deposition by Spray Pyrolysis.....	29
II.2.2.2.2.1.a. <i>Atomization of Precursor Solution</i>	30
Pneumatic atomization.....	30
Ultrasonic nebulized atomization	31
Electrostatic spray pyrolysis	32
II.2.2.2.2.1.b. <i>Aerosol Transport</i>	32
II.2.2.2.2.1.c. <i>Decomposition of Precursor</i>	32
II.2.2.2.2.2. Advantages of Spray Pyrolysis Technique	34
II.3. Characterization methods.....	34
II.3.1. Structural and Morphological Characterizations.....	34
II.3.1.1. X-ray Diffraction (XRD)	34
Crystallites size determination	36
II.3.1.2. Scanning Electron Microscope (SEM)	36

II.3.2. Compositional Analysis	37
II.3.2.1. Energy dispersive x-ray analysis (EDS)	37
II.3.3. Optical studies.....	39
II.3.3.1. Transmission spectroscopy.....	39
Optical band gap.....	41
Urbach energy.....	42
II.3.4. Electrical properties (<i>Four point probe method</i>)	42
II.4. References	43
Chapter III: Effect of precursor nature and molarities on Titanium and Zinc oxides thin films properties.....	47
III.1. Introduction.....	48
III.2. Experimental details	48
III.2.1. Spray pyrolysis system set-up	48
III.2.2. Substrate preparation	49
III.2.2.a. Choice of the substrate	49
III.2.2. b. Cleaning of the substrate	49
III.2.3. Preparation of the films	50
III.2.3.A. Preparation of TiO ₂ films	50
III.2.3.A.1. Preparation of Solutions	50
III.2.3.B. Preparation of ZnO films	51
III.2.3.B.1. Preparation of Solutions	51
III.3. Empirical conditions	52
III.3.A. Section one deposition of TiO ₂ thin films	52
III.3.A.1. Results and discussion	53
Effect of precursor nature and molarities	53
III.3.A.1.1. Film formation mechanism and thickness measurement.....	53
III.3.A.1.2. Structural properties	54
III.3.A.1.2.1. Crystallite size (D)	55
III.3.A.1.2.2. Dislocations Density	56
III.3.A.1.2.3. Microstrain (ϵ)	56
III.3.A.1.3. Morphological study.....	57
III.3.A.1.4. Optical properties	60
III.3.A.1.5. Electrical properties	62
III.3.A.1.6. Conclusion.....	63
III.3.B. Section two deposition of ZnO thin films.....	64
III.3.B.1. Results and discussion.....	64
Effect of precursor nature and molarities	64
III.3.B.1.1. Film formation mechanism and thickness measurement.....	64
III.3.B.1.2. Structural properties.....	65
III.3.B.1.2.1. lattice parameters, Crystallite size (D) and stress determination	67
III.3.B.1.3. Optical properties and Electrical properties.....	69
III.3.B.1.4. Conclusion.....	72
III.5. References.....	72
Chapter IV: Deposition of titanium-doped ZnO films and ZnO:TiO ₂ composite oxide films.....	77
IV.1. Introduction.....	78
IV.A. Section one: Effect of Titanium low doping contents.....	78
IV.A.1. Experimental details.....	78
IV.A.2. Results and discussion	79
IV.A.2.1. Surface thickness of the films.....	79

IV.A.2.2. Structural properties.....	80
IV.A.2.3. Morphology and chemical analysis.....	83
IV.A.2.4. Optical properties.....	88
IV.A.2.5. Electronic Proprieties.....	89
IV.A.2.6. Electrical properties.....	91
IV.A.3. Conclusion.....	92
IV.B. Section tow: Effect of Titanium high doping contents (ZnO: TiO ₂ composites).	93
IV.B.1. Experimental details.....	93
IV.B.2. Result and discussion	94
IV.B.2.1. Film formation mechanism and thickness measurement.....	94
IV.B.2.2. Structural properties.....	95
IV.B.2.3. Morphology and chemical analysis.....	96
IV.B.2.4. Optical properties.....	99
IV.B.2.5. Electrical properties.....	101
IV.B.3. Conclusion.....	102
IV.2. Reference.....	105
General conclusion and perspective.....	108

Figures List

Fig. I. 1. Structure and TiO_6 polyhedra for the TiO_2 phase rutile (Ti (blue); O (red)).....	08
Fig. I. 2. Structure and TiO_6 polyhedra for the TiO_2 phase anatase (Ti (blue); O (red)).....	09
Fig. I. 3. Structure and TiO_6 polyhedra for the TiO_2 phase brookite (Ti (blue); O (red)).....	10
Fig. I. 4. Ball and stick representation of ZnO crystal structures. (a) Cubic rocksalt structure (b) cubic zinc-blende, (c) hexagonal wurtzite.	15
Fig. I. 5. Molecular orbital model of ZnO.....	16
Fig. I. 6. Tetrahedral geometry of sp^3 orbitals for both O and Zn atoms.....	16
Fig. I. 7. Schematic representation the applications of ZnO.	19
Fig. II. 1. Schematic of general elementary steps of a typical CVD process.	27
Fig. II. 2. Classification of CVD methods.....	28
Fig. II. 3. Schematic diagrams of some commonly employed nozzles.....	31
Fig. II. 4. Diagram of the different process stages for the aerosol droplet evolution	33
Fig. II. 5. Mini-Flex (Rigaku) diffractometer.....	35
Fig. II. 6. Schematic diagram of scanning electron microscope.....	37
Fig. II. 7. Scheme of X-ray excitations in EDX analysis.....	38
Fig. II. 8. scanning electron microscope TESCAN VEGA3.....	39
Fig. II. 9. Double beam instrument schematic. The beam splitter is highlighted in yellow, the reference beam in blue, and the sample beam is highlighted in green.....	40
Fig. II. 10. Determination of E_g	41
Fig. II. 11. Schematic of Four-Point Probe.....	43

Fig. III. 1. The pneumatic spray pyrolysis setup.....	49
Fig. III. 2. Modification process of titanium Isopropoxide by acetylacetone (where $R = C_3H_7$ and $R' = C_2H_5$).....	51
Fig. III. 3. XRD patterns of TiO_2 thin film with different concentrations for (S1) TTIP, (S2) $TiCl_3$ precursors.....	55
Fig. III. 4. An Edge Dislocation in a Simple Cubic Lattice.....	56
Fig. III. 5. The top view and cross-section SEM photographs for the TTIP (S1) and $TiCl_3$ (S2) precursors.....	59
Fig. III. 6. Optical transmittance of TiO_2 (S1) for TTIP, (S2) for $TiCl_3$ precursors versus solution concentration.....	60
Fig. III. 7. Variation of band gap and band tail width versus solution concentration for (S1) and (S2) films.....	61
Fig. III. 8. Dependence of electrical resistivity in TiO_2 films on precursor concentration for (S1) TTIP and (S2) $TiCl_3$ precursors.....	63
Fig. III. 9. X-ray diffraction pattern of spray deposited ZnO thin films at different molarities from (A) Zinc chloride $ZnCl_2$ and (B) Zinc acetate $Zn(C_2H_3O_2)_2 \cdot 2H_2O$	66
Fig. III. 10. Variation of the calculated values of crystallites size and stress in ZnO films versus solution concentration, A from $ZnCl_2$, B from $Zn(C_2H_3O_2)_2 \cdot 2H_2O$	67
Fig. III. 11. Transmittance Spectra of the films prepared from zinc chloride ($ZnCl_2$) 'A' and 'B' for ZnO films elaborated from $Zn(C_2H_3O_2)_2 \cdot 2H_2O$ as function of the wavelength	70
Fig. III. 12. The variation of ZnO's optical gap and Urbach energy as a function of molarities.....	71
Fig. IV. A. 1. The variation of the thickness of the undoped ZnO thin film and the 1 at.% to 9 at.% Ti doped ZnO thin film.....	79
Fig. IV. A. 2. X-ray diffraction spectres of ZnO films with different Ti concentrations.....	81
Fig. IV. A. 3. Variation of the calculated values of crystallites size and stress in the films versus doping concentration	83
Fig. IV. A. 4. Top view SEM photographs for deferent doping concentration.....	85

Fig. IV. A. 5. EDX spectra of undoped and Ti-doped ZnO films.....	87
Fig. IV. A. 6. Optical transmittance variation versus Ti doping content.....	89
Fig. IV. A. 7. Variation of band gap and band tail width versus doping concentration.....	90
Fig. IV. A. 8. Dependence of electrical resistivity in TiO ₂ films on doping concentration.....	91
Fig. IV. B. 1. The variation of the thickness of ZnO and ZnO: TiO ₂ composite thin films with different molar ratios.....	94
Fig. IV. B. 2. X-ray diffraction spectra of the ZnO and ZnO: TiO ₂ composite thin films with different molar ratios.....	96
Fig. IV. B. 3. Top view SEM photographs of the ZnO and ZnO: TiO ₂ composite thin films with different molar ratios.....	97
Fig. IV. B. 4. EDAX spectra of the 1:0.5ZnO:TiO ₂ molar ratio thin film.....	98
Fig. IV. B. 5. Variation of atomic ratios of Zn , Ti and Oxygen atoms of the ZnO and ZnO: TiO ₂ composite thin films with different molar ratios.....	99
Fig. IV. B. 6. Optical transmittance of the ZnO and ZnO: TiO ₂ composite thin films with different molar ratios.....	100
Fig. IV. B. 7. Variation of band gap and band tail width of the ZnO and ZnO: TiO ₂ composite thin films with different molar ratios.....	101
Fig. IV. B. 8. Dependence of electrical resistivity of different ZnO: TiO ₂ molar ratios thin film.....	102

Tables List

Table.III.1: Experimental conditions.....	52
Table.III.2: The thickness values of the films.	54
Table.III.3. Structural properties of TiO ₂ versus solution concentration for (S1) and (S2) series.	57
Table.III.4. Experimental conditions.....	64
Table.III.5. the characteristics of the zinc salts used in our experimental study.....	65
Table.III.6. Variation of interplanar distance 'd' and lattice parameters as a function of molar concentration.	67
Table.IV.1. Variation of interplanar distance 'd' and lattice parameters as a function of Ti doping contents.	82
Table.IV.2. Variation of atomic ratios of Zn Ti and Oxygen atoms as a function of Ti doping concentration.	84

General introduction

Nanostructured materials research is nowadays a rapidly growing field of science where the efforts of chemists, physicists, materials scientists, and, more recently, biological scientists and engineers have merged. Nanotechnology, which is defined as the creation and utilization of materials, systems, and devices through control of matter on the nanometer-length scale, is expected to become one of the main driving forces in materials research for the 21st century [1].

Thin Film technology is an important branch of nonmaterial's physic in which the characteristics of different materials such as semiconductors and insulators in thin film form are investigated. Transparent conducting oxide films (TCOs) are electrically conductive materials with comparably low absorption of electromagnetic waves within the visible region of the spectrum. In transparent conducting oxide films (TCOs), the nonmetal part, B, consists of oxygen. In combination with different metals or metal-combinations, A, they lead to compounds, semiconductors, A_yB_z , with different opto-electrical characteristics. These opto-electrical characteristics can be changed by doping, $A_yB_z:D$ (D = dopant), with metals, metalloids or nonmetals. Hence, metals can be part of the compound semiconductor itself, A, or can be a dopant, D [2]. One of the most promising inorganic materials that are used for TCOs is Titanium and Zinc Oxides (ZnO and TiO_2), which are a wide direct band-gap semiconductor. They combine desirable characteristics, such as high transparency and electrical conductivity, easy fabrication, low cost, non-toxic character, and compatibility for large-scale applications. ZnO and TiO_2 thin films can be prepared by a large variety of methods with sputter deposition, chemical vapordeposition, spray pyrolysis, and vacuum evaporation[3].

Recently, a consumption trend of pharmaceutical products has attracted considerable attention during the COVID-19 global pandemic, which leads industries to reorganize their strategies and adapt them to the current market requirements. These products include anti-inflammatories, antibiotics, and blood lipid regulators .Clofibrac acid is a blood lipid regulator that is used all over the world.This compound is considered as a one of the most frequently encountered major drug metabolite detected in the aquatic environment. However, this molecule is recognized to be extremely resistant to biodegradation as well as other removal process like adsorption and hydrolysis, which remain its concentration at

high level in the environment for a long time. Photocatalysis technology has become a promising means of pharmaceutical pollution control. This technique is designed to irradiate of appropriate semiconductors in a manner that generate active species with higher redox capacity[4].

Zinc oxide (ZnO) and Titania (TiO₂) have been found to be very efficient for this purpose Therefore; worldwide very active research is going on the growth of various types of nanostructures of this materials. Coupling of the two semiconductors provides a novel approach to achieve a more efficient charge separation and increased lifetime of the charge carriers. These properties help them offering superior photocatalytic activity[5]. Because of those characteristics, they have also been used in ink degradation, herbicide degradation, humidity sensors, photo-anodes for water splitting and for photo-anodes indye-sensitized solar cells, among other applications[6].

The goal of this thesis is to elaborate thin layers of metal oxides using the pneumatic spray technique and characterize them while simultaneously investigating how their structural, morphological, optical, and electrical properties vary. This research was done at the University of Biskra's Physics of Thin Films and Applications laboratory (LPCMA), and. It is a study that focuses on the characterization of thin layers of zinc and titanium oxide, and improving the quality of these films by examining the effects of operating conditions on the layer's properties (precursor starting solution, molarity), as well as the study of Ti-doped ZnO layers (ZnO:Ti) variation from low content to high amounts of doping to reach such layers with a binary mixture of zinc and titanium oxides, deposited by the pneumatic spray technique utilizing titanium chloride and zinc chloride with molarities of 0.175 M and 0.1 M, respectively, as precursors, on glass substrates at 370 °C.

We have characterized our films by different analysis techniques. Diffraction X-ray analysis (XRD) was used to measure structural properties such as the crystalline quality and nature of the layers, the size of the crystallites, the lattice parameters, and the evaluation of the stresses. Scanning electron microscopy (SEM) made it possible to analyze the surfaces and their morphology and chemical composition by X-ray energy dispersive spectroscopy (EDS). UV-visible spectrophotometry made it possible to discuss the optical characteristics such as: the spectrum of the transmittance, the optical gap energy, the Urbach energy. Finally, the four-point technique was used to measure electrical characteristics such as electrical resistivity.

This thesis consists of four chapters. The first Chapter presents a review of the properties of ZnO and TiO₂. Chapter two presents a general description of different growth and characterizations techniques giving details and description of the experimental spray pyrolysis kit and its method of use. Chapter three was devoted to two sections:

•**Section one:** included deposition of TiO₂ thin films (the study of the influence of precursor solution and molarity on the structural, morphological, optical and electrical properties of titanium oxide (TiO₂)).

•**Section two:** included deposition of ZnO thin films (the study of the influence of precursor solution and molarity on the structural, morphological, optical and electrical properties of zinc oxide (ZnO)).

Chapter four presents the various experimental results obtained (properties structural, morphological, optical and electrical) on thin layers of titanium doped ZnO and ZnO: TiO₂ binary mixture layers elaborated by the spray technique pneumatics.

Finally, we end this manuscript with a general conclusion which let us identify all the significant results that we have obtained during this course of work.

References

- [1] Rogach AL, Eychmüller A, Hickey SG, et al. reviews Infrared-Emitting Colloidal Nanocrystals : Synthesis , Assembly , Spectroscopy , and Applications. *Small* 2007; 3: 536–557.
- [2] Fouad B. Deposition and analysis of Zinc Oxide thin films elaborated using spray pyrolysis for photovoltaic applications. University Mohamed Khider of Biskra, 2018.
- [3] Logothetidis S. Nanostructured Materials and Their Applications. 1st ed. Springer Berlin, Heidelberg, 2012. Epub ahead of print 2012. DOI: 10.1007/978-3-642-22227-6.
- [4] Janani FZ, Khair H, Taoufik N, et al. ZnO-Zn₂TiO₄ heterostructure for highly efficient photocatalytic degradation of pharmaceuticals. *Environ Sci Pollut Res*. Epub ahead of print 2022. DOI: 10.1007/s11356-022-22791-6.
- [5] Khatua L, Panda R, Nayak AK, et al. Efficient UV photocatalytic dye

decomposition activity with cost effective solid state reaction grown Zinc Orthotitanate (Zn_2TiO_4) nanoparticles. *J Alloys Compd* 2018; 764: 895–900.

- [6] Mazabuel-collazos A, Gómez CD. ZnO-TiO₂ nanocomposites synthesized by wet-chemical route: Study of their structural and optical properties. *Mater Chem Phys*. Epub ahead of print 2018. DOI: 10.1016/j.matchemphys.2018.10.007.



Chapter I
Materials System

Chapter I: Material System

This chapter will present a brief review of the properties of ZnO and TiO₂ such as crystal structure, electronic, optical and electrical properties of ZnO and TiO₂.

I.1. Titanium Dioxide

Titanium dioxide is commonly known as Titania. Fumed silica (SiO₂) is the first industrially produced nanostructured material using a gas phase process that has been transferred to other oxides, such as Titania (TiO₂), alumina (Al₂O₃), and zirconia (ZrO₂) which allows the tailoring of their properties based on process simulations. Compared with various wide band gap semiconductors such as ZnO, SnO₂ and Nb₂O₅, titanium dioxide is one of the most attractive photovoltaic materials due to its interesting properties. It has strong oxidizing power, is non-toxic and bio-compatible making it a suitable material for various implants. It is used in many consumer products such as toothpaste, lipstick, paints, food additives and pharmaceuticals. Titanium dioxide exhibits long term photo stability[1].

With an estimated TiO₂ concentration of about 0.7 wt. %, titanium is the ninth most abundant element of the Earth's continental crust. William Gregor is originally discovered titanium (which was named by menackanite) in ilmenite in 1791[2].

Titanium (IV) is the most stable valence state while Ti (II) and Ti (III) are readily oxidized to the tetravalent state. Accordingly, the titanium-oxide system shows a quite diverse phase diagram with a lot of different structures and stoichiometries TiO_x with x=2/3, 1, 3/2, 5/3, 2, 7/4, (2n-1)/n (n=4... 10). By increasing n, the phase structures resemble more and more closely that of TiO₂[3].

I.1.2. Titania polymorphs

Titanium dioxide (TiO₂) belongs to the family of transition metal oxides[4]. It is the only naturally occurring oxide of titanium at atmospheric pressure[5]. TiO₂ occurs in Nature in three different forms which, in order of abundance, are rutile, anatase, and brookite. The rutile form is widely used as a white pigment and opacifier[6]. However, the anatase phase represents the technologically most interesting crystallographic form of titanium dioxide since, in many cases; it exhibits a higher photocatalytic activity than other TiO₂ polymorphs. Furthermore, mesoporous TiO₂ films in DSSCs are predominantly of the anatase

phase[03]. The rarer mineral brookite is not used commercially; this, coupled with its relatively complicated structure, has led to few studies of its properties[6].

Various oxygen deficient TiO_2 crystal structures referred to as the Magnéli phases ($\text{Ti}_n\text{O}_{2n-1}$) also exist. In these compounds ordered, oxygen vacancies lead to the formation of planes where instead of corner-shared or edge-shared TiO_6 octahedra, there are face shared octahedra. As a result, the Ti cations can interact electronically which gives rise to increased electrical conductivity in these materials[7].

Another five high-pressure phases of TiO_2 have been reported:

- TiO_2 II or srilankite, an orthorhombic polymorph of the lead oxide structure.
- Cubic fluorite-type polymorph.
- Pyrite-type polymorph.
- Monoclinic baddeleyite-type polymorph.
- Cotunnite-type polymorph the stability of these phases has been discussed in several publications. However, these are of minor significance for research and development applications[5].

I.2.1.A. Rutile

The vast majority of studies of the bulk and surface properties of TiO_2 have been of the rutile phase. The rutile structure, illustrated in **Fig. I. 1**, belongs to the $P4_2/mnm$ tetragonal space group. The unit cell is defined by the lattice vectors **a** and **c** and contains two TiO_2 units with Ti ions at (0,0,0) and $(\frac{1}{2}, \frac{1}{2}, \frac{1}{2})$ and O ions at $\pm(u,u,0)$ and $\pm(u+\frac{1}{2}, \frac{1}{2}-u, \frac{1}{2})$.

The unit-cell parameters have been determined and subsequently verified several times using x-ray and neutron diffraction and are found to be $\mathbf{a}=4.587 \text{ \AA}$, $\mathbf{c}=2.954 \text{ \AA}$, and $\mathbf{u}=0.305$ at 15 K. Each Ti ion is octahedrally coordinated to six O ions. The TiO_2 octahedron is distorted, with the apical Ti-O bond length (1.98 \AA) being slightly longer than the equatorial Ti-O bond length (1.95 \AA). The four equatorial O ions are coplanar occupying a rectangular arrangement with the long edge (2.954 \AA) along the **c** direction and the short edge (2.53 \AA) lying diagonally across the plane defined by the **a** direction. The TiO_6 octahedra form chains that share edges along the **c** direction and share vertices in the **a-b** plane [6].

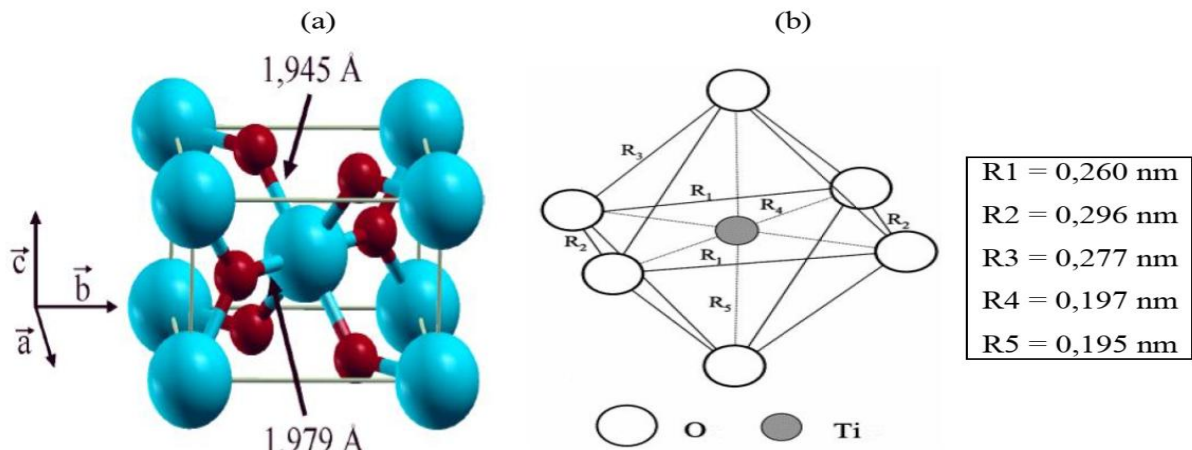


Fig. I. 1. structure and TiO_6 polyhedra for the TiO_2 phase rutile (Ti (blue); O (red) [5].

I.1.2. B. Anatase

The anatase structure, shown in **Fig. I. 2**, is characterized by the tetragonal space group $I4/amd$. The unit cell contains two TiO_2 units with Ti ions at $(0,0,0)$ and $(0, 1/2, 1/4)$ and O ions at $(0,0,u)$, $(0,0,-u)$, $(0, 1/2, u+1/4)$ and $(0, 1/2, 1/2-u)$. As with rutile, **a**, **c**, and **u** have been measured several times using both x-ray and neutron diffraction to be 3.782 \AA , 9.502 \AA , and 0.208 , respectively, at about 15 K. Each Ti ion is octahedrally coordinated to six O ions. The Ti-O octahedron is not regular and the Ti-O bond distances are similar to those in rutile (1.98 and 1.93 \AA for the long and short Ti-O bond lengths respectively). The octahedral form zigzag chains along the **a** and **b** directions with each octahedron sharing four edges [6]. From the experimental data, it can be seen that the rutile unit cell is more compact although the Ti-O bond lengths in both structure are almost similar. As suggested by Hanaor and Sorrell, anatase can be converted to rutile under the affect of pressure rather than temperature (they observed no phase transformation as the temperature was raised up to 2500 K)[8].

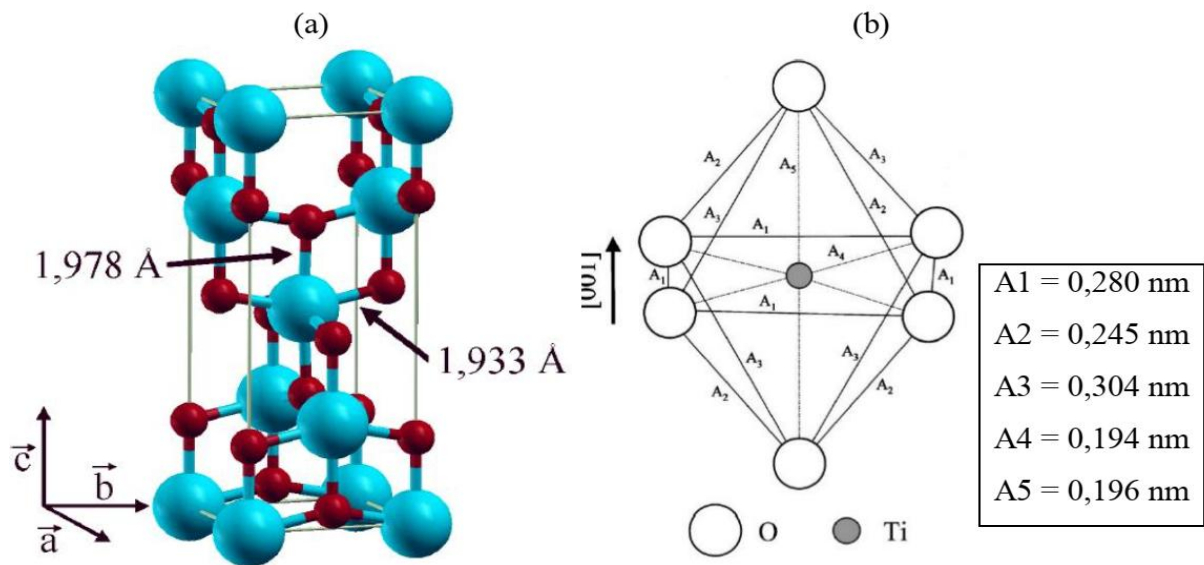


Fig. I. 2. structure and TiO_6 polyhedra for the TiO_2 phase anatase (Ti (blue); O (red) [5].

I.1.2. C. Brookite

Brookite is the least studied TiO_2 photocatalyst due to the difficulties usually encountered in order to obtain it as a pure phase. It has an orthorhombic crystalline structure with a unit cell described by the space group $Pbca$ [9]. The unit-cell parameters of Brookite are found to be $a=9.184\text{\AA}$, $b= 5.447\text{\AA}$, $c= 5.145\text{\AA}$ [10]. The structure is composed of octahedra, each with a titanium atom at its center and oxygen atoms at its corners **Fig. I. 3**. The octahedra share edges and corners with each other to such an extent as to give the crystal the correct chemical composition[8]. Due to stronger distortions in TiO_2 brookite, all bond lengths and bond angles slightly differ from each other, thus leading to the formal loss of local symmetry and C_1 symmetric TiO_6 units[11].

A complementary view of the crystal structure is given by the threefold coordination of O ions in trigonal-planar-type Ti_3O building blocks. While the Ti_3O units exhibit a Y-shaped conformation in rutile, the anatase units are closer to a T-shape. In brookite, both T- and Y-shaped Ti_3O units are present[11].

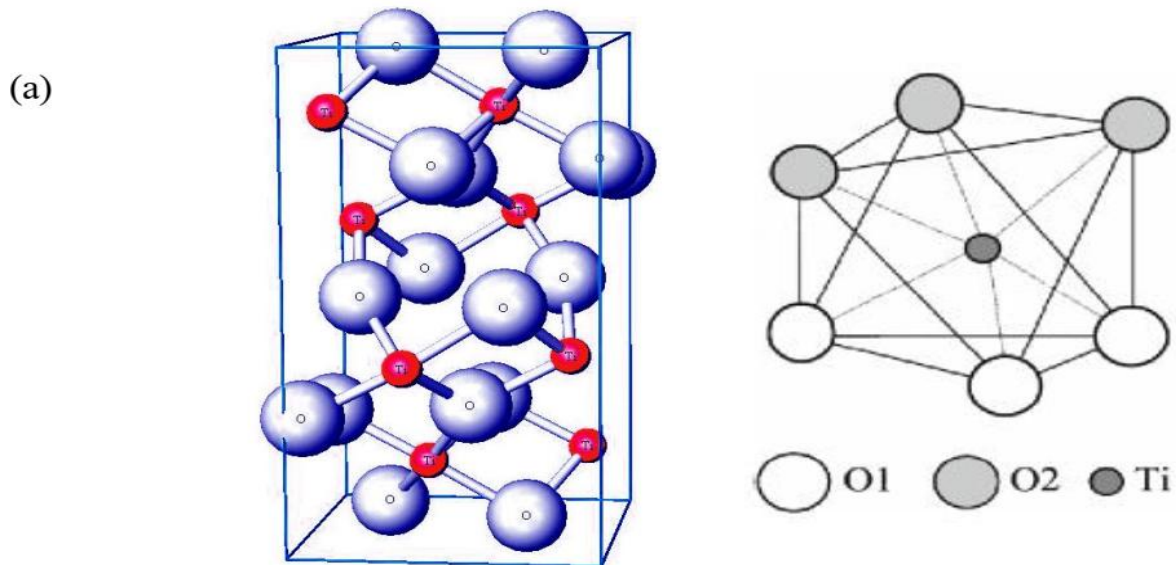


Fig. I. 3. structure and TiO_6 polyhedra for the TiO_2 phase brookite (Ti (blue); O (red) [5].

I.1.3. Electronic properties

The general topology of the electronic band structure was found to be similar for both TiO_2 anatase and rutile. As expected for a mostly ionic compound, the electronic bands are very flat. However, the most striking difference in the band structures of anatase and rutile is the deeper minimum in the conduction band of anatase which indicates a much smaller effective electron mass in anatase being 10 times lower compared to rutile. In contrast, the effective hole mass seems to be higher in anatase compared to rutile resulting in substantial differences in the electron transport properties of the two polymorphs. The electron transport is clearly favored in anatase due to the much higher electron mobility in the conduction band. Because of the high band gap of anatase, thermally excited intrinsic charge carriers are generated only in very small numbers at ambient temperatures. Consequently, electrical currents are usually sustained by extrinsic charge carriers. For example, oxygen vacancies produce band gap states which are associated with Ti^{3+} ions acting as electron donors. In heavily doped anatase films, even a Mott transition to metallic conduction occurs. The higher photoactivity of TiO_2 anatase compared to rutile can be partially attributed to the Fermi level of the anatase which is about 0.1 eV higher than that of rutile. However, no clear and widely accepted explanation is available yet[3].

I.1.4. Electrical and optical properties

Anatase and rutile TiO_2 are n-type semiconductors with band gaps of 3.2 and 3.0 eV, respectively. The conductivity of TiO_2 is dependent on the oxygen deficiency through the creation of defects such as oxygen vacancies, Ti^{3+} and Ti^{4+} interstitials, and crystallographic shear planes (CSP). Oxygen deficiency is easily created in TiO_2 , especially when the preparation is done in a vacuum. The amount of oxygen deficiency and thus conductivity can also be adjusted after preparation by heat treatment in oxygen rich or reducing atmospheres. The nature and amount of other impurities can also largely affect the electrical properties of TiO_2 . Hydrogen impurities for example can increase the electrical conductivity. Impurities can be incorporated intentionally or they can be residues from the preparation process. Thus the electrical properties of TiO_2 depend strongly on the preparation method and sample history. Various molecules can cause a measurable change in the conductivity when they interact with the TiO_2 surface. For this reason, TiO_2 has been studied for various gas sensing applications[7].

The dielectric constant (k) of TiO_2 is 40 for anatase and 86-170 (depending on crystal orientation) for rutile. TiO_2 has therefore been studied as a high- k insulator for metal-oxide-semiconductor field-effect transistors (MOSFET) and dynamic random access memories (DRAM). The biggest limitation of the use of TiO_2 as an insulator is the high leakage caused by its relatively small band gap and n-type conductivity. Especially the easy creation of oxygen deficiency contributes to the increased conductivity[7].

TiO_2 is transparent to visible wavelengths as can be concluded from its band gap energy. The refractive index of TiO_2 is the highest of all oxides. The index is even higher than that of diamond, and thus large and pure TiO_2 crystals have gem-like reflectance, refraction and brilliance and are suitable for use in jewelry. The high refractive index has also enabled the wide use of TiO_2 as a white pigment and also in many other optical applications. Because TiO_2 absorbs UV light and is biocompatible it is used in sun screens[7].

I.1.5. Doping of TiO_2

An effective way of modifying the electronic properties of TiO_2 is doping, the deliberate insertion of impurities into the TiO_2 lattice. In the case of TiO_2 , the mechanism is much more complicated than in silicon solar cells, due to the defect ridden nature of TiO_2 and doping

mainly affects the trap states and electronic structure of TiO_2 , which is illustrated by the improvements that are made by doping with elements of equal valency as the host TiO_2 ions. Doping can be achieved by either replacing the Ti^{4+} cation or the O^{2-} anion. Cationic dopants are typically metals, whereas anionic dopants are non-metals. Since the lower edge of the CB is made up of Ti^{4+} 3d bands, replacing Ti^{4+} by a different cation is thus expected to heavily affect the CB structure. The upper edge of the VB consists of O^{2-} 2p bands and replacing O^{2-} by a different anion affects the VB energy. The atomic radius of the dopant should not differ much from the ion it replaces to prevent lattice distortion, introducing new defects that may hamper device performance because the dopant induces oxygen vacancies. Dopants often inhibit the growth rate of the TiO_2 nanoparticles, resulting in smaller particles. This is in many cases beneficial since assemblies made from smaller particles have a larger surface area per volume of mesoporous TiO_2 compared to large particle assemblies[12].

Because of the large band gap of TiO_2 , the utilization of solar and indoor light is very inefficient. Narrowing the band gap or creating a separate energy states in the band gap by doping are common solutions for increasing the absorption of visible light,

Doping TiO_2 with elements such as N, S, C and F is frequently used to shift the absorption toward visible light. Especially N, S and C doping is expected to decrease the band gap of TiO_2 . The addition of foreign atoms can also cause a number of energy states in the band gap. The nature of these states depends strongly on the preparation method.

Doping TiO_2 with nitrogen is currently regarded as the most promising solution for visible light photocatalysis. The work of Asahi et al. is often referred to as the pioneering publication on nitrogen doped TiO_2 photocatalysts. In their study, first-principles calculations were first conducted to examine the effects of substitutional doping of C, N, S, P and F for O in anatase TiO_2 . The samples showed good photocatalytic activity under visible light. The photocatalytic activities of the nitrogen doped samples under UV light were also relatively good. Carbon doping has been reported to lead to visible light active photocatalysts; Khan et al. demonstrated that a $\text{TiO}_{2-x}\text{C}_x$ material prepared by a controlled combustion of a titanium sheet in a natural gas flame could be used in photochemical water splitting by visible light. Besides C, N, S and F, other anionic dopants in TiO_2 have been explored, but to a lesser extent. Iodine doped TiO_2 nanoparticles were found to degrade phenol under visible light. Co-doping with chlorine and bromine has been reported to increase the photocatalytic water splitting activity

of TiO₂. Co-doped TiO₂ materials have been studied. A good example is nitrogen and fluorine codoped TiO₂ prepared by the spray-pyrolysis technique. The beneficial effects of both dopants have been combined in a single material and the results show better performance than single element doped TiO₂ prepared in a similar way[7].

I.2. Zinc oxide

Zinc oxide (ZnO) is an “old” semiconductor that has attracted the attention of researchers for a long time because of its applications in science and industry such as piezoelectric transducers, optical waveguides, acousto-optic media, conductive gas sensors, transparent conductive electrodes, and so on.

ZnO, which crystallizes in the wurtzite structure, is a direct band-gap semiconductor with a room temperature band gap of 3.37 eV, an exciton binding energy of 60 meV, and other useful properties. ZnO can be grown at relatively low temperatures below 500°C. The band gap of ZnO can be tuned by forming alloys of ZnMgO, ZnCdO, etc. Magnetic semiconductors can be obtained from ZnMnO, ZnCrO, and so on, which have wonderful applications in spintronics and other fields[13].

I.2.1. Brief Historical Review of Research and Development on ZnO

Zinc oxide (ZnO) powder has been widely used as a white paint pigment and industrial processing chemical for nearly 150 years. In the early 1900s, white, polycrystalline ZnO powder was extensively applied in medical technology and in the cosmetics and pharmaceutical industries. In the 1930s, some research activities on ZnO, including the photoluminescence and electroluminescence properties of ZnO. After the invention of the semiconductor transistor before 1950, the semiconductor age began and systematic studies on ZnO as a compound semiconductor were also started. Following the rediscovery of ZnO and its potential applications in the 1950s, science and industry alike began to realize that ZnO had many interesting novel properties that were worth further investigation. Research on ZnO entered into a “modern rediscovery” after the mid-1950s. In 1960, the good piezoelectric properties of ZnO were discovered, which led to the first electronic application of ZnO as a thin layer for surface acoustic wave devices. Efforts have been made toward fabrication of large-size ZnO substrates of excellent structural perfection. A variety of ZnO Substrate growth techniques are being explored, the underlying basis for which was developed in the

1960s and 1970s. Owing to the renewed need for large high-quality single crystals, these methods are being revamped for producing large area wafers reproducibly and economically. Until the 1970, doping and implantation of impurities into ZnO were studied. It was found that the *n*-type conductivity can be obtained rather easily from ZnO, and that as-grown, unintentionally doped ZnO is always *n*-type because of high concentration of background donors which are mainly H, O vacancy, V_O , Zn interstitial Zn_i , and group III elements, especially Al [13].

I.2.2. Basic Properties of ZnO and Related Alloys

In this section, crystal structure, electronic band structure, doping, electrical and optical properties of the ZnO will be discussed in detail.

I.2.2.1. ZnO Surfaces

ZnO oxide is one of the prototypical metal oxide gas sensing materials. Its properties have obtained a lot of early attention in the surface science community and have been recently revisited. Its current popularity is also related to the many different nano-structural forms and shapes ZnO self-organizes in under various growth conditions. ZnO crystallizes in three forms: cubic zinc-blende, hexagonal wurtzite and the rarely observed cubic rocksalt structure, which are schematically shown in **Fig.I.4**.

Wurtzite is the thermodynamically favored form of ZnO at ambient conditions and zinc blende can be stabilized by growth on cubic substrates, while the rocksalt structure is a high-pressure meta-stable phase. The lattice constants of wurtzite ZnO are $a = 3.25 \text{ \AA}$ and $c = 5.2 \text{ \AA}$. This hexagonal lattice consists of two interconnecting hexagonal-close-packed (hcp) sublattices of Zn^{2+} and O^{2-} , with each anion surrounded by four cations at the corners of a tetrahedron, and vice versa. The tetrahedral coordination of Zn and O is typical of sp^3 covalent bonding. The ionic character of the material gives rise to a polar repeat-unit along the *c*-axis. As a consequence of this polar symmetry, the (0001) and the (000 $\bar{1}$) surfaces of wurtzite ZnO exhibit different bulk terminations, with the first one terminated by Zn-atoms and the latter by O-atoms. This means that if we cleave a crystal along the (0001) plane we obtain two distinctively different surface [14]. The polar nature of the ZnO is responsible for many interesting properties viz., piezoelectricity, spontaneous polarization, crystal growth, etching, and defect generation[15].

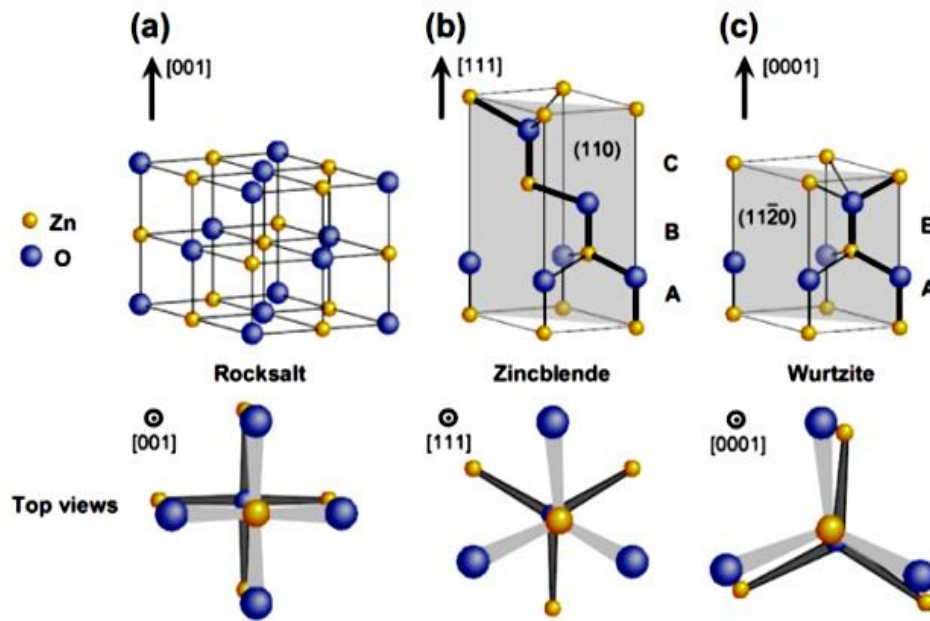


Fig. I. 4. Ball and stick representation of ZnO crystal structures. (a) Cubic rocksalt structure (b) cubic zinc-blende, (c) hexagonal wurtzite [16].

I.2.2.2. Optical Properties of ZnO

Most of the applications of ZnO films are certainly related to its optical properties. Since the band gap energy of ZnO is 3.37 eV at room temperature, it is transparent in both the visible and near ultraviolet–visible wavelength region. The exciton binding energy is quite high (60 meV), and it luminesces in the ultraviolet (UV) region (around 380 nm) making ZnO a possible future contender for UV and blue-light-emitting devices. This large exciton binding energy permits excitonic recombination above room temperature, and, as a result, optically pumped lasing has been observed in epitaxial or polycrystalline ZnO thin films.[17] The ZnO band-gap is a direct one with energy of 3.44 eV at 4 K and 3.37 eV at room temperature. For comparison, the respective values for wurtzite GaN are 3.50 eV and 3.44 eV. It also exhibits exciton binding energy of 60 meV, compared with 25 meV in GaN. This large exciton binding energy (compared to the one for other inorganic semiconductors) indicates that efficient excitonic emission in ZnO can persist at room temperature and higher. Since the oscillator strength of excitons is typically much larger than that of direct electron–hole transitions in direct-gap semiconductors, its exciton binding energy makes ZnO a promising material for optical devices that are based on excitonic effects. ZnO is a tetrahedrally-bonded semiconductor and the electronic structure together with its major intrinsic defects (such as

zinc vacancy V_{Zn} , zinc interstitial Zn_i , oxygen vacancy V_O , oxygen interstitial O_i) can be understood using the molecular orbital theory. [18]

The model, however, is a very simple one: the zinc atom possesses a full d-shell (10 electrons), for this reason, its sp^3 orbitals have in reality a strong d-character. ZnO has a rather strong ionic binding, consequently, the conduction band (CB) arises essentially from the Zn^{2+} 4s orbitals and the upper valence bands (VB) from the O^{2-} 2p states with an admixture of Zn^{2+} 3d levels[18].

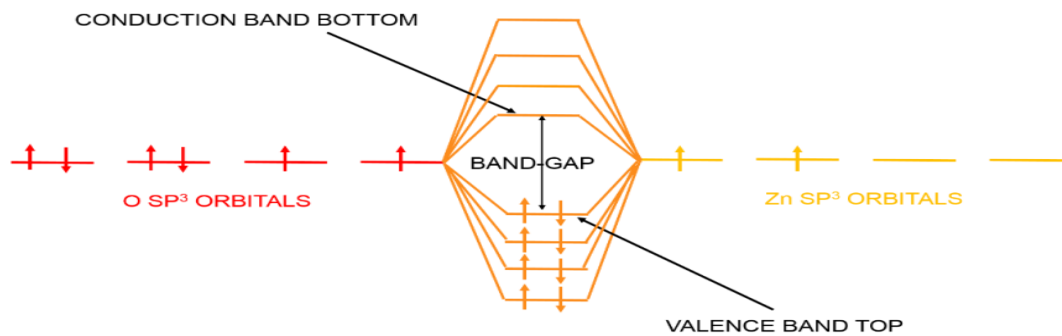


Fig. I. 5. Molecular orbital model of ZnO.

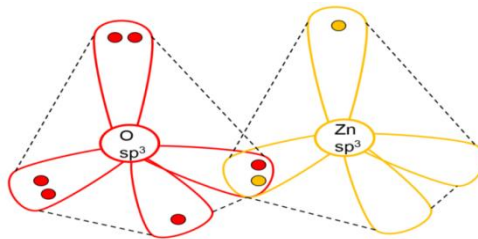


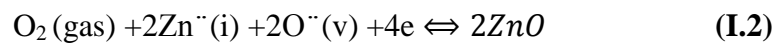
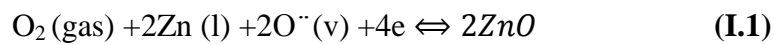
Fig. I. 6. Tetrahedral geometry of sp^3 orbitals for both O and Zn atoms.

The sp^3 orbitals have a tetrahedral configuration, the coordination number for both oxygen and zinc in the wurtzite structure is 4 (each oxygen atom bonds with 4 Zinc atoms and vice versa).

I.2.2.3. ZnO Electrical Properties

Electrical investigation of zinc oxide date back to 1912, when somerille measured the resistivity of cylindrical ZnO rods up to temperatures of 1200°C. The reported data at the beginning of the twentieth century scattered significantly, depending on the preparation of the samples and the used electrical contacts. Today we know that this was caused by the difficult

preparation of compact zinc oxide samples and by the missing understanding of semiconductors at that time. At the beginning of the 1930s, Wagner investigated the dependence of the electrical properties of oxides on their stoichiometry. These investigations were devoted to the proof of the theory of defect equilibria by Schottky and Wagner for ionic crystals. As well as Hauffe and Block could show that the oxygen content of the crystals, varied by annealing at different oxygen partial pressures, strongly determines the electrical carrier concentration and hence the conductivity due to a reaction balance between oxygen vacancies (2.1) or interstitial zinc atoms (2.2) and electrons in the conduction band according to :



Where l, v, and i, mean lattice place vacancy and interstitial position, which gives, Von Baumbach and Wagner argued that the zinc interstitial is more probable because of the smaller ionic radius of the Zn^{++} ions (74pm) compared with the oxygen ion (138). What could not be decided for decades was the question whether the oxygen vacancy or the zinc interstitial constitutes the donor. In conclusion, it was found that the conductivity of ZnO depends significantly on the stoichiometry, adjusted by the oxygen or zinc partial pressure during growth or annealing[19].

I.2.2.4. Dopants in ZnO

As already explained, the conductivity of ZnO depends significantly on the stoichiometry. This means, intrinsic defects in ZnO (Zn_i or V_O) constitute an intrinsic dopant in ZnO. In 2000, it was established that H-related unintentional dopants form a shallow donor in ZnO, which causes the intrinsic n-type behavior of ZnO, as suggested by a pioneering group led by van der Walle.

Highly conductive and efficient ZnO-based TCO can be obtained by extrinsic doping with IIIA (B, Al, Ga, In) and IIIB (Sc, Y, La) elements that act as shallow donors according to the simple H-like substitution donor model of Be. There are other reports on doping with IVA (Ti, Zr, Hf) and IVB (Si, Ge, Sn) and non-metal anions, such as Cl and F, to enhance the conductivity of ZnO thin films[20].

Titanium is another promising dopant atom for ZnO. Many previous studies have examined the doping of Ti in ZnO (TZO)[21–23]. Ti^{4+} has a radius of 0.68 Å, which is smaller than that of Zn^{2+} , 0.74 Å, and could be incorporated as interstitial and acted as a scattering site. However, only a small amount of doped Ti^{4+} could induce more electrons and avoid acting scattering centers. Chung et al. [24] investigated the properties of Ti-doped ZnO films and reported that the lowest resistivity of TZO films was achieved as the Ti addition was 1.34%. Lin et al. [25] studied the effects of substrate temperature on the properties of TZO films by simultaneous RF and DC magnetron sputtering. Also, Ti doped ZnO films with different concentrations were grown on glass substrates at 400 °C by a spray pyrolysis technique[26, 27]. It was found that the quality of the ZnO films improved when doped with Titanium.

The effort to increase the conductivity without degrading the transparency was paralleled by a more elaborate strategy in which phase-segregated two-binary and ternary TCOs were synthesized and characterized. The phase-segregated two-binary systems include ZnO-SnO₂, CdO-SnO₂, and ZnO-In₂O₃, ZnO-TiO₂. In spite of the expectations, the electrical and optical properties of the two-binary TCOs were much inferior to those of ITO. The phase diagram of the ternary TCOs could be schematically presented by a three-dimensional or four-dimensional phase combination of the most common ternary TCO materials, based on known binary TCO compounds. Accordingly, the ternary TCO compounds could be formed by combining ZnO, CdO, TiO₂, SnO₂, InO_{1.5} and GaO_{1.5} to obtain Zn₂SnO₄, ZnSnO₃, Zn₂TiO₄, CdSnO₄, ZnGa₂O₄, GaInO₃, Zn₂In₂O₅, Zn₃In₂O₆, and Zn₄In₂O₇. Other binary TCOs were synthesized from known binary TCOs and also from non-TCO compounds, such as In₆WO₁₂ and the p-type CuAlO₂[28].

The ZnO-TiO₂ system has always been of scientific and technological interest, initially for potters because of its application as paint pigments and fusion thermistors, as well as for carrying out basic studies such as dielectric material and in luminescence phenomena. Considering the reaction in solid state that can occur in a mixture of ZnO and TiO₂, when subjected to the action of temperature, it is possible that the mixed oxides are formed: Zn₂TiO₄, ZnTiO₃, and Zn₂Ti₃O₆, which have structural similarities (Zn₂TiO₄-spinel with TiO₂-anatase and ZnTiO₃ with TiO₂-rutile). Zn₂Ti₃O₈ meanwhile is based on the Zn₂TiO₄ phase and its crystalline structure is derived from the spinel but with defects. In the rutile and the ZnTiO₃ the connection of the TiO₆octahedrals promotes the formation of chains and/or

layers while in the anatase and in the spinel (Zn_2TiO_4 and $Zn_2Ti_3O_8$) three-dimensional structures are formed[29].

I.2.3. ZnO thin films applications

Zinc oxide can be called a multifunctional material thanks to its unique physical and chemical properties. It is already widely used in our society, and indeed it is a key element in many industrial manufacturing processes. **Fig.I .7.** Represents a schematic of the ZnO application.

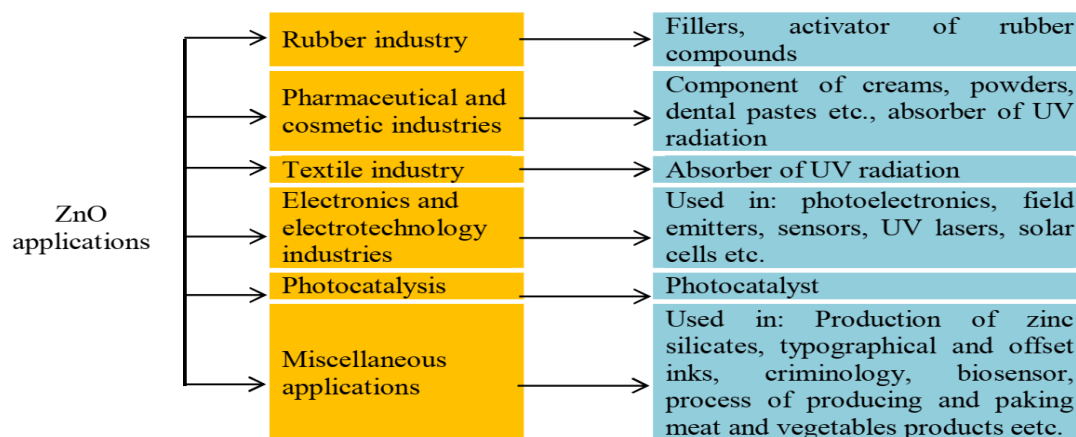


Fig. I .7. Schematic representation the applications of ZnO[30].

I.2. References

- [1] Gokilamani N, Muthukumarasamy N, Thambidurai M, Et Al. Solanum Nigrum And Eclipta Alba Leaf Pigments For Dye Sensitized Solar Cell Applications. J Sol-Gel Sci Technol 2014; 69: 17–20.
- [2] Meinhold G. Rutile And Its Applications In Earth Sciences. Earth-Science Rev 2010; 102: 1–28.
- [3] Kley CS. Atomic-Scale Characterization And Control Of Metal-Organic Templates And Photosensitizers On Surfaces. Lausanne, EPFL, 2013. Epub Ahead Of Print 2013. DOI: 10.5075/Epfl-Thesis-5884.
- [4] Gupta SM, Tripathi M. A Review Of Tio2 Nanoparticles. Chinese Sci Bull 2011; 56: 1639–1657.

-
- [5] Hanaor DAH, Sorrell CC. Review Of The Anatase To Rutile Phase Transformation. *J Mater Sci* 2011; 46: 855–874.
- [6] Muscat J, Swamy V, Harrison NM. First-Principles Calculations Of The Phase Stability Of Tio₂. *Phys Rev B - Condens Matter Mater Phys* 2002; 65: 2241121–22411215.
- [7] Pore V. Atomic Layer Deposition And Photocatalytic Properties Of Titanium Dioxide Thin Films. University Of Helsinki, 2010.
- [8] Vu NH, Le H V., Cao TM, Et Al. Anatase-Rutile Phase Transformation Of Titanium Dioxide Bulk Material: A DFT+U Approach. *J Phys Condens Matter*; 24. Epub Ahead Of Print 2012. DOI: 10.1088/0953-8984/24/40/405501.
- [9] Di Paola A, Bellardita M, Palmisano L. Brookite, The Least Known Tio₂ Photocatalyst. 2013. Epub Ahead Of Print 2013. DOI: 10.3390/Catal3010036.
- [10] Azouani R. Élaboration De Nouveaux Nanomatériaux Photocatalytiques Actifs Sous Rayonnement Visible. Université Paris 13, 2009.
- [11] Landmann M, Rauls E, Schmidt WG. The Electronic Structure And Optical Response Of Rutile, Anatase And Brookite Tio₂. *J Phys Condens Matter*; 24. Epub Ahead Of Print 2012. DOI: 10.1088/0953-8984/24/19/195503.
- [12] Roose B, Pathak S, Steiner U. Doping Of Tio₂ For Sensitized Solar Cells. *Chem Soc Rev* 2015; 44: 8326–8349.
- [13] Feng ZC. Handbook Of Zinc Oxide And Related Materials: Volume Two: Devices And Nano-Engineering. 2012.
- [14] Aleksander, Gurlo A. Integrated Analytical Systems. In: Carpenter MAAKSM (Ed) Metal Oxide Nanomaterials For Chemical Sensors. New York, USA: Springer-Verlag New York Pp. 513–539. Integrated Analytical Systems. 1st Ed. NY,USA: Springer-Verlag New York. Epub Ahead Of Print 2003. DOI: 10.1007/978-1-4614-5395-6.
- [15] Ramachandra Rao MS, Okada T. Zno Nanocrystals And Allied Materials. 1st Ed. Springer New Delhi, 2014. Epub Ahead Of Print 2014. DOI: 10.1007/978-81-322-1160-0.
-



- [16] Ong CB, Ng LY, Mohammad AW. A Review Of Zno Nanoparticles As Solar Photocatalysts: Synthesis, Mechanisms And Applications. *Renew Sustain Energy Rev* 2018; 81: 536–551.
- [17] Saniee NF. Structural And Optical Properties Of Transparent Conducting Si-Doped Zno Thin Films Grown By Pulsed Laser Deposition. University Of Birmingham, [Http://Www.Nanoarchive.Org/7248/](http://www.nanoarchive.org/7248/) (2005).
- [18] Intilla L. Study Of Zno Properties Applied To Thin Film Transistors. UCL (University College London), 2016.
- [19] Ellmer K, Klein A, Rech B. Transparent Conductive Zinc Oxide: Basics And Applications In Thin Film Solar Cells. Springer Berlin Heidelberg, 2007.
- [20] Mallick A, Basak D. Revisiting The Electrical And Optical Transmission Properties Of Co-Doped Zno Thin Films As N-Type Tcos. *Prog Mater Sci* 2018; 96: 86–110.
- [21] Chang HP, Wang FH, Chao JC, Et Al. Effects Of Thickness And Annealing On The Properties Of Ti-Doped Zno Films By Radio Frequency Magnetron Sputtering. *Curr Appl Phys* 2011; 11: S185–S190.
- [22] Lu JJ. Conductivity Enhancement And Semiconductor – Metal Transition In Ti-Doped Zno Films. *Opt Mater (Amst)* 2007; 29: 1548–1552.
- [23] Ganesh R, Pala S, Tang W, Et Al. CO Oxidation By Ti- And Al-Doped Zno : Oxygen Activation By Adsorption On The Dopant. *J Catal* 2009; 266: 50–58.
- [24] Chung J, Chen J, Tseng C. The Influence Of Titanium On The Properties Of Zinc Oxide Films Deposited By Radio Frequency Magnetron Sputtering. *Appl Surf Sci* 2008; 254: 2615–2620.
- [25] Lin S, Huang J, Lii D. Effect Of Substrate Temperature On The Properties Of Ti-Doped Zno Films By Simultaneous Rf And Dc Magnetron Sputtering. *Mater Chem Phys* 2005; 90: 22–30.
- [26] Rajasekaran M, Arunachalam A, Kumaresan P. Structural, Morphological And Optical Characterization Of Ti-Doped Zno Nanorod Thin Film Synthesized By Spray Pyrolysis Technique. *Mater Res Express*; 7. Epub Ahead Of Print 2020. DOI: 10.1088/2053-

1591/Ab815d.

- [27] Sridhar R, Manoharan C, Ramalingam S, Et Al. Spectroscopic Study And Optical And Electrical Properties Of Ti-Doped Zno Thin Films By Spray Pyrolysis. *Spectrochim Acta - Part A Mol Biomol Spectrosc* 2014; 120: 297–303.
- [28] Afre RA, Sharma N, Sharon M, Et Al. Transparent Conducting Oxide Films For Various Applications: A Review. *Rev Adv Mater Sci* 2018; 53: 79–89.
- [29] Mazabuel-Collazos A, Gómez CD. Zno-Tio₂ Nanocomposites Synthesized By Wet-Chemical Route: Study Of Their Structural And Optical Properties. *Mater Chem Phys*. Epub Ahead Of Print 2018. DOI: 10.1016/J.Matchemphys.2018.10.007.
- [30] Fouad B. Deposition And Analysis Of Zinc Oxide Thin Films Elaborated Using Spray Pyrolysis For Photovoltaic Applications. University Mohamed Khider Of Biskra, 2018.



***Chapter II Thin films Preparation
and characterization techniques***

II.1. Introduction

There is a steadily growing interest in the research on oxide surfaces and films, due to their challenging fundamental properties and to their actual and potential applications in catalytic systems, chemical sensors, electronic and magnetic devices, and functional and aesthetic coatings. Special efforts have been directed at the study of thin oxide films. Such two-dimensional systems are emerging as important new materials where the relevant phenomena are induced by the extreme vertical confinement, and new phases and structures are stabilized, which cannot be obtained in bulk form. Last but not least, the possible use of thin oxide films as model systems to substitute for bulk oxides has been shown to be very appealing.

Critical properties basically depend on the reduced dimensionality, as well as on the stoichiometry, defectivity, and morphology of the films, on the extent of the crystalline order, and on the sharpness of the interfaces between film and substrate or between different films in multilayers, which are to a great extent determined by the preparation method. Therefore a main driving force in the development of oxide materials in the form of thin films has been the progressive improvement of the fabrication procedures.

A wide range of preparation methods exist for the thin film materials. The deposition method has generally a large impact on the resulting film properties as well as on the production costs. The vast varieties of thin film materials, their deposition, processing and fabrication techniques, spectroscopic characterization, optical characterization probes, physical properties, and structure-property relationships are the key features of such devices and basis of thin film technologies.

Most deposition techniques follow these three major sequences:

1. Synthesis of the deposition species,
2. Conveyance from source to substrate,
3. Deposition and adhesion of the source onto the substrate and subsequent film growth.

In this section, the most important deposition methods are reviewed, with the main emphasis on spray pyrolysis which is used for this work.

II.2. Thin films dépositions techniques

There are several types of thin films deposition techniques, priority will be given to the two major deposition techniques used for thin films. The prominent subsets of deposition techniques are physical vapor deposition (PVD) and chemical vapor deposition (CVD). The distinguishing feature between PVD and CVD is in the vapor. In PVD, the vapor is made up of atoms and molecules that simply condense on the substrate, and for CVD, the vapor undergoes a chemical reaction on the substrate which resulted into a thin film [1] .

II.2.1. Physical vapor deposition (PVD) process

Physical vapor deposition (PVD) is used to describe variety of methods to deposit thin solid films by the condensation of a vaporized form of the solid material onto various surfaces. Namely, PVD process involves physical ejection of material as atoms or molecules and condensation and nucleation of these atoms onto a substrate. The vapor phase material can consist of ions or plasma and is often chemically reacted with gases introduced into the vapor, called reactive deposition, to form new compounds. The thicknesses of deposited layers could be from few nanometers to thousands of nm. Every PVD process can be defined by three basic steps [2]:

- (1) Generation of the deposition or vapor-phase species: material can be converted to a vapor phase by evaporation, sputtering, or ion bombardment.
- (2) Transport of the species to the substrate: transport of vapor species from the source to the substrate can occur under thermal scattering or molecular flow conditions (without collisions between atoms and molecules). Alternatively, if the partial pressure of the metal vapor or gas species in the vapor state is high enough for some of these species to be ionized (by creating a plasma), there will be a large number of collisions in the vapor phase during transport to the substrate.
- (3) Film deposition on the substrate: once the atoms or molecules are deposited, the film nucleates on the substrate and grows by a number of processes. Microstructure and composition of the film can be modified by bombardment of the growing film by ions from the vapor phase, resulting in sputtering and re-condensation of the film atoms and enhanced surface mobility of the atoms in the near surface and surface of the film.

II.2.2. Chemical Methods

The use of chemical deposition methods has allowed the large-scale production of thin oxide films on complex-shaped objects at lower cost. The main disadvantage is the reduced control over the deposition and the risk of residues left from the precursors as compared with cleaner PVD methods. These methods can be roughly divided into two main groups, one based on chemical vapor deposition (CVD), the second based on liquid precursors. All these techniques have been extensively used recently for the growth of doped and undoped oxide nanostructured materials with potential applications in areas ranging from electronics, optics, and energy storage to biomedical sciences[3].

II.2.2.1. Chemical vapor deposition (CVD) process

CVD is a generic term for deposition of the thin film via series chemical reaction. The process of material synthesis occurs when the constituent of the target in the vapor phase reacts via a chemical process near the surface or onto the surface of the substrate, leading to the growth of the thin film. Note that the mechanisms behind CVD differ drastically from the PVD process. In PVD, thin film formation is caused by condensation of atoms or molecules on the surface of the substrate due to evaporation, ion bombardment, or sputtering. On the other hand, CVD is a thermodynamically complex process involving chemical reactions under specific conditions such as temperature, pressure, reaction rates, and momentum, mass, and energy transport. The quality of the film can be controlled and modified by using the appropriate combination of process parameters. There are various types of chemical reaction possible during CVD. The CVD reaction types possible are pyrolysis, reduction, oxidation, compound formation, disproportionation, and reversible transfer[1].

The CVD technique consists of developing materials in the form of thin layers from gaseous precursors that chemically react to form these layers on a heated substrate, as shown in **Fig. II. 1**. The CVD process can be summarized in five steps[4]:

- Transporting reactive gas species to the substrate.
- Adsorption of the reactants on the surface.
- Surface reaction and film growth.
- Desorption of volatile secondary products.
- Transport and evacuation of gaseous by-products to the reactor outlet.

CVD process usually characterized by volatile reaction of by-products and unused precursor species. Many CVD reactions by-products are very hazardous volatile by-products such as H₂, Cl₂, HCl, HF or water vapour. Proper safety precaution is needed when using CVD. Venting, scrubbing of by-products and unreacted compounds are essential in CVD processes. Today, a variety of different CVD methods are available that can be employed to synthesize different thin films materials. According to the characteristics of the processing parameters (pressure, temperature, precursor nature, gas flow state, wall/substrate temperature, depositing time, and activation manner), these methods can be categorized into seven main types based on temperature, pressure, wall/substrate, nature of precursor, depositing time, gas flow state and activation/power source[5], as demonstrated in **Fig. II. 2**.

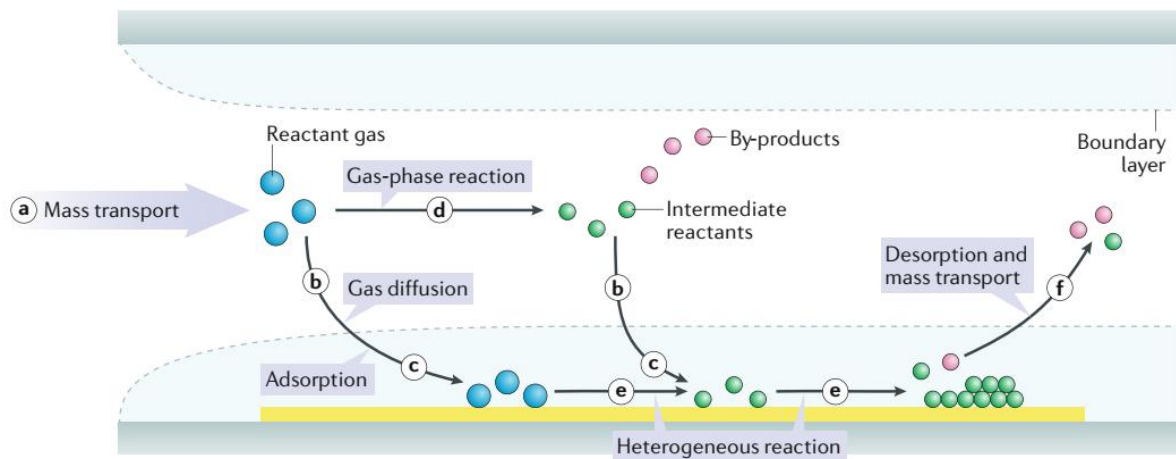


Fig. II. 1. Schematic of general elementary steps of a typical CVD process. First, reactant gases (Blue circles) are transported into the reactor (step a). Then, there are two possible routes for the reactant gases: directly diffusing through the boundary layer (step b) and adsorbing onto the substrate (step c); or forming intermediate reactants (green circles) and by-products (red circles) via the gas-phase reaction (step d) and being deposited onto the substrate by diffusion (step b) and adsorption (step c). Surface diffusion and heterogeneous reactions (step e) take place on the surface of substrate before the formation of thin films or coatings. Finally, by-products and unreacted species are desorbed from the surface and forced out of the reactor as exhausts (step f). CVD, chemical vapor deposition [6].

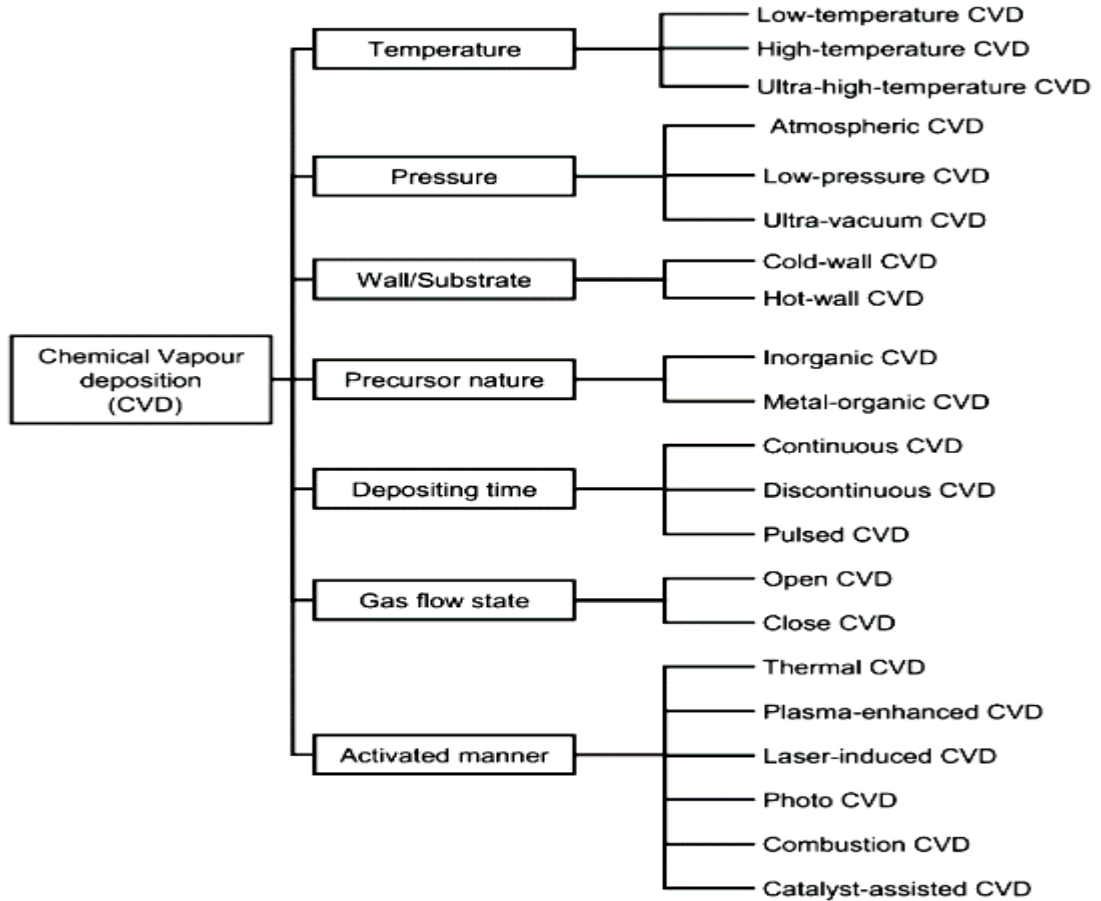


Fig. II. 2. Classification of CVD methods[5].

II.2.2.2. Chemical solution deposition techniques (CSD)

Film fabrication by CSD typically begins with the solution synthesis in the chemistry lab. The main precursors are salts, carboxylates, or other metallo-organic compounds such as metal alkoxides and metal β -diketonates, which can often be purchased commercially or synthesized in-house by common chemical synthesis strategies. Next, the coating solution is deposited by a number of methods. Spin and dip coating in various modifications are the by far most frequently applied techniques. Aerosol deposition (often denoted as spray coating) and, more recently, ink-jet printings are more sophisticated methods allowing for a more conformal coating or structured coating with reduced material consumption[7].

I.2.2.2.1. Sol–Gel

The sol–gel process is one of the most used liquid-precursor-based techniques in the preparation of thin oxide films. The sol-gel process may be described as: "Formation of an oxide network through polycondensation reactions of a molecular precursor in a liquid. [8]" .The starting materials used in the preparation of the sol are usually inorganic metal salts or metal organic compounds such as metal alkoxides $M(OR)_z$ where R is an alkyl radical ($R = CH_3, C_2H_5,$ etc.) [9].

A **sol** is a stable dispersion of colloidal particles or polymers in solvent. The particles may be amorphous or crystalline. An aerosol is particles in a gas phase, while a sol is particles in a liquid [10].

A **gel** consists of a three dimensional continuous network, which encloses a liquid phase, In a colloidal gel, the network is built from agglomeration of colloidal particles. In a polymer gel the particles have a polymeric sub-structure made by aggregates of sub-colloidal particles [11]. The particle concentration, viscosity, and stability of the sol–gel influence the deposition parameters and film quality. The deposition of films in the sol–gel process proceeds usually through application of a precursor solution on one side of a rapidly rotating substrate (spin coating) or by immersion in the precursor solution (dip coating). A final heating step removes the remaining solvent from the surface [3].

II.2.2.2.2. Spray Pyrolysis (SP)

Spray pyrolysis is an aerosol process commonly used to form a wide variety of thin films materials including noble metals, metal oxides, spinel oxides, chalcogenides and superconducting compounds [12]. It was used as early as 1910 to obtain transparent oxide films, after that this technique has been developed extensively by several researchers; the process involves a thermally stimulated reaction between clusters of liquid/vapor atoms of different chemical species [13]. It is based on the pyrolytic decomposition of a metallic compound dissolved in a liquid mixture when it is sprayed onto a preheated substrate [14].

II.2.2.2.2.1. Models for Film Deposition by Spray Pyrolysis

There are too many processes that occur either sequentially or simultaneously during film formation by spray pyrolysis. These include precursor solution atomization, droplet transport and evaporation, spreading on the substrate, drying and decomposition of the precursor salt.

Chapter II Thin films Preparation and characterization techniques

Understanding these processes will help to improve film quality. Thin-film deposition using spray pyrolysis can be divided into three main steps: atomization of the precursor solution, transportation of the resultant aerosol, and decomposition of the precursor on the substrate [15].

II.2.2.2.1.a. Atomization of Precursor Solution

Precursor solution composition alters the final chemical characteristics of the material targeted, so the nature of the solvent should be considered at first stage. The solvent in the precursor solution is chosen attending to the solubility of the precursor compound and on its physical properties such as density and viscosity as well as on the final byproducts that will generate and how neutral for their disposal they will be. The preferred choice is water or a mixture of water and an alcohol, which will dissolve many inorganic salts (such as chlorides, some nitrites and fluorides). Organic salts will require organic solvents that, when properly selected, could render excellent precursor solutions [16].

Since the aerosol droplet size distribution, determined by the aerosol generation mechanism, will set the morphological characteristics of the final material produced[16]. the key is to understand the basic atomization process of the atomization device in use. In particular, it is important to know which type of atomizer is best suited for which application and how the performance of the atomizer is affected by variations in liquid properties and operating conditions. Some of them are briefly given below [15].

Pneumatic atomization

Expansion of a pressurized liquid stream through a nozzle is the simplest form of droplet generation. An aerosol generated by pneumatic atomization will be entrained within a gas flow created by the compressed gas input. The pressure of aerosol deposition processes is typically in the neighborhood of atmospheric pressure [7].The velocity of the liquid stream is limited by the nozzle diameter and thermodynamics of expansion. Nominal size of droplets is in the range of 50 micrometers in diameter and the size distribution is relatively wide. Productivity is the best among the droplet generators introduced in this section. A two-fluid nozzle is similar to a pressurized nozzle except that the liquid solution is passed through together with a pressurized gas [17].so that the shear force exerted on the liquid is larger than in a pressurized nozzle. The

droplet size is controlled by the ratio of gas and liquid. Droplet size distribution is relatively narrow [18].

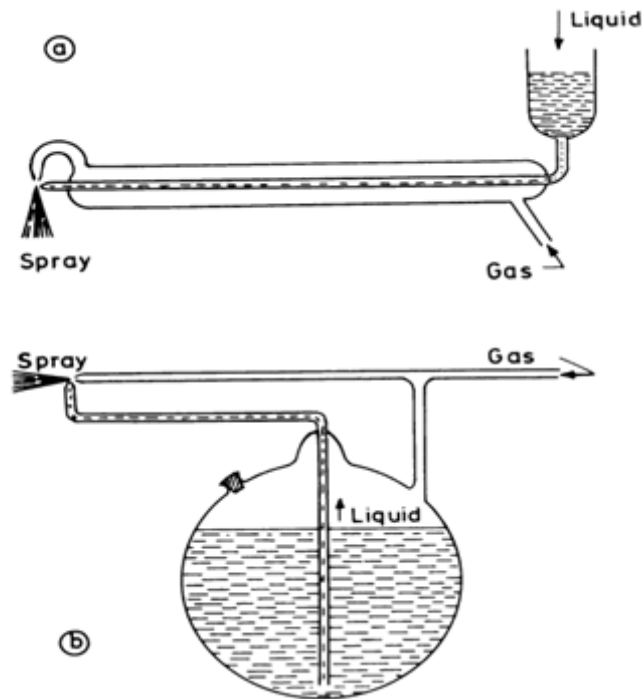


Fig. II. 3. Schematic diagrams of some commonly employed nozzles [13].

Ultrasonic nebulized atomization

Ultrasonic pulverization of an aerosol is based on vibration and cavitation effects induced by the exposition of a liquid solution to an ultrasonic beam (typically a few tens kHz to about 1 MHz frequency) of sufficient intensity. The aerosol is atomized from the liquid, either contained in a vessel crimped with an ultrasonic transducer ceramic, or passed through an ultrasonically excited vibrating nozzle, and then conveyed with a carrier gas onto the substrate surface [17]. The droplets have very small sizes with a narrow size distribution and no inertia in their movement so that they can be transported the carrier gases. The pyrolysis of an aerosol, produced by the ultrasonic spraying is known as the pyrosol process. The advantage in this method is that the gas flow rate is independent of the aerosol flow rate [12]. Ultrasonic atomizers are commonly used in the laboratory, but give low production rates. Thus, further studies must be conducted to develop droplet generators which will be practical for industrial applications [19].

Electrostatic spray pyrolysis

Droplets can also be formed by electrostatic processes. This method involves a high dc voltage applied between a capillary, in which the liquid solution is passed through, and a ground electrode substrate. Beyond a critical voltage (typically several kV) at the capillary outlet, the surface of the solution becomes unstable and an electrostatic spray is formed, which is attracted toward the substrate by the electrostatic force [17]. The nozzle-to-substrate distance is kept small, about 6 mm [12]. Such a phenomenon is called electrostatic atomization or electrospraying. The main challenge here is scale-up to allow larger liquid throughputs [19].

II.2.2.2.1.b. *Aerosol Transport*

Once the aerosol is generated, it has to be transported to the material synthesis area with a gas flow set to minimize coalescence of the drops throughout the transport process, and also to render a desired synthesis rate. Since the carrier gas will be closely present during the synthesis process, whether it is chosen to be an inert or a reactive gas becomes relevant. Thus, if the carrier gas is air, the synthesis is limited to compounds that are as stable like or even better than oxides. In the case of metals, the carrier gas has to be an inert gas which in some cases is combined with a reduction gas (N_2 and H_2 , as in the case of forming gas) [16]. During transportation it is important that as many droplets as possible are transported to the substrate without forming powder or salt particles [15].

II.2.2.2.1.c. *Decomposition of Precursor*

The decision whether the final chemical reaction takes place on a gas phase or on a hot substrate will determine if the material synthesized is a powder or a film coating. At the reactive zone, several parameters are determinant as to what type of material synthesis process occurs, such as temperature, droplet size and their speed. The reactive zone is, in the case of film deposition, the space near the surface of the hot substrate (a few millimeters above the surface of the substrate), **Fig. II. 4.** shows a diagram of the different stages at which the droplet is subjected as it approaches the hot substrate for two cases a fixed droplet size and speed, different (increasing from A to D, **Fig. II. 4. a**) temperature of the substrate and fixed substrate temperature and speed of different droplet sizes (decreasing droplet size from A to D, **Fig. II. 4. B**).

Chapter II Thin films Preparation and characterization techniques

At low temperature (large initial droplet size), the solvent within the droplet is not completely vaporized and the liquid droplet hits the substrate and upon contact with it vaporizes leaving a ring-shaped dry precipitate on the substrate (process A).

At low or intermediate temperature values (large or medium droplet size) the solvent is vaporized, and a dry precipitate (an amorphous precursor salt) hits the substrate surface where a pyrolysis reaction takes place (process B).

At intermediate or high temperatures (medium or small droplet size) the droplet goes through all previously described stages. Near the substrate surface the dry precipitates are vaporized, propitiating a chemical vapor reaction (CVD) on the surface of the substrate (process C).

Finally, for high temperature (small droplet sizes) the vaporized precipitates undergo a chemical reaction in the vapor phase before they reach the substrate surface (process D) [16].

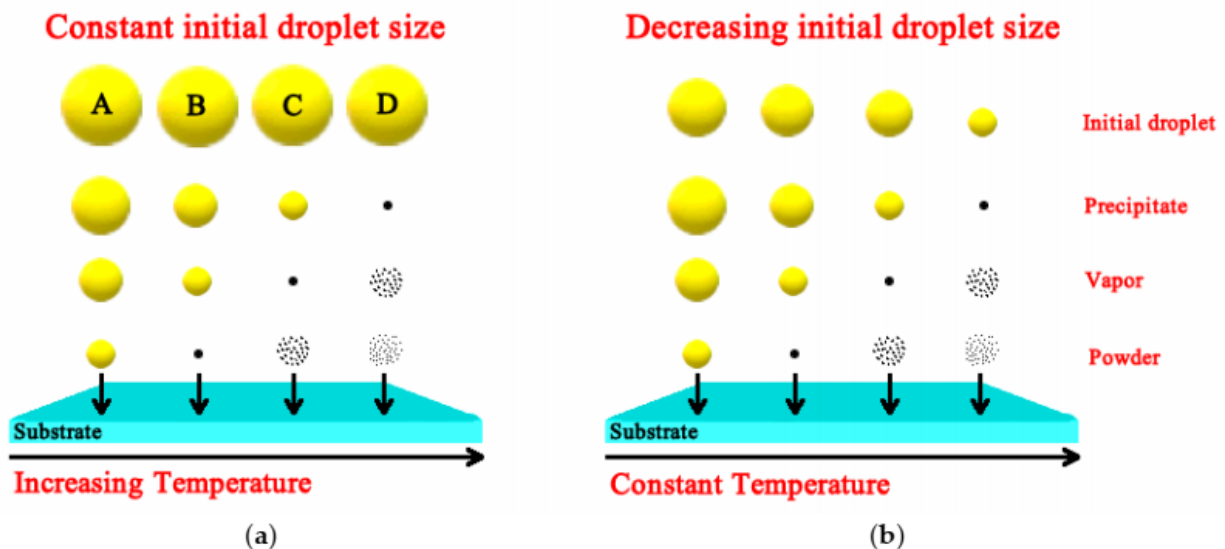


Fig. II. 4. Diagram of the different process stages for the aerosol droplet evolution as it approaches the hot substrate for two cases: (a) Constant initial droplet size and increasing substrate temperature, (b) constant substrate temperature and decreasing initial droplet size.

It is believed that the processes A and D lead to rough or non-adherent films. Adherent films were obtained by CVD at low temperatures (process C). However, type A or B allows formation of high quality adherent films too. Moreover, the process C can rarely occur in most spray pyrolysis depositions, because either the deposition temperature is too low for the vaporization of a precursor or the precursor salt decomposes without melting and vaporization [15].

II.2.2.2.2. Advantages of Spray Pyrolysis Technique

Despite its simplicity, SP have a number of advantages [12]:

- (1) It offers an extremely easy way to dope films with virtually any element in any proportion by merely adding it in some form to the spray solution.
- (2) Unlike closed vapor deposition methods, SP does not require high quality targets and/or substrates nor does it require vacuum at any stage, which is a great advantage if the technique is to be scaled up for industrial applications.
- (3) The deposition rate and the thickness of the films can be easily controlled over a wide range by changing the spray parameters, thus eliminating the major drawbacks of chemical methods such as sol-gel which produces films of limited thickness.
- (4) Operating at moderate temperatures (100–500°C), SP can produce films on less robust materials.
- (5) Unlike high-power methods such as radio frequency magnetron sputtering (RFMS), it does not cause local overheating that can be detrimental for materials to be deposited. There are virtually no restrictions on substrate material, dimension or its surface profile.
- (6) By changing composition of the spray solution during the spray process, it can be used to make layered films and films having composition gradients throughout the thickness.

The major interest in spray pyrolysis is due to its low cost, while it is increasingly being used for some commercial processes, such as the deposition of a transparent layer on glass.

Depend on the available equipment in our laboratory of thin films and applications of university of Biskra, which is able to supply suitable conditions for synthesis via Spray Pyrolysis (SP) and further treatments of the desired product. The present work is an attempt to summarize the basic types of equipment, and conditions for obtaining of thin films for various applications, via two kinds of spray pyrolysis method which are pneumatic spray pyrolysis [14].

II.3. Characterization methods

II.3.1. Structural and Morphological Characterizations

II.3.1.1. X-ray Diffraction (XRD)

Crystalline structure of the samples can be recognized through X-Ray Diffraction (XRD). This technique consists in shooting a monochromatic beam of X-Rays on the sample and collecting

Chapter II Thin films Preparation and characterization techniques

the diffracted X-Rays with a detector. Varying the incidence angle of the beam creates a series of peaks and valleys depending on the different kind of interference created by the diffracted rays. There is constructive interference when the atomic layer separation is a whole multiple of the wavelength used to investigate the sample. This happens for a definite series of angles determined by Bragg's law [20]:

$$2d_{hkl} \sin \theta = n\lambda \quad (\text{II.1})$$

d_{hkl} : The atomic spacing,

θ : incident angle of X-ray,

λ : The wavelength.

The X-ray diffraction is a non-destructive structural analysis method for determining the crystal structure of materials in the form of bulk materials, powders or thin films [4]. This technique can detect every kind of atoms provided that they are located in crystallographic planes, therefore amorphous materials cannot be detected. The signal measured greatly depends on the sample crystal quality [20]. to identify compounds and/or phases is performed by comparing the results obtained with the reference values listed in the standard files JCPDS (Joint Committee for Powder Diffraction Standards) [4].

In this work, we used a Mini-Flex (Rigaku) diffractometer (**Fig. II. 5.**) With a source of Cu-K α 1 radiation has a wavelength of 0.15405 nm



Fig. II. 5. Mini-Flex (Rigaku) diffractometer.

Crystallites size determination

According to the Scherrer equation, there is a relationship between the broadening of a peak in a diffraction pattern and the average size of sub-micrometric crystallites, D [21]:

$$D = \frac{k\lambda}{\beta \cos \theta} \quad (\text{II.2})$$

Where k is a constant determined by the material (we used the value $k = 0.89$, λ is the incident radiation wavelength, β is the FWHM (full width at half maximum) of the peak and θ is its position according to Bragg's law. Scherrer constant κ is usually taken to be 0.9, but its value depends greatly on the crystallite shape. Note that β is an angular width, in terms of 2θ (not θ), and not a linear width. However, this equation is a rough estimation valid only for crystallites smaller than half a micron of diameter and is based on the assumptions of a perfect crystal lattice and an incident beam composed of parallel and monochromatic radiation [20].

II.3.1.2. Scanning Electron Microscope (SEM)

The scanning electron microscope (SEM) is one of the most heavily used instruments in the research field. The image in scanning electron microscope is produced by scanning the sample with a focused high-energy electron beam. The principle involved in imaging is to make use of the scattered secondary electrons when a finely focused electron beam impinges on the surface of the specimen. The electrons are produced by a thermal emission source, such as heated tungsten filament, or by using field emission cathode. The anode, which is positive with respect to the filament, forms powerful attractive forces for electrons. This causes electrons to accelerate toward the anode. The image in an SEM is produced by scanning the sample with a focused electron beam and detecting the secondary and backscattered electrons produced due to the interaction of the primary electron beam. These electrons are collected by a secondary detector or a backscatter detector, converted to a voltage, and amplified. The amplified voltage is applied to the grid of the cathode ray tube (CRT) that causes the intensity of the spot of light to change. Intensity of the emitted electron signal displayed as brightness on a cathode ray tube. The image consists of thousands of spots of varying intensity on the face of a CRT that correspond to the topography of the sample. Secondary electron imaging provides high resolution imaging of fine surface morphology and for this the samples must be electrically conductive [22–24].

This imaging can produce very high-resolution images of the sample surface, revealing details about 1 to 5 nm in size. The produced images have a very large depth of field yielding a

characteristic three-dimensional appearance useful for understanding the surface structure of the sample [24].

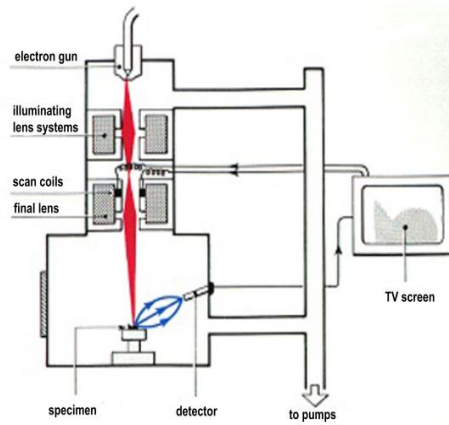


Fig. II. 6. Schematic diagram of scanning electron microscope.

II.3.2. Compositional Analysis

II.3.2.1. Energy dispersive x-ray analysis (EDS)

Energy-dispersive X-ray spectroscopy is a non-destructive analytical technique employed to identify specific elements present in the sample and their relative proportions. With an x-ray spectrometer added to the SEM, EDS element mapping and point analysis can be performed on a chosen scanned area or point image of a sample produced by electron microscopy [25]. When an electron impinges on a specimen, it may scatter with an inner-shell electron of a specimen atom, transferring energy sufficient for the inner-shell electron to emerge from the specimen. The empty state is then reoccupied by an electron from an elevated state, and the difference in potential energy between the two states is either transferred to a bound electron, which then can leave the atomic bond as Auger electron, or is emitted as X-ray quantum [26].

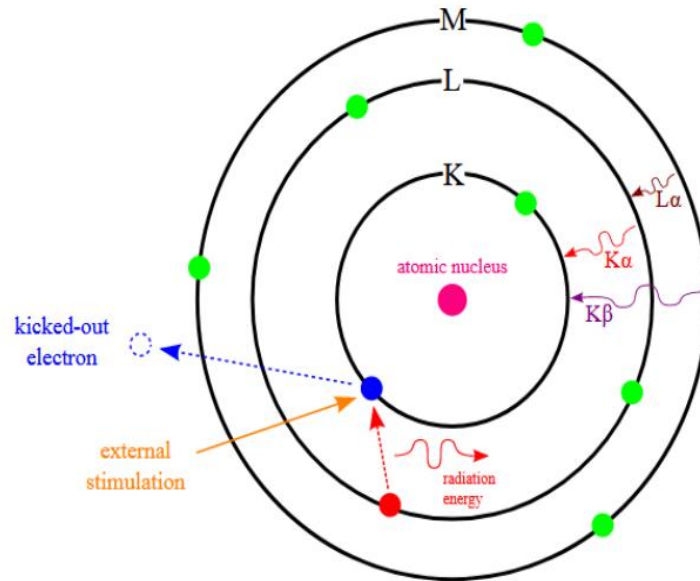


Fig. II. 7. Scheme of X-ray excitations in EDX analysis.

This amount of energy is predicted by the laws of quantum mechanics. The x-ray detector in the EDAX is reverse biased semiconductor pin or Schottky diode.

$$I(x)=I_0exp[-\mu /\rho]\rho x \quad (\text{II.3})$$

Where (μ/ρ) is the mass absorption coefficient, ρ the detector material density, $I(x)$ the x-ray intensity in the detector and I_0 is the incident xray intensity. The mass absorption coefficient is characteristic of a given element at specified x-ray energies and it varies with atomic number of the target. Thus, by measuring the energy of the x-rays emitted by a specimen during electron beam bombardment, the identity of the atom from which the x-ray was emitted can be established. The output of an EDAX analysis is an EDAX spectrum, which is a plot of how frequently x-ray is received for each energy level. The higher a peak in a spectrum, the more concentrated the element is in the specimen [23].

In this work the compositional analysis were carried out using TESCAN VEGA3.



Fig. II. 8. Scanning electron microscope TESCAN VEGA3.

II.3.3. Optical studies

II.3.3.1. Transmission spectroscopy

Optical photons incident on any material may be reflected, transmitted or absorbed. The absorption of light in a semiconductor can lead to

1. Photoionisation of semiconductor atom: this is excitation of valence electrons to the conduction band. The energy required is greater than or equal to the band gap.
2. Photoionisation of impurity atoms: this leads to the transition of electron from the donor level to the conduction band or from the valence band to the acceptor level.
3. Excitation of electrons from the valence band to an imperfection level.
4. Formation of excitons.
5. Excitation of free carriers to a higher energy state in the same band.
6. Excitation or absorption of phonons.
7. Excitation of crystal vibrations.

Chapter II Thin films Preparation and characterization techniques

Of all these absorption processes the first three directly give rise to photoconductivity. The optical transmittance studies are useful for the identification of band gap, impurity states, refractive index, extinction coefficient etc [24]. The technique is based on the measurement of light absorption by a sample, typically using commercially available spectrometers at reasonable cost. As illustrated in **Fig. II. 9**, the intensity of light from a light source, e.g. a lamp, is measured by a light detector, e.g. photodiode, photomultiplier tube (PMT) PMT or charge coupled device (CCD) detector, without (blank) and with a sample between the light source and detector. If the sample absorbs light at some wavelength, the transmitted light will be reduced. The intensity of the transmitted light plotted as a function of light wavelength will give a spectrum of the sample absorption [27].

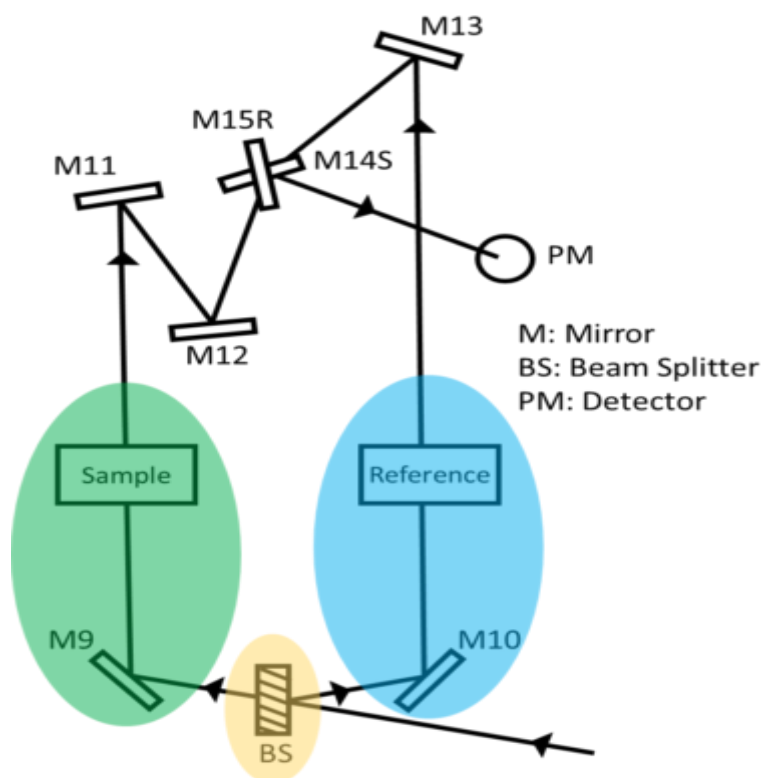


Fig. II. 9. Double beam instrument schematic. The beam splitter is highlighted in yellow, the reference beam in blue, and the sample beam is highlighted in green.

Based on Beer's law, the absorption coefficient can be deduced from the transmission spectra using the relation,

$$I = I_0 e^{-(a)d} \quad (\text{II.4})$$

Chapter II Thin films Preparation and characterization techniques

Where, I is the transmitted intensity and I_0 is the incident intensity of the light and d is the thickness of the film.

In the present investigation, The optical transmittance spectra has been recorded from 250nm to 2500nm wavelength using a UV-VIS-NIR spectrophotometer (JASCO V-770) at room temperature This spectrophotometer is a double beam system with single monochromator with the wavelength range of 190 nm to 2700 nm. This spectrometer has PbS photocell detector. Since the spectrophotometer is interfaced with computer the recorded spectrum is obtained directly from the computer.

Optical band gap

The absorption is expressed in terms of a coefficient ($\alpha h\nu$), which is related to the energy gap E_g according to the equation,

$$\alpha h\nu = A(h\nu - E_g)^N \quad (\text{II.5})$$

Where A is a constant, h is the Plank's constant, ν the frequency of the incident beam and $N=1/2$ for allowed direct transitions, $N=2$ for allowed indirect transitions. Optical band gap was determined using the $(\alpha h\nu)^2$ versus $h\nu$ plot by extrapolating the linear portion of the curve to $h\nu$ axis [22].

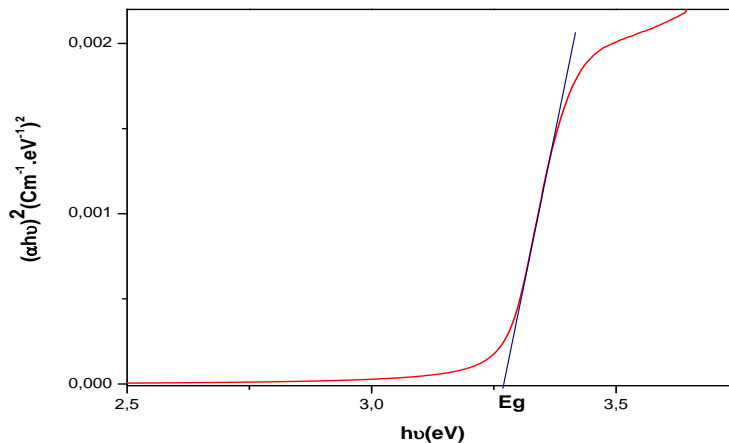


Fig. II. 10. Determination of E_g .

Urbach energy

For semiconductors, fundamental absorption near the energy band gap increases exponentially, and the absorption edge is called the Urbach tail. Urbach energy (E_U) indicates the width of the localized states in the band gap. Such tails can originate from disorder of the perfect crystal, e.g. from defects or doping, and the fluctuation of electronic energy bands due to lattice vibrations.

The Urbach energies are determined by following equation [28, 29]:

$$\alpha = \alpha_0 e^{\left(\frac{h\nu}{E_U}\right)} \quad (\text{II.6})$$

where α_0 is constant. The E_U is the Urbach energy. If it takes the logarithm of (II.5) the following equation can be written:

$$\ln(\alpha) = \ln(\alpha_0) + \frac{h\nu}{E_U} \quad (\text{II.7})$$

The experimental value of the Urbach energy could be estimated from the slope of ($\ln \alpha$) versus energy ($h\nu$) plots of the films [30].

II.3.4. Electrical properties (*Four point probe method*)

The use of thin films as resistors, contacts and interconnections has lead to extensive study of conductivity. Investigations of the electrical resistivity as a highly structure sensitive properties make it possible to gain insight into the structural and electrical properties of the film which is important from both the theoretical and practical point of view.

The most common method for measuring resistivity is the four-point probe method shown in **Figure II. 11**. The probes are equally spaced. A small current I from a constant-current source is passed through the outer two probes and a voltage V is measured between the inner two probes [31]. Since negligible contact and spreading resistance are associated with the voltage probes, one can obtain a fairly accurate estimation of the sheet resistance (R_{sh}) from the following relation

$$R_{Sh} = 4.532\left(\frac{V}{I}\right) \quad (\text{II.8})$$

Chapter II Thin films Preparation and characterization techniques

In the above configuration, a correction factor of 4.532 is used for all samples. And the conductivity (σ) values of films could be calculated from the following formula:

$$\sigma = \frac{1}{\rho} = \frac{1}{(R_{sh} \times d)} \quad (\text{II.9})$$

Where ρ is the resistivity of the films and d : thickness of the film [32].

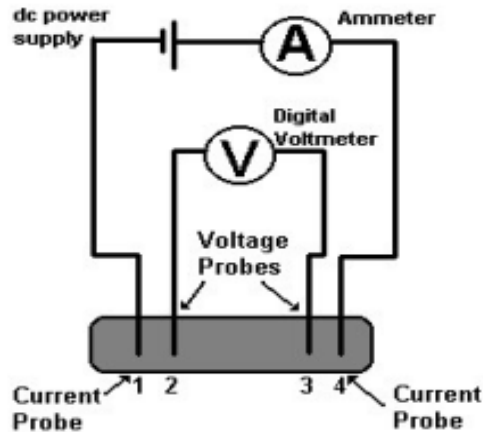




Fig. II. 11. Schematic of Four-Point Probe[33].

II.4. References

- [1] Abegunde OO, Akinlabi ET, Oladijo OP, Et Al. Overview Of Thin Film Deposition Techniques. AIMS Mater Sci 2019; 6: 174–199.
- [2] Petkoska AT, Nasov I. Surface Engineering Of Polymers - Case Study : PVD Coatings On Polymers. Zast Mater 2014; 55: 3–10.
- [3] Gianfranco P, Valeri S. Oxide Ultrathin Films. 2011. 
- [4] Abdeouahab N. Preparation And Characterization Of Thin Films Nanostructures Based On Zno And Other Oxides. Larbi Ben M'hidi University, 2019.
- [5] Saeed M, Alshammari Y, Majeed SA, Et Al. Chemical Vapour Deposition Of Graphene—

Chapter II Thin films Preparation and characterization techniques

- Synthesis, Characterisation, And Applications: A Review. *Molecules*; 25. Epub Ahead Of Print 2020. DOI: 10.3390/Molecules25173856.
- [6] Campbell SA, Smith RC. Chemical Vapour Deposition. *High-K Gate Dielectr* 2003; 0123456789: 65–88.
- [7] Schneller T, Waser R, Kosec M, Et Al. Chemical Solution Deposition Of Functional Oxide Thin Films. 2013. Epub Ahead Of Print 2013. DOI: 10.1007/978-3-211-99311-8.
- [8] Aguilar GV. Introductory Chapter: A Brief Semblance Of The Sol-Gel Method In Research. In: Aguilar GV (Ed) *Sol-Gel Method*. Rijeka: Intechopen. Epub Ahead Of Print 2018. DOI: 10.5772/Intechopen.82487.
- [9] Blamire MG. *Functional Metal Oxides: New Science And Novel Applications*. 2013. Epub Ahead Of Print 2013. DOI: 10.1002/9783527654864.
- [10] Tolosana-Moranchel Á, Faraldos M, Bahamonde A. Methodologies Of Synthesis Of Titania And Titania-Graphene Photocatalysts. In: *Materials Science In Photocatalysis*. Elsevier, 2021, Pp. 83–94.
- [11] Parvez M, Haque E, Akter M, Et Al. Synthesis Of Bismuth Ferrite Nanoparticles By Modified Pechini Sol-Gel Method. *Int J Sci Eng Investig* 2020; 9: 29–31.
- [12] Patil PS. Versatility Of Chemical Spray Pyrolysis Technique. *Mater Chem Phys* 1999; 59: 185–198.
- [13] Grosso D, Boissière C, Faustini M. Thin Film Deposition Techniques. *Sol-Gel Handb* 2015; 1-3: 277–316.
- [14] MOHAMED O. Synthesis And Characterization Of Zinc Oxide (Zno) Thin Films Deposited By Spray Pyrolysis For Applying: Electronics And Photonics. Mohamed Khiderof Bistrka, 2018. 
- [15] Perednis D, Gauckler LJ. Thin Film Deposition Using Spray Pyrolysis. *J Electroceramics* 2005; 14: 103–111.
- [16] Falcony C, Aguilar-Frutis MA, García-Hipólito M. Spray Pyrolysis Technique; High-K Dielectric Films And Luminescent Materials: A Review. *Micromachines* 2018; 9: 1–33.
- [17] Sakka S. *Handbook Of Sol-Gel Science And Technology: Processing, Characterization*

Chapter II Thin films Preparation and characterization techniques

- And Applications, Volumes I–III Set Edited By Sumio Sakka (Professor Emeritus Of Kyoto University). Kluwer Academic Publishers: Boston, Dordrecht, London. 2005. Lx + 1980 Pp. 1500.00. J Am Chem Soc 2005; 127: 6135.
- [18] Jung DS, Park S Bin, Kang YC. Design Of Particles By Spray Pyrolysis And Recent Progress In Its Application. Korean J Chem Eng 2010; 27: 1621–1645.
- [19] Gurav A, Kodas T, Pluym T, Et Al. Aerosol Processing Of Materials. Aerosol Sci Technol 1993; 19: 411–452.
- [20] Stefani D. Growth And Characterization Of Nanostructured Au Doped Zinc Oxide Thin Films By RF Magnetron Co-Sputtering. Università Degli Studi Di Padova, 2015.
- [21] Saad Rahmane, Mohamed Salah Aida, Abdelouahad Chala, Hachemi Ben Temam DA. Elaboration Of Transparent Undoped Zno And Al-Doped Zno Thin Films By Spray Pyrolysis And Their Properties. Plasma Process Polym 2007; 356–358.
- [22] Vimalkumar TV. Highly Conductive And Transparent Zno Thin Film Using Chemical Spray Pyrolysis Technique: Effect Of Doping And Deposition Parameters. Cochin University Of Science And Technology, 2011.
- [23] Aravind A. Synthesis And Characterization Of 3d-Transition Metals Doped Zno Thin Films And Nanostructures For Possible Spintronic Applications Department Of Physics Cochin University Of Science And Technology Cochin - 682 022 , Kerala , India October 2012. COCHIN UNIVERSITY OF SCIENCE AND TECHNOLOGY, 2012.
- [24] Gokilamani N. NATURAL DYE SENSITIZED NANOCRYSTALLINE Tio 2 THIN FILMS FOR SOLAR CELL APPLICATIONS. Anna University, Chennai-600 025, 2014.
- [25] Yanru GT. Synthesis Of Multi- - - Segmented Tio 2 / Pt Nanorods For Photocatalytic Hydrogen Production. Imperial College London, 2014.
- [26] Abou-Ras D, Kirchartz T. Advanced Characterization Techniques For Thin Film Solar Cells. Germany: Wiley-VCH, 2011.
- [27] Zhang JZ. OPTICAL PROPERTIES AND SPECTROSCOPY OF NANOMATERIALS. California, Santa Cruz, USA: World Scientific Publishing Co. Pte. Ltd, 2015.
- [28] Yilmaz M, Turgut G. Titanium Doping Effect On The Characteristic Properties Of Sol-

Chapter II Thin films Preparation and characterization techniques

Gel Deposited ZnO Thin Films. *Kov Mater* 2015; 53(5): 333–339.

- [29] Grundmann M. *The Physics Of Semiconductors: An Introduction Including Devices And Nanophysics*. Second Edi. 2010. Epub Ahead Of Print 2010. DOI: 10.1007/978-3-642-13884-3.
- [30] Jemaa I Ben, Thimont FCLPY. Structural , Optical And Electrical Investigations On Nb Doped TiO₂ Radio-Frequency Sputtered Thin Films From A Powder Target. *J Mater Sci Mater Electron*. Epub Ahead Of Print 2016. DOI: 10.1007/S10854-016-5471-8.
- [31] Sze SM, Ng KK. *Physics Of Semiconductor Devices: Third Edition*. 2006. Epub Ahead Of Print 2006. DOI: 10.1002/9780470068328.
- [32] Abdelkrim A, Rahmane S, Nabila K, Et Al. Polycrystalline SnO₂ Thin Films Grown At Different Substrate Temperature By Pneumatic Spray. *J Mater Sci Mater Electron* 2017; 28: 4772–4779.
- [33] Saniee NF. *Structural And Optical Properties Of Transparent Conducting Si-Doped ZnO Thin Films Grown By Pulsed Laser Deposition*. University Of Birmingham, [Http://Www.Nanoarchive.Org/7248/](http://www.nanoarchive.org/7248/) (2005).

Chapter III *Effect of precursor
nature and molarities on Titanium and
Zinc oxides thin films properties*

III.1. Introduction

In this chapter we present some of the optical, structural, electrical and morphological properties of titanium and zinc oxides films prepared by spray pyrolysis starting from different concentrations of different precursor solutions in order to enhance their properties to be used in photocatalytic and photovoltaic applications.

III.2. Experimental details

III.2.1. Spray pyrolysis system set-up

Fig.III.1. shows the experimental set-up of our spray pyrolysis system which is built in our laboratory in the university of Biskra, it consists of:

An atomizer: It makes it possible to transform the solution into a jet of very fine droplets, placed on an adjustable holder in order to control the distance nozzle-substrate.

A compressor (*JUN- AIR, 6-S type*): It allows compressing the carrier gas (the air). By suitable way it is connected with the nozzle for generating and guiding droplets with considerable velocity toward the heated substrate.

A substrate holder: a steel holder with a diameter of 20 cm putted on and heated by an electric resistance, the resulting temperature on the surface of the substrate is measured by a chromel-alumel thermocouple fixed on the steel holder.

Temperature controller: The temperature adjustment is realized by using a numerical thermo-regulator (**EC 3-133; EVERY CONTROL**).

Solution flow rate regulator: it is a small reserve of solution source which supplies by gravity the spray pyrolysis with a low solution flow rate which can be controlled by changing the difference of solution level between reserve and atomizer.

Other elements: are materials used to measure deposition time (chronometer), other laboratory instrument such as electronic circuits and transformers.

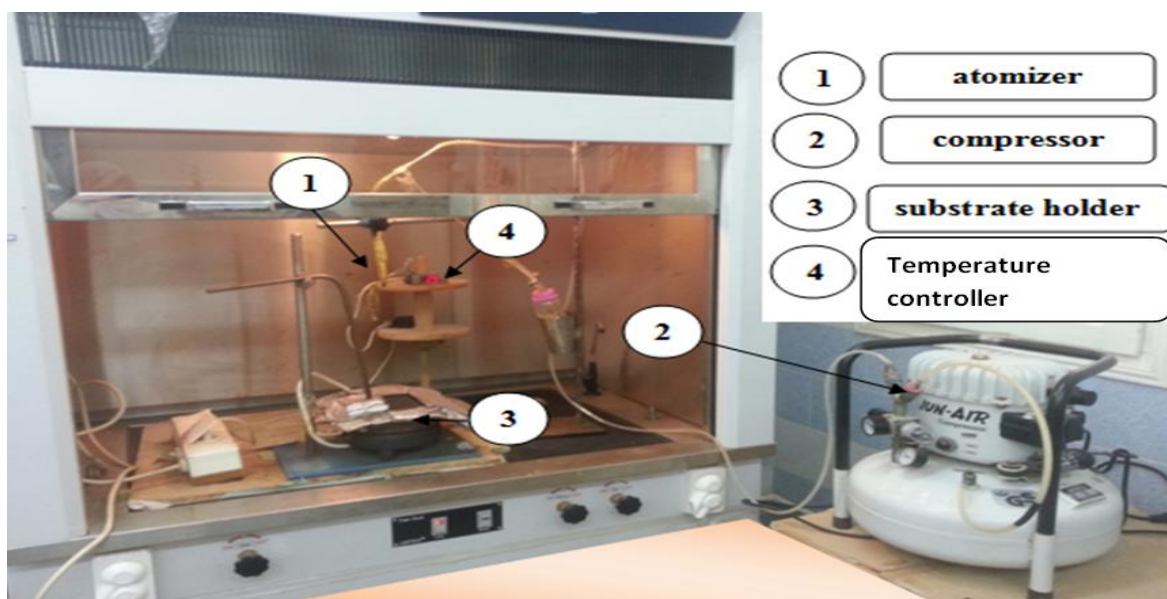


Fig. III. 1. The pneumatic spray pyrolysis setup.

III.2.2. Substrate preparation

III.2.2.a. Choice of the substrate

For laboratory work, we therefore chose to use glass slides (TLC Silicagel 60F254) of format $(2.5 \times 1.5) \text{ cm}^2$ and about 2 mm thick. The choice of glass is due to many reasons such that it allows performing a good optical characterization of films, due to its transparency in UV-Visible wavelength range. It is adopted because the good thermal expansion it exhibits with ZnO and TiO_2 ($\alpha_{\text{glass}}=8.5 \cdot 10^{-6} \text{ K}^{-1}$, $\alpha_{\text{ZnO}}=7.2 \cdot 10^{-6} \text{ K}^{-1}$ and $\alpha_{\text{TiO}_2} = 8.4 \cdot 10^{-6} \text{ K}^{-1}$) so as to minimize thermal stresses at the interface substrate layer. It must be an isolator layer so it will not affect the conductivity measurement, and for economic reasons.

III.2.2. b. Cleaning of the substrate

Before a substrate can be coated, it must be cleaned. The forces that hold films together and to the substrate are all short-range interatomic and intermolecular forces. These forces are extremely powerful, but their short range means that we can think of each atomic layer as being bound to the neighboring layers only, and being little affected by material further removed from it. Thus, the adhesion of a thin film to the substrate depends

Chapter III Effect of precursor nature and molarities on Titanium and Zinc oxides thin films properties

critically on conditions at the substrate surface, substrate cleaning is therefore of paramount importance.

Firstly the substrates are cut using a pen with diamond point then it should be cleaned to remove organic contamination (grease, dust, etc.). Grease will probably require treatment with an alcohol such as ethanol and acetone, after that it is necessary to rinse them intensively with distilled water. Thus, gentle cleaning of both surfaces of the substrate is carried out using a soft lint-free paper (optical paper). Then the cleaned substrate is immersed in a bath of distilled water, then an ethanol bath. The degreasing in each bath lasts five minutes and is followed by rinsing with distilled water. The substrates should never be allowed to dry themselves or stains will certainly occur, which are usually impossible to remove. So we must dry them thoroughly and immediately with a blow drier. Finally Substrates should be handled as little as possible after cleaning and, since they never remain clean for long, placed immediately in the spraying machine and the coating operation started.

To avoid the thermal crash and the deformation or the breaking of glass substrates after deposition of the films we maintain the sample for enough time until the temperature reaches the ambient temperature.

III.2.3. Preparation of the films

III.2.3.A. Preparation of TiO₂ films

III.2.3.A.1. Preparation of Solutions

The following two distinct titanium precursors were used to create TiO₂ thin films: The first precursor solutions were prepared using Titanium Tetra Isopropoxide (TTIP) Ti[OCH(CH₃)₂]₄ and acetylacetonate (acac) (CH₃COCH₂COCH₃) as stabilizer in molar ratios of 0.2, 0.25, 0.3, and 0.35:1.5. Acetylacetonate behaves as a nucleophilic reactant and replaces the alkoxy group, thus giving rise to new molecular precursor. In the hydrolysis reaction of acetylacetonate alkoxides, less electronegative ligands (alkoxy groups) are rather quickly withdrawn while the more electronegative ligands (acetylacetonate groups) persist as a complex ion with the metallic group [1].

Titanium (IV) compounds are sensitive to moisture and water due to rapid hydrolysis, and this causes some operation difficulties in solution preparation. Hydrolysis could be avoided by using ethanol (C₂H₅OH) as a solvent in the preparation of TTIP solution [2], with the

volume of 20 ml. It was shown that the coordination number of titanium increases from four $[\text{Ti}(\text{OPr}^i)_4]$ to five $[\text{Ti}(\text{OPr}^i)_3\text{acac}]$ by the modification with acetylacetonate, then to six $[\text{Ti}(\text{OH})_x(\text{OEt}^i)_{3-x}\text{acac}]$ with oligomeric species formed during the dilution with ethanol. The acetylacetonate modification process for titanium isopropoxide followed by dilution with ethanol is schematically depicted in **Fig.III.2**. The environment of Ti with six fold coordination resembles that of Ti in tetragonal TiO_2 anatase. In addition, through the acetylacetonate modification, titanium isopropoxide is transformed to a stable complex against hydrolysis with no precipitate forms [1].

The solutions were stirred for 3 h and further aged at room temperature under atmospheric pressure, the final product undergoes a pyrolytic reaction to form TiO_2 thin films. The films prepared: using these solutions are denoted by (S1).

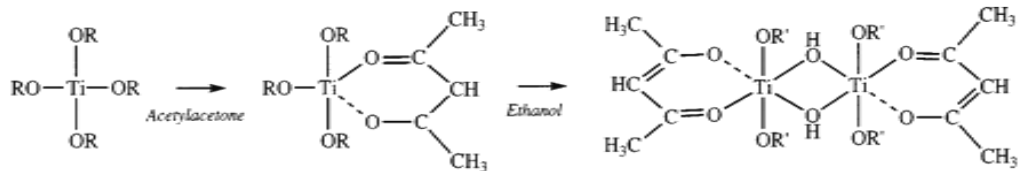
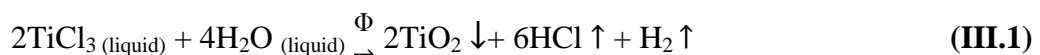


Fig. III. 2. Modification process of titanium Isopropoxide by acetylacetonate (where $R = \text{C}_3\text{H}_7$ and $R' = \text{C}_2\text{H}_5$).

For the second precursor which is denoted by (S2), Titanium (III) chloride (TiCl_3) was dissolved in distilled water to obtain the final solutions with the concentrations: 0.125, 0.15, 0.175 and 0.2 M.

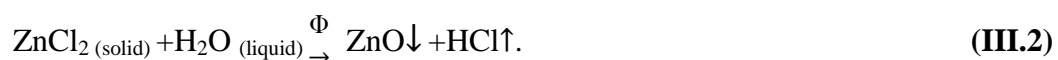
Titanium (III) chloride reacts with water

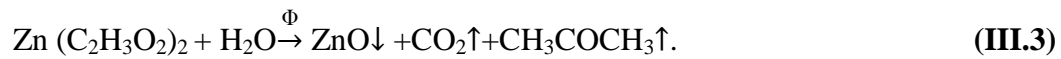


III.2.3.B. Preparation of ZnO films

III.2.3.B.1. Preparation of Solutions

We used zinc chloride (ZnCl_2) and zinc acetate ($\text{Zn}(\text{C}_2\text{H}_3\text{O}_2)_2$) as the source materials for ZnO in our experiments, which were dissolved in distilled water (solvent) at various concentrations such as 0.05, 0.1, 0.2 and 0.3M and 0.1, 0.2, 0.3 and 0.4M respectively. The generated droplets start reacting in the spacing above heated substrate at elevated temperature ($>200^\circ\text{C}$). The chemical reactions occur as follows [3]:





In addition to the un-doped ZnO thin layer, we prepared a series of titanium-doped ZnO thin layers, with titanium chloride (TiCl_3) serving as the titanium source.

III.3. Empirical conditions

For the manufacture of thin films with different properties, and in order to custom applications, we must know the characteristics that can be changed in the experimental study, we will see the relationship between the parameters and their effects on the thin-film structural, optical, and electrical properties.

In order to optimize the deposition parameters, we have divided the deposition process into two sections:

- **Section one:** included deposition of TiO_2 thin films
- **Section two:** included deposition of ZnO thin films

III.3.A. Section one deposition of TiO_2 thin films

In the section one we present some of the optical, structural, electrical and morphological properties of titanium oxide films prepared by spray pyrolysis starting from different concentrations of different precursor solutions in order to enhance their properties to be used in photocatalytic and photovoltaic applications. These parameters and their variations are reported on the following table:

Table.III.1. Experimental conditions

Series	Precursor solutions	Substrate temperature (°C)	Molar concentration M	Deposition time (min)
Series 01	Titanium Tetra-isopropoxide $\text{Ti}[\text{OCH}(\text{CH}_3)_2]_4$ (S1)	550	0.2	3
			0.25	
			0.3	
			0.35	
Series 02	Titanium chloride TiCl_3 (S2)	550	0.125	3
			0.15	
			0.175	
			0.2	



III.3.A.1. Results and discussion

➤ Effect of precursor nature and molarities

III.3.A.1.1. Film formation mechanism and thickness measurement

Deposition of TiO₂ films from titanium chloride and TTIP solutions was carried out under the above-stated conditions. A thermal decomposition occurs to the fine droplets of the solutions after their falling over the hot substrate surface resulting in well-adherent (hardly peeled with scotch tape test), and uniform titanium dioxide thin films with transparent color for (S1) and slightly transparent whitish color for (S2).

The surface thickness of the films was carried out by gravimetric method using a sensible balance type PHYWE *SA2004B* with precision of 10⁻⁴g using the relation [4]:

$$d = m / (g * A) \quad \text{(III.4)}$$

Where A: surface area of the film; m: mass of the film; and g: density of the deposited material.

The thickness values of the films are found to be between 76 and 160 nm for (S1) and between 178 and 784 nm for (S2) as listed in **Table.III.2**. The film thickness increases continuously with increasing molar concentration due to relative increase in amount of the sprayed titanium.

It is clear for the 0.2 M sample in the two precursors used, that the thickness of TiO₂ thin films elaborated with titanium chloride is almost ten times greater than the obtained with TTIP. The difference in the precursor properties alters the films growth mechanism which originates the difference in. The pyrolytic reaction on the surface of the substrate produces the formation of the films. When using TTIP as a starting solution the decomposition of this compound may require intermediate reactions. While when using titanium chloride, the reaction on the surface is spontaneous. Indriana Kartini [5], suggest that increasing the concentration of acetylacetonate more than 1 tends to slow down the crystal phase formation. He suggests that the formation of Ti-complex that makes the Ti precursor bulkier and the groups of Isopropoxide are replaced by acac groups and Ti(IV) acetylacetonate tris-isopropoxide is formed with moderate reactivity [6]. This leads to the fact the excess amount of acac restrains the interaction between Ti-molecules which causes a suspension of the crystal growth. As a result, it delays the growth velocity of TiO₂ films.

Table.III.2. The thickness values of the films.

Molar Concentration (M)	TTIP Thickness (nm)	Molar Concentration (M)	TiCl ₃ Thickness (nm)
0,2	76.43	0,125	178,715
0,25	120.5	0,15	388
0,3	127.8	0,175	525,58
0,35	160.97	0,2	784,323

III.3.A.1.2. Structural properties

XRD patterns of the TiO₂ films deposited at different solution concentration are shown in **Fig.III.3**. For (S2) films we can see the poor crystallinity of the structure in most of the samples, except for 0.175 M sample where appears one peak in the position $2\theta = 37.7^\circ$, which can be related to the (103) direction of Anatase crystallographic phase (JCPDS card No. 00-001-0562) and confirms that the deposited film is a TiO₂ film with a tetragonal structure. This poor crystallinity is very likely due to the non stability of the starting solution regarding the aerial oxidation of Ti⁺³ ions in presence of humidity [7], which can be seen while preparing the starting solution, accompanied by a color-changing of the solution from violet to the transparent color which is probably due to the colorless titanyl ions (TiO²⁺). For 0.2 M sample, the peak (103) disappears probably attributed to the growth velocity due to the quantity of solution falling on the substrate.

So, for better control of the crystallinity of the films; chemical equilibrium and reactions in the starting solution study is desirable which can give clues to the size of the critical nucleus, above which particles prefer to grow rather than shrink.

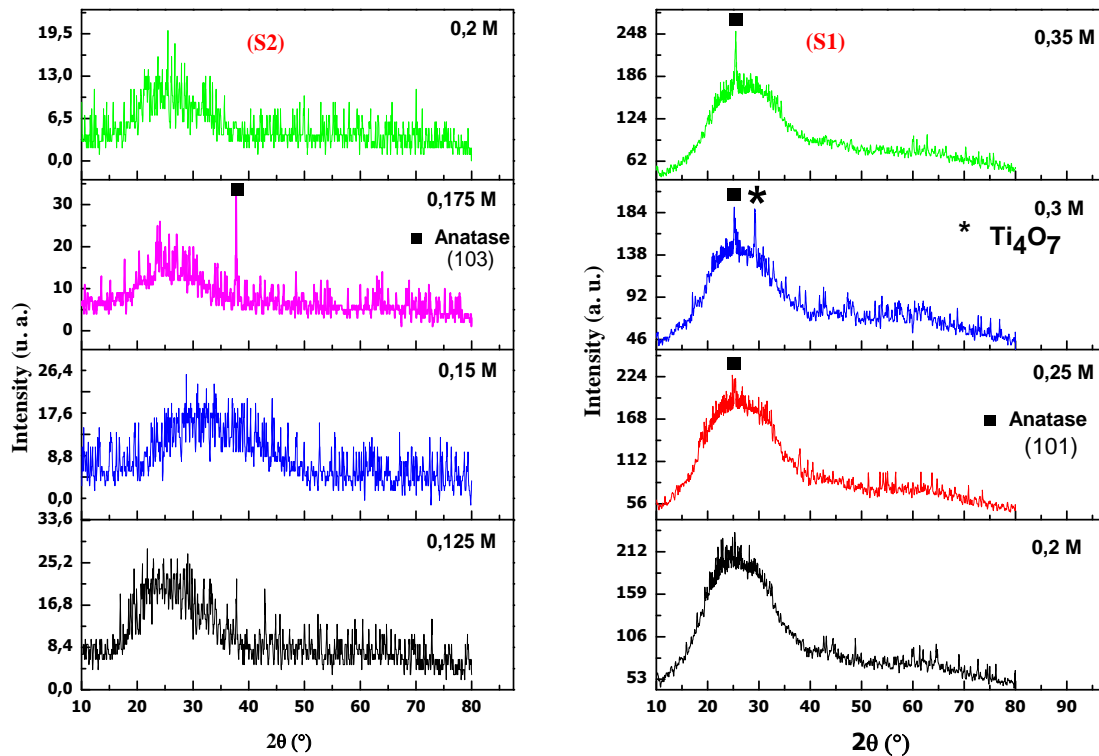


Fig. III. 3. XRD patterns of TiO_2 thin film with different concentrations for (S1) TTIP, (S2) TiCl_3 precursors.

The XRD patterns for (S1) samples shows that the crystallinity is better than that in (S2), it is observed that the films exhibit characteristic peak of Anatase crystal plane (101) (JCPDS card No. 00-001-0562). For 0.3 M sample, the appearance of a new peak in the position $2\theta = 29.2^\circ$ which may be revealed to the $(1\bar{2}2)$ direction of Magnéli-phase Ti_4O_7 (JCPDS card No.018-1402). We note that with the increasing of precursor concentrations the intensity of the plane (101) increases while the plane $(1\bar{2}2)$ disappears meaning that the crystallites size increases and the crystallinity becomes better.

As can be seen there is a difference between the films deposited using TTIP and TiCl_3 sources and of course this is due to the nature of each source and the used solvent in starting solution, plus the chelating agent used in TTIP solution, also to their concentration, all this parameters can affect the crystallographic nature of the films.

III.3.A.1.2.1. Crystallite size (D)

The crystallite size D of the TiO_2 samples was estimated using the Scherer formula (equation (II.2)). It can be seen from the table below (table III.3) that for (S1) samples

there is an increasing of crystallites size by increasing the molar concentration this is may be happening due to the coalescence of nucleation sites, the nucleation sites combine to form the bigger ones. Those lasts grow by successive clustering of nucleation sites during deposition.

III.3.A.1.2.2. Dislocations Density

The number of dislocations in a material is defined as the dislocation density δ the total dislocation length per unit volume or the number of dislocations intersecting a unit area which are given by [8]:

$$\delta = \frac{1}{D^2} \quad (\text{III.5})$$

Crystallographic lattices are never perfect, but contain lattice faults that may be characterized by their spatial extension as zero-dimensional point defects, one-dimensional line defects or two-dimensional area defects. A dislocation causes the neighboring atoms to shift from their ideal lattice sites and thereby introduces a strain field in the surrounding volume see **Fig.III.4**. The strain field may extend over a distance of some micrometers from the core of the dislocation and the defect line thus affects a large volume [9]

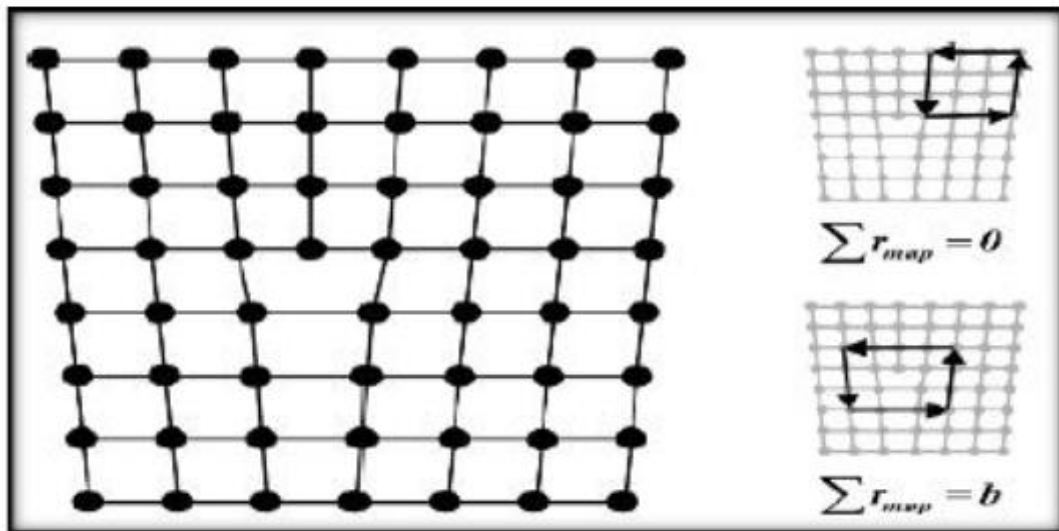


Fig. III. 4. An Edge Dislocation in a Simple Cubic Lattice [9].

III.3.A.1.2.3. Microstrain (ϵ)

The micro strains are caused during the growth of thin films, and will be raised from stretching or compression in the lattice to make a deviation. So the strain broadening

is caused by varying displacements of the atoms with respect to their reference lattice position [9]. The strain values (ϵ) of the TiO₂ films are calculated from the formula [3]:

$$\epsilon = \frac{\beta \cos \theta}{4} \quad (\text{III.6})$$

It can be observed that the strain is reduced with the increase of the precursor concentration which can be explained by the improvement of the crystallinity of the (S1) films. For (S2) series due to the poor crystalline nature of the films we couldn't calculate the crystallite size, strain and dislocation density for most of the samples except for the 0.175 M. In general for all the samples low strain and small crystalline size have been obtained.

Table.III.3. Structural properties of TiO₂ versus solution concentration for (S1) and (S2) series.

Samples solution concentration (M)	(S1) series			Samples solution concentration (M)	(S2) series		
	D (nm) (103)	strain ϵ	dislocation density δ (lines/nm ²)		D (nm) (101)	strain ϵ	dislocation density δ (lines/nm ²)
0,2	/	/	/	0,125	/	/	/
0,25	22,8	0,0015	0,0019	0,15	/	/	/
0,3	23,0	0,0015	0,0018	0,175	29,1	0,0011	0,0011
0,35	34,5	0,0010	0,00083	0,2	/	/	/

III.3.A.1.3. Morphological study

The surface morphology of the spray-deposited titanium oxide thin films were characterized and analyzed using Zeiss-SMT LEO 1540 XB scanning electron microscopy at Hungarian Academy of Sciences, Centre for Energy Research. as shown in **Fig.III.5**. The top view SEM photographs were taken using magnifications of about 50,000 for the TTIP and 1000, 5000 for the TiCl₃ starting solutions, the cross-sectioned photographs magnifications were 100,000 and 50,000 respectively.

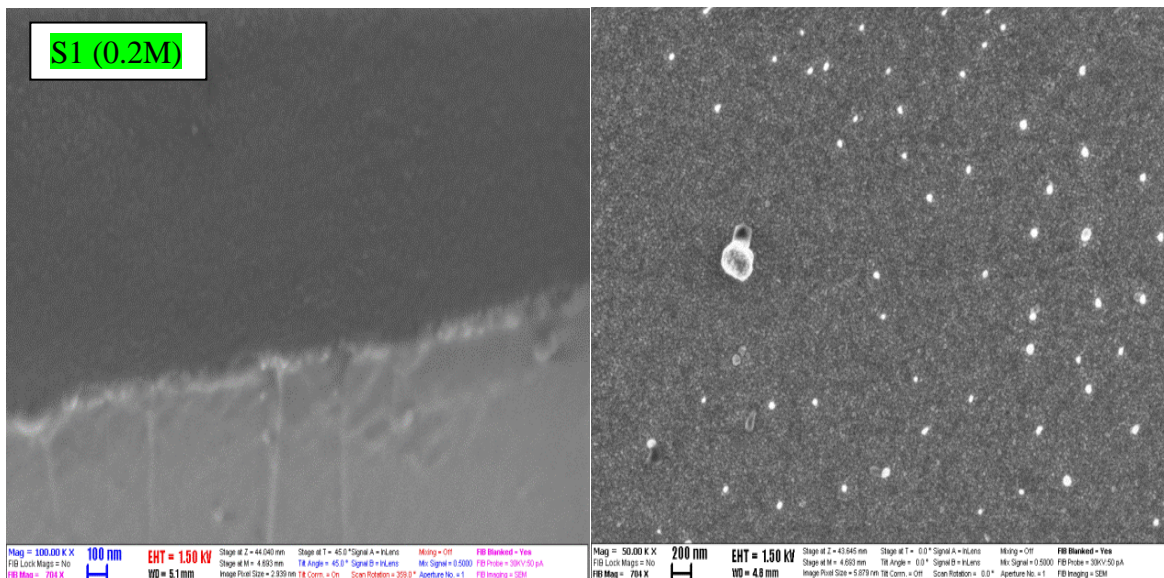
These images show that the surface morphology depends clearly on the nature of the used precursor. The films elaborated with TTIP are characterized by uniform, pinhole, and pore-free, dense and crack-free TiO₂ films as given in **Fig.III.5**. The cross-sectioned micrographs indicate that the TiO₂ films are well-adhered to the glass substrate and there is no delaminating of the film. We can see that nano-scale grains distributed uniformly over the substrate and their size increases slightly as the precursor solution concentration

increases which is due to the increase in the deposited rate confirmed by the values of the thicknesses of the deposited films. Similar feature were found by M. Alzamani and collaborators [10].

For the films formed with the TiCl_3 solution we can see a different microstructure developed over the glass substrate, a rough surface consisting of nano or micro-pores in an irregular shape with splashes distributed randomly like holo particles, those splashes possibly derives from a high growth rate. Moreover, no grain or grain boundaries appear in the films, this confirms the amorphous structure of the films.

It seems like particles of TiO_2 were assembled to form a fibrous structure, it is remarkable that the microstructure becomes porous and the number of splashed grains are found to decrease while their size is increasing with the increase in precursor concentrations. The same aspect was also reported for TiO_2 thin films elaborated by the spray pyrolysis technique[10,11].

The cross-sectioned images of the TiO_2 film shown in **Fig.III.5**. indicate a stack of nano layers. The uneven growth of the layered structure was evident from the observed images.



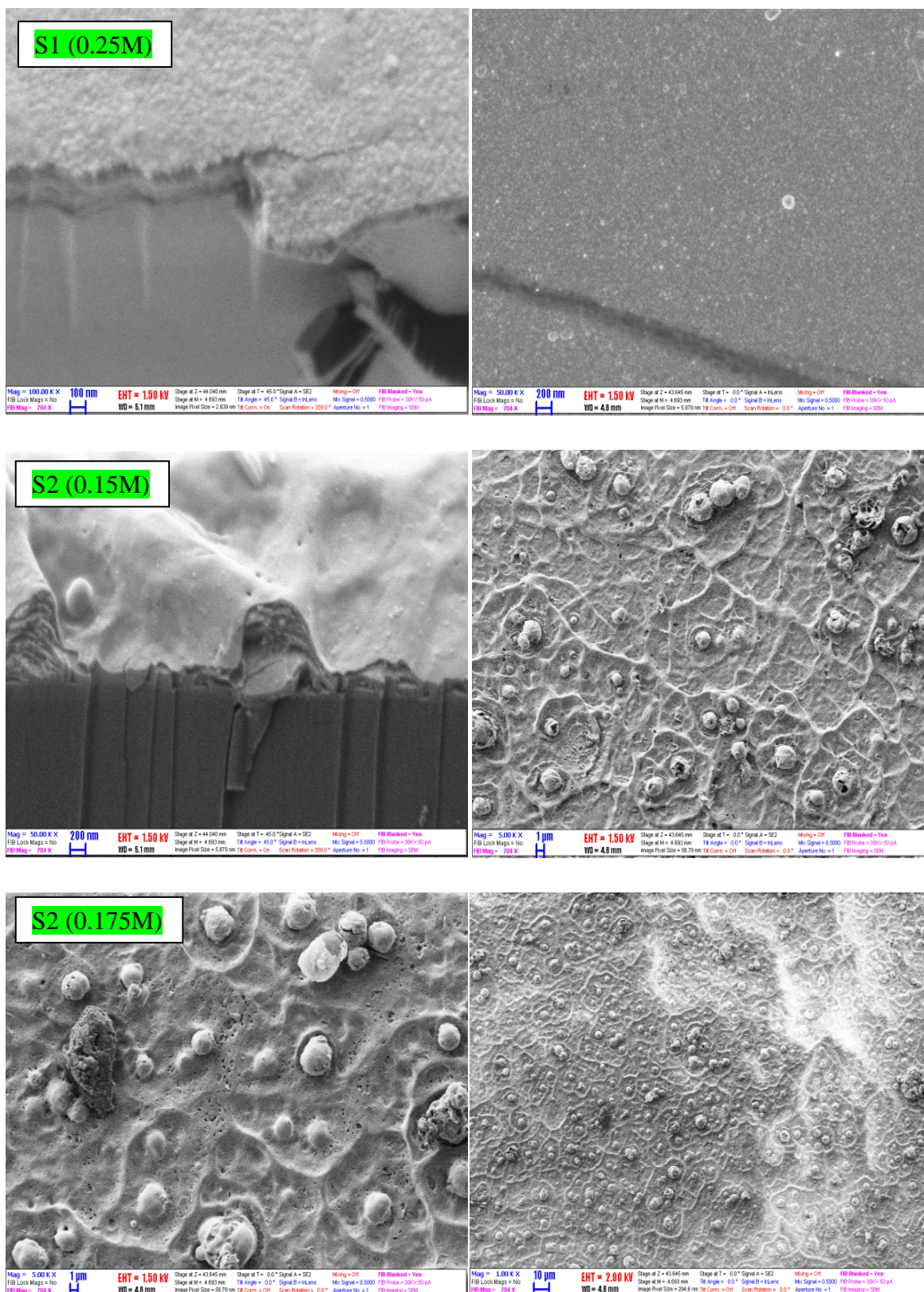


Fig. III. 5. The top view and cross-section SEM photographs for the TTIP (S1) and $TiCl_3$ (S2) precursors.

III.3.A.1.4.Optical properties

Fig.III.6. Shows the optical transmittance curves for (S2) and (S1) as a function of the wavelength for the TiO₂ films deposited with different concentrations. In the visible region, it is seen that transmittance for (S2) films decreases with the increase of solution concentration. The reduction of transmittance at higher molar concentration is due to the increase in the thickness of the films. The films deposited at 0.125 M exhibit a high optical transmittance (>80 %). Also the 0.125M film does not cross the 0 point of the y-axis in the low wavelength side at 300 nm this is probably resulting from uniform coverage on the glass substrate or due to the formation of pinholes. Moreover, we can see the absence of interference fringes, which is due to the multiple reflections at the two film edges, i.e. at the film/air, and the film/substrate interfaces. Their absence is owing to the roughness of the interface air/film, hence at this interface; incident light is diffused rather than reflected in one direction. On the other side, for (S1) we can see the presence of interference fringes that support a smooth morphology (as it is clear from the SEM photographs), and the optical transmittance achieves 90 % for 0.3 M sample. The difference in transmittance originates from the difference in the film's thickness. Also, it can be seen in **Fig.III.6** a region of 380–400 nm which is the region of the absorption edge in the layers due to the fundamental absorption (transition between the valence, and the conduction band). The absorption edge for (S1) films shifts towards the higher energy; this indicates that the optical gap is larger than in (S2) films.

The estimation of the optical band gaps (E_g) of the films is based on Tauc formula for direct band gap semiconductors and the Urbach energy E_U , which characterizes the disorder in the film, calculation details are given in [12,13].

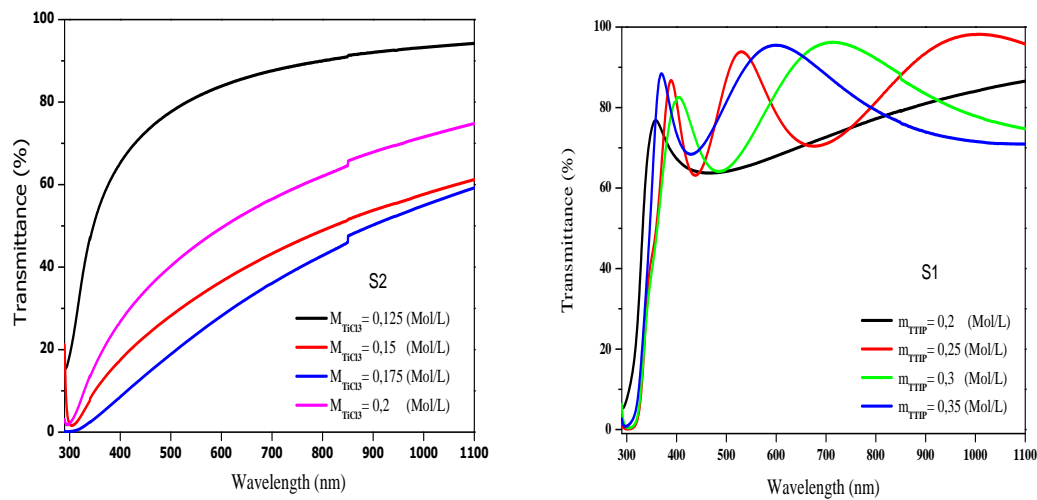


Fig. III. 6. Optical transmittance of TiO_2 (S1) for TTIP, (S2) for $TiCl_3$ precursors versus solution concentration.

From **Fig.III.7**, we have found that the calculated optical band gap (E_g) as expected; is larger in (S1) films and it had a decreased form for both (S1) and (S2) with the increase of solution concentration, this decrease is confirmed by the increase in band tail width (Urbach energy) which is may result from the structural defects appearing in the film due to their preparation conditions; this could give rise to the allowed states near the conduction band in the forbidden region [15]. These allowed states may merge with the conduction band with the increasing of solution concentration, resulting in the reduction of the band gap.

The value of the band tail width for the films elaborated with titanium chloride is higher than the value for the films prepared with TTIP; this is due to the presence of the amorphous phase in these films, which is in god agreement with XRD analysis.

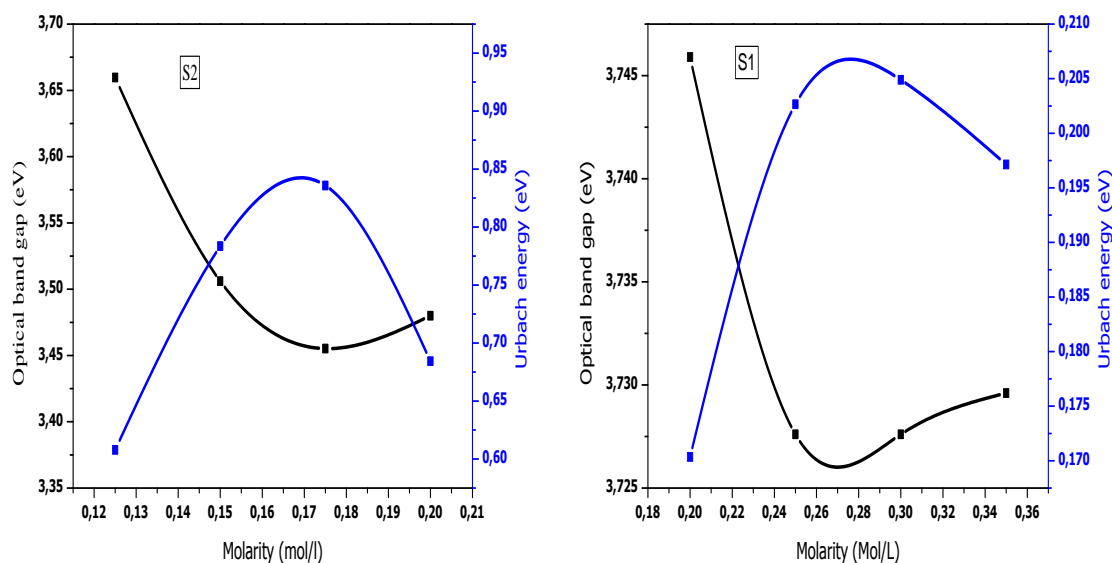


Fig. III. 7. Variation of band gap and band tail width versus solution concentration for (S1) and (S2) films.

III.3.A.1.5. Electrical proprieties

The stoichiometric TiO_2 is an insulating material with an extremely high resistivity above 10^8 ($\Omega\cdot\text{cm}$), but the sub oxidized TiO_2 with an excess of titanium is an n type semiconductor showing unique properties[16].

As we can see from **Fig.III.8**. The variation of the resistivity of the TiO_2 films is unversed for the tow precursors; however, the values are near to each other. For (S1), the resistivity of the TiO_2 thin films decreases from $6.5 \cdot 10^3$ to $9.4 \cdot 10^2$ ($\Omega\cdot\text{cm}$) with the increase in precursor concentration. The variation of resistivity is attributed to carrier concentration and/or mobility changing [15]. So, in one hand, with the increase of the concentration the thickness of the film increases leading to an increase in carrier concentration, and in the other hand an increase of crystallite size leads to a decrease in the trapping states at grain boundaries resulting to the increase of the carrier's mobility as it is shown clearly by the XRD patterns and SEM analyses. For (S2) we can see that the resistivity values are increasing from $3.2 \cdot 10^3$ to $4.06 \cdot 10^4$ ($\Omega\cdot\text{cm}$) with the rise of the precursor concentration which may be due to poor crystalline properties. The grain boundaries play the role of trap centers due to incomplete atomic bonds within and hence depleting the free charge carriers. The extra free carriers become immobilized as trapping states increase[17].

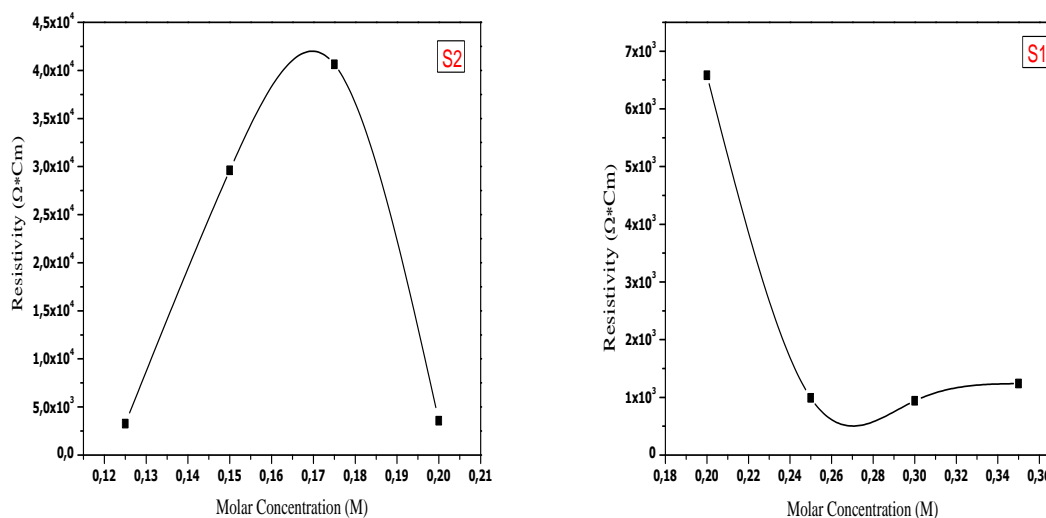


Fig. III. 8. Dependence of electrical resistivity in TiO_2 films on precursor concentration for (S1) TTIP and (S2) $TiCl_3$ precursors.

III.3.A.1.6. Conclusion

In this section, we had compared the properties of TiO_2 thin films deposited from two precursor solutions with different concentrations. The films obtained from $TiCl_3$ were thicker than the films obtained from TTIP which is related to the growth velocity affected by the properties of each precursor.

XRD patterns show the poor crystallinity of the films of both of them with the appearance of characteristic peaks of anatase. The investigation of the SEM micrographs shows that the films obtained from TTIP were well adherent, uniform, pore-free, dense and crack-free with nano-scale grains, whereas films obtained from $TiCl_3$ were rough and consist nano or micro-pores in an irregular shape with splashes distributed randomly, also no grain or grain boundaries appear in those films which confirms their amorphous structure.

Optical properties were strongly affected by the nature of the starting solution too; we have seen the presence of interference fringes in (S1) and their absence in (S2) thin films, also the transmittance was decreasing with the increase of solution concentration. The reduction of transmittance at higher molar concentration is due to the increase in the thickness of the films. Moreover, we have found that the calculated optical band gap (E_g) is larger in (S1) films and it had a decreased from for both (S1) and (S2) with the increase of solution

Chapter III Effect of precursor nature and molarities on Titanium and Zinc oxides thin films properties

concentration, this decrease is confirmed by the increase in band tail width (Urbach energy). The variation of the resistivity of the TiO₂ films with the increase in precursor concentration is inverted for the low precursors; however, the values are near to each other. The resistivity variation is attributed to carrier concentration and/or mobility changing. The thin film prepared by TiCl₃ at 0.175M could have good photocatalytic properties since it has a porous morphology besides anatase crystallographic phase which is well known as the most suitable structure for photocatalytic application.

III.3.B. Section two deposition of ZnO thin films

In section 2, we discuss some of the optical, structural, electrical, and morphological characteristics of zinc oxide films elaborated by spray pyrolysis, starting from various concentrations of various precursor solutions, to improve their capabilities for use in photocatalytic and photovoltaic applications. The following table reports these parameters and their variations:

Table.III.4. Experimental conditions

Series	Precursor solutions	Substrate temperature (°C)	Molar concentration M	Deposition time (min)
Series 01	ZnCl ₂	370	0.05	3
			0.1	
			0.2	
			0.3	
Series 02	Zn(C ₂ H ₃ O ₂) ₂ 2H ₂ O	370	0.1	3
			0.2	
			0.3	
			0.4	

III.3.B.1. Results and discussion

➤ Effect of precursor nature and molarities

III.3.B.1.1. Film formation mechanism and thickness measurement

The dissolved substances or chemicals that are dissolved in the solvent (starting solution) in accordance with the specified stoichiometric ratio determine the composition of the final particle.

Table.III.5. the characteristics of the zinc salts used in our experimental study.

Zinc chloride:	Zinc acetate:
Appearance: solid of variable shape, hygroscopic and white	Appearance: Crystalline solid, white with acetic acid odor
The molecular formula: $ZnCl_2$	The molecular formula: $Zn(C_2H_3O_2)_2 \cdot 2H_2O$
Physical state: Solid	Physical State: Solid
Molecular weight: 136.301 g/mol	Molecular weight: 219.38 g/mol
Density: 2.9g/ml	Density: 1.735 g/ml at 20°C
Melting point: 290°C	Melting point: 237°C

The estimated thickness values of the samples are between 380 and 500 nm for the $ZnCl_2$ precursor solution, and around 300 nm for the precursor solution $Zn(C_2H_3O_2)_2 \cdot 2H_2O$

III.3.B.1.2. Structural properties

The X-ray diffraction pattern of ZnO films of different precursors and concentrations deposited at an optimized substrate temperature of 375 °C is shown in **Fig.III.9**. The XRD measurement exposed that most of the as-grown film layers were polycrystalline in nature. The four leading diffraction peaks in the XRD patterns of ZnO thin films for both precursors clearly show peaks corresponding to (100), (002), (101), and (103) planes of ZnO Wurtzite hexagonal structure with the preferred orientation is along the (002) plane. The designation of diffraction lines is caused by comparing with JCPDS files of ZnO (JCPDS 36-1451). For films deposited from $ZnCl_2$ source (A). The intensity of the diffraction peaks becomes sharper as the precursor concentration decreases; this effect may be due to the high growth rate which affects the nucleation, as a result new sites are hosting the formation of thin films. This faster nucleation has consequences on the thin films structural properties.

Porosity of the samples also could cause a deterioration of the crystallinity of the layers as the precursor concentration increases.

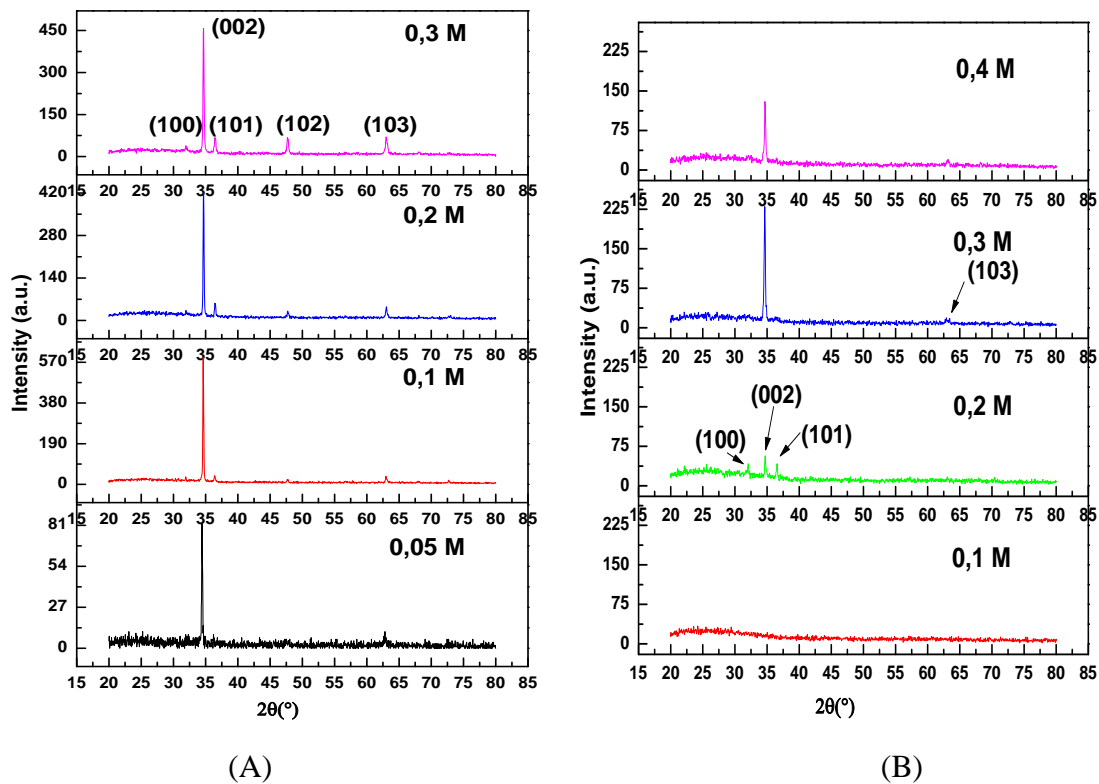


Fig. III. 9. X-ray diffraction pattern of spray deposited ZnO thin films at different molarities from (A) Zinc chloride $ZnCl_2$ and (B) Zinc acetate $Zn(C_2H_3O_2)_2 \cdot 2H_2O$.

Fig.III.9.B exhibits the XRD pattern of the ZnO thin films deposited from Zinc acetate with various molarities. It observed that the deposited sample with a molarity of 0.1M is amorphous, after this molarity all the films were crystallized in the wurtzite hexagonal phase and there are four orientations identified as (100), (002), (101), (103) planes respectively, the (002) direction perpendicular to the substrate was the preferential orientation along the c-axis By increasing the molar concentration of precursors from 0.2M to 0.3M, the intensity of preferential orientation (002) was increased due to the increasing of the amounts of the zinc species in solution. This amount of material in the film, being the number of intensity counts directly proportional to the film volume. Specifically, the diffracted intensity is proportional to the effective volume of the crystalline material in the sample. Thus, it is expected that increasing the film thickness produces more intensity counts. A slight decrease in the intensity of the peak was observed with increasing molar concentration to 0.4M could be due to faster growth kinetic creation more nucleation centers.

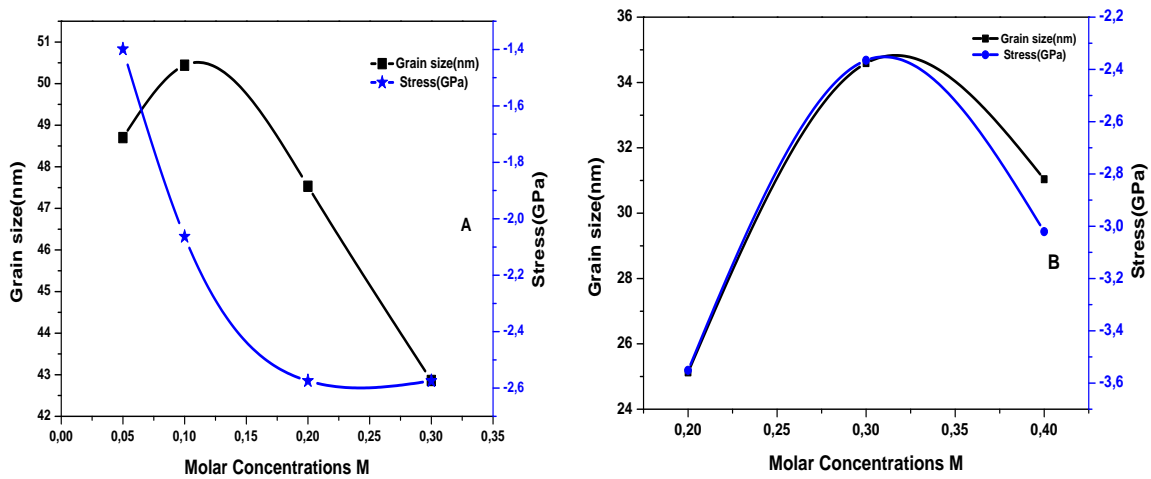


Fig. III. 10. Variation of the calculated values of crystallites size and stress in ZnO films versus solution concentration, A from ZnCl₂, B from Zn(C₂H₃O₂)₂ · 2H₂O.

III.3.B.1.2.1.lattice parameters, Crystallite size (D) and stress determination

The interplanar distance 'd' values of the films are determined by Bragg's law equation (II.1), The lattice constant values of undoped and Ti doped ZnO thin films are calculated by the following relation[18]:

$$\frac{1}{d^2} = \frac{4}{3} \left(\frac{h^2 + k^2 + hk}{a^2} \right) + \left(\frac{l^2}{c^2} \right) \quad (\text{III.7})$$

The results are tabulated in **Table.III.6**. It is found that the lattice constant values are slightly lower than the standard values of $a_0 = 3.2498 \text{ \AA}$ and $c_0 = 5.2066 \text{ \AA}$ (JCPDS card no: 36-1451).

Table.III.6: Variation of interplanar distance 'd' and lattice parameters as a function of molar concentration.

ZnCl ₂ Molar concentration	d (Å°)	A (Å°)	C (Å°)	Zn(C ₂ H ₃ O ₂) ₂ · 2H ₂ O Molar concentration	d (Å°)	A (Å°)	C (Å°)
0.05	2,602	3,187	5,205	0.1	2,583	3,163	5,166
0.1	2,590	3,172	5,181	0.2	2,589	3,171	5,179
0.2	2,586	3,1683	5,173	0.3	2,586	3,167	5,172
0.3	2,587	3,1688	5,174	0.4	2,583	3,163	5,166

The film strain of the c-axis (ε_{zz}) can be determined by the formula [19]:

$$\varepsilon_{zz} = (c - c_0)/c_0 \times 100\% \quad (\text{III.8})$$

Where ' c_0 ' is the lattice constant in unstrained ZnO powder.

For hexagonal crystals, the stress (σ_{film}) in the plane of the film can be calculated using the biaxial strain model[19]:

$$\sigma_{film} = \frac{2C_{13}^2 - C_{33}^{film} (C_{11} + C_{12})}{2C_{13}} \varepsilon_{ZZ} \quad (\text{III.9})$$

$$C_{33}^{film} = \frac{0.99C_{33}^{crystal}}{(1 - \varepsilon_{ZZ})} \quad (\text{III.10})$$

where $C_{11} = 209.7\text{GPa}$, $C_{12} = 121.1\text{GPa}$, $C_{13} = 105.1\text{GPa}$, and $C_{33} = 210.9\text{GPa}$ are the elastic stiffness constants of bulk ZnO. The grain size values of the films are calculated by the Scherer formula (equation (II.2))

Fig.III.10.A. Shows the variation of the stress and crystallite size of the ZnO thin films from ZnCl_2 and $\text{Zn}(\text{C}_2\text{H}_3\text{O}_2)_2 \cdot 2\text{H}_2\text{O}$ source, it was found that crystallite size are in the range of 42-50 nm and 35-39 nm respectively, it could be observed that crystallites size of ZnO films from the first source (ZnCl_2) are greater than the second one this is resulting from the values of stress in the films deposited from both sources.

The stress in the films has a negative sign indicating that the films are in a state of compressive stress. The measured film stress is mainly caused by the growth process itself. The lattice constant ' c ' of ZnO films is smaller than the bulk ZnO. It is suggested that the compressive stress is generated during deposition due to the high amount of the materials arriving to the substrate with low mobility because of the temperature freezing of structural defects at the used temperature [20].

Small growing islands weakly bonded to the surface are initially mobile and can accommodate the continuously increasing lattice parameter by moving or changing their structure. At some island size, which depends on the strength of the bonding to the substrate, the number of bonds that need breaking will be too large for it to be energetically favorable for the islands to move or change shape. The smaller than bulk lattice parameter of the islands will be frozen in at this point and no longer increase with island size. Island growth will continue epitaxially on with the smaller than bulk lattice parameter resulting in a compressive film stress [21].

The magnitude of the steady state compressive stress varies with deposition rate, where high rates lead to a smaller stress magnitude[22] .

As mentioned previously lower steady state compressive stresses are also seen for lower homologous temperatures. The deposition rate and temperature dependence indicate that kinetics play a large role in the generation of the compressive steady state stress[21]. The magnitude of the surface stress would be a function of the deposition conditions (e.g. the deposition rate and temperature), and the adatom surface self diffusivity. In the pre-coalescence regime of Volmer-Weber, a compressive surface stress could lead to a net compressive ‘film’ stress through Spaepen’s argument [23].

The crystallites size of all films has a decreased aspect which is resulting from the fast growth rate of the films as the concentration increases. Generally, the smaller crystallites size the higher photocatalytic activity. The most important Remarque in this section is that the films formed for molar concentration equal to 0.05 mol/l using Zinc chloride precursors are the less strained and have the highest crystallites size.

III.3.B.1.3.Optical properties and Electrical properties

The transmission spectra of the ZnO layers, covering the range of wavelengths between 300 and 900 nm, are grouped on **Fig.III.11**. It is apparent that both spectra have the same overall look and are made up of two regions: a zone of high transparency between 400 and 800 nm, where the transmission value ranges from 45 to 85% for ZnO films elaborated from ZnCl₂ and from 80 to 95% for ZnO films elaborated from Zn (C₂H₃O₂)₂ .2H₂O. These values, reported by several authors [24–26], give the thin layers of ZnO the character of transparency in the visible.

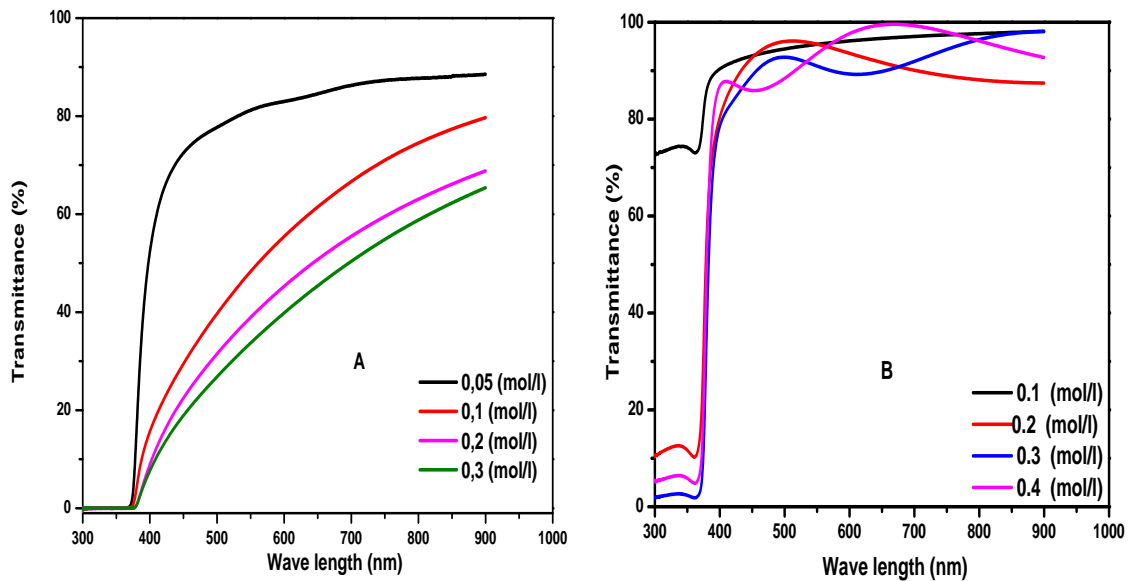


Fig. III. 11. Transmittance Spectra of the films prepared from zinc chloride (ZnCl_2) 'A' and 'B' from $\text{Zn}(\text{C}_2\text{H}_3\text{O}_2)_2 \cdot 2\text{H}_2\text{O}$ as function of the wavelength.

The difference in transmittance between the two sources may be resulting from the morphological properties of the films, we can estimate that the films elaborated from $\text{Zn}(\text{C}_2\text{H}_3\text{O}_2)_2 \cdot 2\text{H}_2\text{O}$ are porous and have smoother surface morphology on the other hand we could conclude that films elaborated from ZnCl_2 are dense and rough. The second region corresponds to the fundamental absorption ($\lambda < 400 \text{ nm}$) in ZnO films, this absorption is due to the interband electrical transition. The variation of the transmission in this region is exploited for the determination of the gap. In general, for the ZnCl_2 starting solution, a general reduction in transmission is observed as a function of the molarities of the solution in the visible range, which is interpreted by the increase in thickness with the increase in molarities.

The optical spectra's of films from $\text{Zn}(\text{C}_2\text{H}_3\text{O}_2)_2 \cdot 2\text{H}_2\text{O}$ source revealed that transmittance increases with increasing molarities due to decreasing surface roughness and crystalline size. The film with 0.1M shows the lowest transmittance in visible light transmittance due to high surface roughness which scattered more light.

Also, we can see that there are no interference fringes for ZnO films elaborated from ZnCl_2 , which results from multiple reflections at the two film edges. Due to the roughness of the air/film interface, incident light at this interface is diffused rather than reflected in

one direction. On the other hand, we can observe interference fringes in films elaborated from $\text{Zn}(\text{C}_2\text{H}_3\text{O}_2)_2 \cdot 2\text{H}_2\text{O}$, which support a smooth surface morphology.

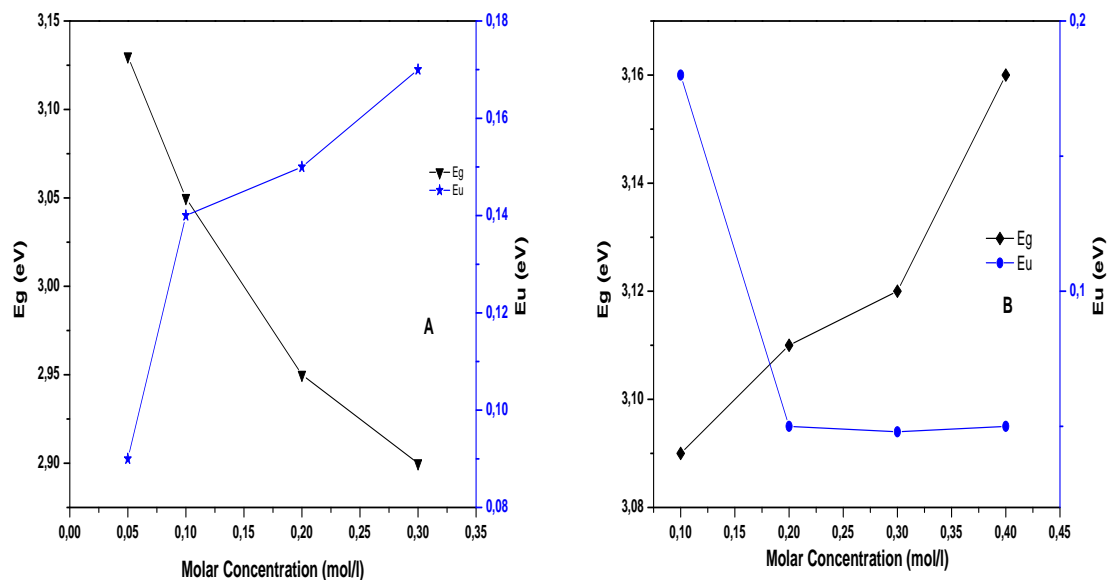


Fig. III. 12. The variation of ZnO's optical gap and Urbach energy as a function of molarities 'A' ZnCl₂ and 'B' from Zn (C₂H₃O₂)₂ ·2H₂O.

Using the prior relations (mentioned in chapter II), we determined the gap energy and disorder (Urbach energy) values. The variations in the gap energy and disorder for various molarities and solutions are depicted in **Fig.III.12**. With an increase in $\text{Zn}(\text{C}_2\text{H}_3\text{O}_2)_2 \cdot 2\text{H}_2\text{O}$ solution concentration, it is seen that the gap energy increases in the range of 3,09 to 3,16 eV which are similar to the values found by Taskin M and Nikam S V et al [27, 28]. This phenomenon is related to the increase in the number of major porters (free electrons), which characterize the type n of ZnO-based semiconductor, and can be interpreted as an increase in film thickness as explained by the "Burstein-Moss" effect [29]. On the other hand, it is noted that the disorder decreases at a range of 0,18 to 0,05 eV with an increase in solution molarities.

The **Fig.III.12.A** shows the variation of the optical gap and the disorder for ZnO films prepared at various molarities using zinc chloride; it is seen that the gap energy decreases in the range of 3,13 to 2,9eV which are similar to the values found by M.N. Amroun et al [24]. This may be due to the oxygen vacancy created during the growth with the increase

in Zn concentration or defect states [30]. We can infer that the reduction in visible light transmission is caused by the large concentration of oxygen vacancies in the ZnO samples. In addition to its function as a trap center, oxygen also acts as a source of impurities near the valence band, which causes the band gap to narrow.

The measured resistivity of ZnO films prepared from the two sources using four point was found in the same order which is $10^1 \Omega \cdot \text{cm}$ and are in good agreement with that reported by many authors [31–34]. The conductivity of ZnO depends significantly on the stoichiometry, adjusted by the oxygen or zinc content during growth or annealing [35].

III.3.B.1.4. Conclusion

ZnO thin films were successfully deposited by spray pyrolysis method. The effects of molarities and starting solution sources were studied upon structural, optical and electrical properties. XRD analysis for both sources confirmed that the prepared ZnO thin films have a good quality Wurtzite hexagonal structure with a preferred orientation (002) direction. All the structural parameters were affected by changing molarity. The crystallinity of the films improved by increasing molar concentrations for Zinc acetate source while at high concentrations of Zinc chloride we found a deterioration of crystallinity as the molar concentration increases. Highest transmittance is exhibited by the ZnO film with molarity 0.4M for Zinc acetate source and with 0.05M for Zinc chloride. The optical energy gap increased from 3.09 to 3.16 eV for Zinc acetate source and decreased from 3.13 to 2.9 eV for Zinc chloride, proportionally with the increase of molarity. Resistivity is observed for ZnO films prepared from both sources at the average $10^1 \Omega \cdot \text{cm}$. Therefore, we concluded that the synthesized zinc oxide thin films with good crystallite size, transmittance, band gap energy and conductivity requires adequate molarity such as 0.05 M for Zinc chloride starting solution source.

III.5. References

- [1] Moon J, Li T, Randall CA, et al. Low temperature synthesis of lead titanate by a hydrothermal method. *J Mater Res* 1997; 12: 189–197.
- [2] Wang WN, Lenggono IW, Terashi Y, et al. One-step synthesis of titanium oxide

Chapter III Effect of precursor nature and molarities on Titanium and Zinc oxides thin films properties


- nanoparticles by spray pyrolysis of organic precursors. *Mater Sci Eng B Solid-State Mater Adv Technol* 2005; 123: 194–202.
- [3] Komaraiah D, Radha E, Vijayakumar Y, et al. Optical, Structural and Morphological Properties of Photocatalytic ZnO Thin Films Deposited by Spray Pyrolysis Technique. *Mod Res Catal* 2016; 05: 130–146.
- [4] Abdelkrim A, Rahmane S, Nabila K, et al. Polycrystalline SnO₂ thin films grown at different substrate temperature by pneumatic spray. *J Mater Sci Mater Electron* 2017; 28: 4772–4779.
- [5] Kartini I, Lu GQ. STUDY OF THE FORMATION OF MESOPOROUS TiO₂ USING ISOPROPOXIDE PRECURSORS UNDER LESS WATER CONDITIONS. *Indones J Chem* 2010; 5: 15–22.
- [6] Wang CC, Ying JY. Sol-gel synthesis and hydrothermal processing of anatase and rutile titania nanocrystals. *Chem Mater* 1999; 11: 3113–3120.
- [7] Ashton JF, Hons BS. *Some Aspects of the Solution Chemistry of Titanium (III)*. Tasmania University, Australia, 1977. Epub ahead of print 1977. DOI: <https://doi.org/10.25959/23235602.v1>.
- [8] Abdelkrim A, Rahmane S, Abdelouahab O, et al. Effect of solution concentration on the structural, optical and electrical properties of SnO₂ thin films prepared by spray pyrolysis. *Optik (Stuttg)* 2016; 127: 2653–2658.
- [9] Yaseen NT. *Design and Fabrication of Antireflection ZnO Thin Film by Using Different Techniques*. AL-Nahrain University, 2017.
- [10] Alzamani M, Shokuhfar A, Eghdam E, et al. Progress in Natural Science : Materials International Influence of catalyst on structural and morphological properties of TiO₂ nanostructured films prepared by sol – gel on glass. *Prog Nat Sci Mater Int* 2013; 23: 77–84.
- [11] Gapale DL, Arote SA, Palve BM, et al. Influence of precursor solution concentration on the structural, optical and humidity sensing properties of spray-deposited TiO₂ thin films. *J Semicond*; 39. Epub ahead of print 2018. DOI:

Chapter III Effect of precursor nature and molarities on Titanium and Zinc oxides thin films properties

10.1088/1674-4926/39/12/122003.

- [12] More AM, Gunjkar JL, Lokhande CD, et al. Systematic interconnected web-like architecture growth of sprayed TiO₂ films. *Micron* 2007; 38: 500–504.
- [13] Tauc J. Optical Properties of Amorphous Semiconductors. In: Tauc J (ed) *Amorphous and Liquid Semiconductors*. Boston, MA: Springer US, pp. 159–220.
- [14] Urbach F. The Long-Wavelength Edge of Photographic Sensitivity and of the Electronic Absorption of Solids. *Phys Rev* 1953; 92: 1324.
- [15] Abdelkrim A, Rahmane S, Abdelouahab O, et al. Optoelectronic properties of SnO₂ thin films sprayed at different deposition times. *Chinese Phys B* 2016; 25: 1–7.
- [16] Ju Y, Wang M, Wang Y, et al. Electrical properties of amorphous titanium oxide thin films for bolometric application. *Adv Condens Matter Phys*; 2013. Epub ahead of print 2013. DOI: 10.1155/2013/365475.
- [17] Anitha N, Anitha M, Raj Mohamed J, et al. Influence of tin precursor concentration on physical properties of nebulized spray deposited tin disulfide thin films. *J Asian Ceram Soc* 2018; 6: 121–131.
- [18] Yilmaz M, Turgut G. Titanium doping effect on the characteristic properties of sol-gel deposited ZnO thin films. *Kov Mater* 2015; 53(5): 333–339.
- [19] Puchert MK, Timbrell PY, Lamb RN. Postdeposition annealing of radio frequency magnetron sputtered ZnO films. *J Vac Sci Technol A Vacuum, Surfaces, Film* 1996; 14: 2220–2230.
- [20] Angayarkanni A. Effect of stress on optical band gap of ZnO thin films with substrate temperature by spray pyrolysis. DOI: 10.1016/j.jallcom.2009.05.116.
- [21] Magnfält D. *Growth Stages*. Linköping University, Sweden, 2014.
- [22] Del Vecchio AL, Spaepen F. The effect of deposition rate on the intrinsic stress in copper and silver thin films. 2007. Epub ahead of print 2007. DOI: 10.1063/1.2712150.
- [23] Spaepen F. Interfaces and stresses in thin films. *Acta Mater* 2000; 48: 31–42.

- [24] Amroun MN, Salim K, Kacha AH. Molarities effect on structural optical and electrical properties of nanostructured zinc oxide deposited by spray pyrolysis technique. *Int J Thin Film Sci Technol* 2021; 10: 67–73.
- [25] Sâad RAHMAN. Elaboration Et Caracterisation De Couches Minces Par Spray Pyrolyse Et Pulverisation Magnetron. Universite Mohamed Kheider - Biskra, http://thesis.univ-biskra.dz/1064/1/phy_d1_2008.pdf (2008).
- [26] M B GiliR , R Chu MB. Effects of Molarity Variation on The Optical Property and Topography of ZnO Thin Films Deposited Via Spray Pyrolysis Effects of Molarity Variation on The Optical Property and Topography of ZnO Thin Films Deposited Via Spray Pyrolysis. *J Phys Conf Ser*; 1191. Epub ahead of print 2019. DOI: 10.1088/1742-6596/1191/1/012050.
- [27] Taskin M. Study the Effect of Molar Concentration on the Optical and Surface Properties of ZnO Thin Films Prepared by Spray Pyrolysis. *Appl Sci Reports*; 3. Epub ahead of print 2014. DOI: 10.15192/pscp.asr.2014.3.3.109111.
- [28] Nikam S V, Jadhav BT, Chivate SM, et al. Structural, morphological and optical attributes of ZnO thin films deposited via spray pyrolysis process: Impact of molarity variation. *IOP Conf Ser Mater Sci Eng* 2022; 1258: 012012.
- [29] Burstein E. Anomalous Optical Absorption Limit in InSb. *Phys Rev* 1953; 93: 632–633.
- [30] Munirah, Khan ZR, Aziz A, et al. Influence of zinc concentration on band gap and sub-band gap absorption on ZnO nanocrystalline thin films sol-gel grown. *Mater Sci Pol* 2017; 35: 246–253.
- [31] Barir R, Benhaoua B, Benhamida S, et al. Effect of Precursor Concentration on Structural Optical and Electrical Properties of NiO Thin Films Prepared by Spray Pyrolysis. *J Nanomater* 2017; 2017: 433–439.
- [32] **BENRAMACHE. S, AOUN. Y, LAKEL. S,** et al. The effect of film thickness on the structural, optical and electrical properties of ZnO thin films deposited by ultrasonic spray deposition. *Mater Today Proc* 2019; 27: 0–31.

- [33] مذكرة زوييري بلال.pdf. university mohamed khider biskra, 2021. 
- [34] Majumder SB, Jain M, Dobal PS, et al. Investigations on solution derived aluminium doped zinc oxide thin films. Mater Sci Eng B Solid-State Mater Adv Technol 2003; 103: 16–25.
- [35] Ellmer K, Klein A, Rech B. Transparent Conductive Zinc Oxide: Basics and Applications in Thin Film Solar Cells. Springer Berlin Heidelberg, 2007.

Chapter IV ***Deposition of
titanium-doped ZnO films and
ZnO:TiO₂ composite oxide films***

IV.1. Introduction

The zinc oxide thin film properties can be easily tailored by using suitable impurity material. Therefore, it is of scientific interest to fine tune the deposition parameters in order to obtain good quality coatings using a simple process. In this section, we report synthesis route to produce pure and Ti doped nanocrystalline ZnO thin films. To get a better understanding of the effect of Ti ion concentration on the morphological, structural and optical properties of the ZnO deposited films, they have been systematically studied using scanning electron microscopy, X-ray diffraction, UV-visible spectroscopy and four point prob.

We focus on the synthesis of Ti doped ZnO using TiCl₃ using spray pyrolysis technique, in this work, which is a suitable precursor. Because of the intense hydrolysis of the alkoxide in air, the use of alkoxide necessitates strict control of experimental conditions such as pH, humidity, etc. The high cost of alkoxide also prevents such a process from being commercialized.

- **IV.A. Section one: Effect of Titanium low doping contents**

IV.A.1. Experimental details

Titanium doped Zinc oxide thin films with different concentrations (0, 1, 3, 5, 7, 9 at. %) were prepared on glass substrates by spray pyrolysis method. The fabrication of the undoped Zinc oxide (ZnO) was carried out using dissolved Zinc (II) Chloride (ZnCl₂) in distilled water to obtain a final solution (M=0.05 mol/L) as the source element, titanium Chloride (TiCl₃) was used as the titanium (Ti) doping source, The prepared solutions were stirred at room temperature and the resultant solutions were sprayed onto glass substrates at 370 °C for 3min to obtain clear thin films with good properties.

IV.A.2. Results and Discussion

IV.A.2.1. Surface Thickness of the Film

The surface thickness of the films was carried out by gravimetric method using the relation(III.4).The results are shown in **FigIV.A.1.**for the undoped ZnO and 1 at.% to 9at.% Ti doped ZnO respectively.As the doping concentration increases, the film thickness decreases from 368 to 212 nm. The contribution of the doping precursor disrupts the growth of the layer and reduces the growth velocity. **The interference between zinc and titanium spraying particle fluxes reduces the mean free path of both of them and reduces their scattering effect resulting to a lower growth rate which causes the film thickness decreases [1].** As it is clear all the values are lower compared to that of the undoped sample.

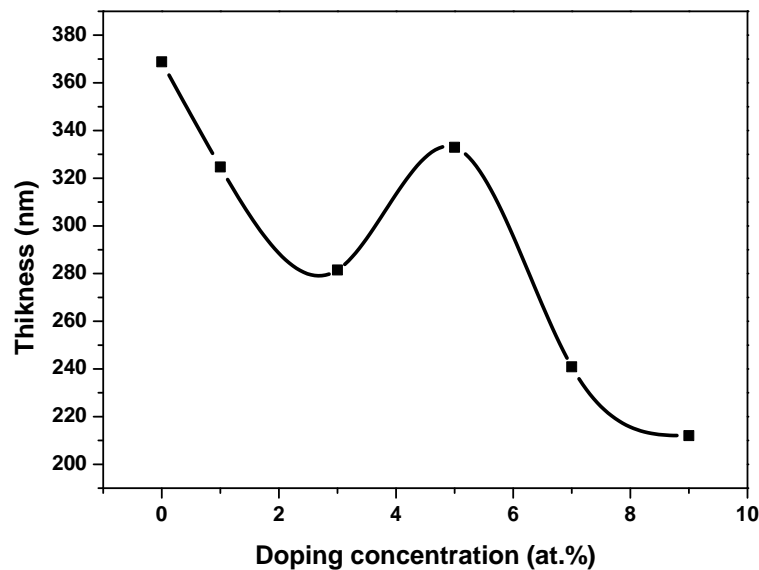


Fig. IV. A. 1. The variation of the thickness with Ti doping concentration.

IV.A.2.2. Structural properties

X-ray diffraction patterns of Ti doped ZnO thin films are shown in **Fig.IV.A.2**.The diffraction pattern exhibits characteristic peaks (wurtzite) corresponding to 2 theta values 34.42°,36.25°, 47.53° and 62.86° as (002), (101), (102) and (103) respectively. The crystalline nature (Hexagonal) and purity of the sample are confirmed by comparing the data with JCPDS (card No: 36-1451).

The result reveals an increase in the intensity while the width of the (002) diffraction peak becomes narrower when Ti doping concentration increases from 1 at.% to 5 at.% which means that there is an enhancement of crystallization and the growth of crystallites. At greater values of Ti doping concentration the intensity of (002) peak decreases and width becomes broad .This was due to the decreases of crystallization and the growth of crystallites.

from 1 at.% to 5 at.% we can see a shifting of the (002) diffraction peak into lower angles .It is well known that the (002) plane of ZnO consists of alternate planes of Zn²⁺ and O²⁻ and thus is charged positively or negatively, depending on surface termination [2]. So adding low content of Ti⁴⁺ ions could disturb the charge of the (002) plane, If Ti⁴⁺ ions substitute Zn²⁺ sites, the repulsive force in this plane would increase because of extra positive charge. This effect can enlarge the lattice parameters, thus leading to the observed decrease of the diffraction angle.

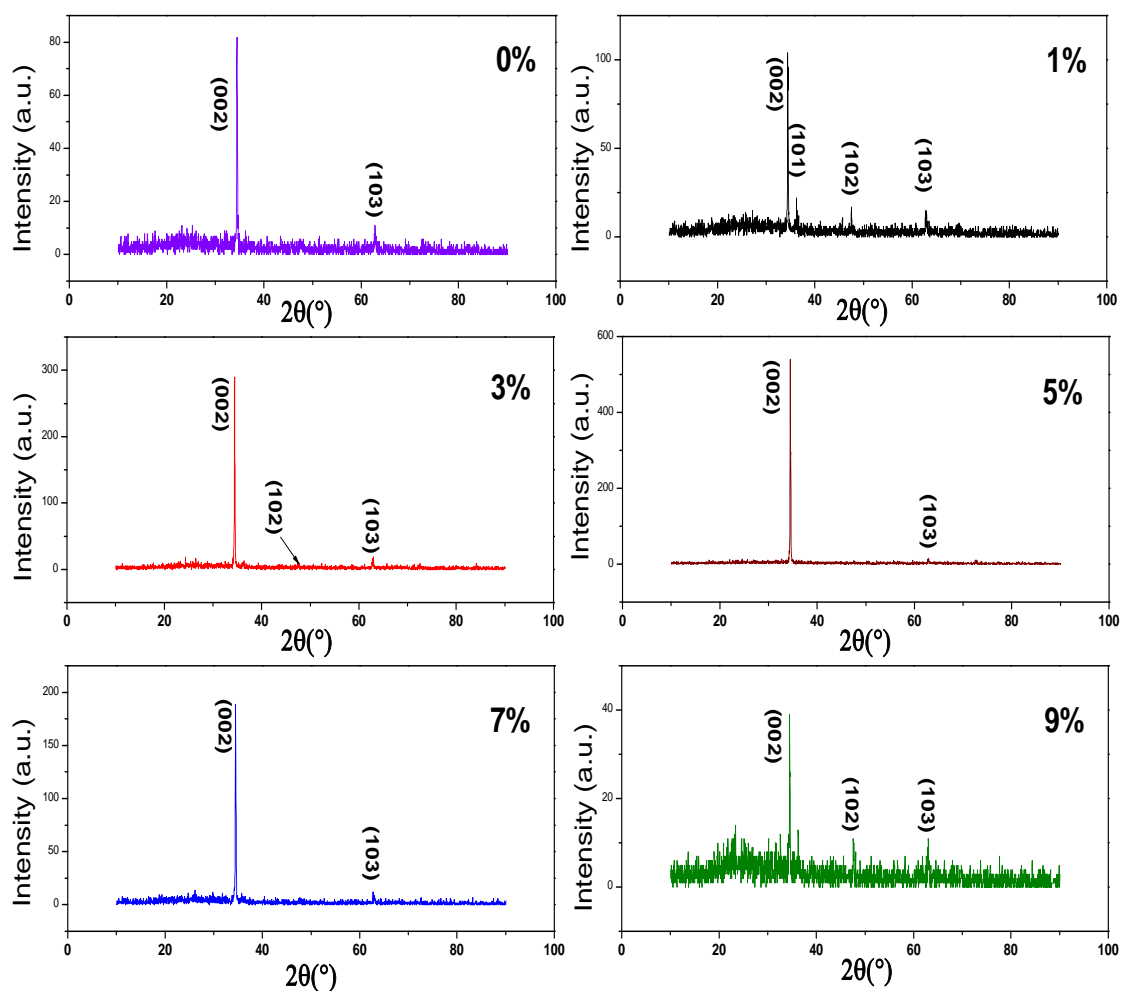


Fig. IV. A. 2. X-ray diffraction spectres of ZnO films with different Ti doping concentrations.

While from 5at.% to 9 at.% we can see a shifting of the (002) diffraction peak into higher angles in addition, a reappearance of (102) and (103) diffraction peaks. It is suggested that the concentration of substitution **Ti saturates at 5 at. %** and the additional Ti atoms are probably in interstitial form then it segregates to the non-crystalline region in grain boundaries leading to the shrinkage of the grain size.

The interplanar distance ‘d’ values of the films are determined by Bragg’s law equation (II.1), The lattice constant values of undoped and Ti doped ZnO thin films are calculated by the relation(III.7)[3]. The results are tabulated in **Table IV.1**. It is found that the lattice constant values are slightly lower than the standard values of $a_0 = 3.2498 \text{ \AA}$ and $c_0 = 5.2066 \text{ \AA}$ (JCPDS card no: 36-1451).

Table.IV.1. Variation of interplanar distance ‘d’ and lattice parameters as a function of Ti doping concentrations.

doping contents	d	A	C
(%)	\AA	\AA	\AA
0	2,60287	3,18784	5,20574
1	2,60609	3,19179	5,21219
3	2,60661	3,19242	5,21322
5	2,60343	3,18853	5,20686
7	2,6029	3,18787	5,20579
9	2,59906	3,18318	5,19813

The film strain of the c-axis (ϵ_{zz}) can be determined by the formula (III.8)[4]. For hexagonal crystals, the stress (σ_{film}) in the plane of the film can be calculated using the biaxial strain model(III.9) (III.10)[4]. The grain size values of the films are calculated by the Scherer formula (equation (II.2)). **Fig.IV.A.3.** represents the variation of the calculated values of crystallites size and stress in the films as we can see undoped sample is free stress, The stress values of Ti 1at.% and 5at.% doped ZnO films are positive, which indicates tensile strains which are proportional to a intensive stress. The intensive stress values of Ti doped ZnO rises because of the increment in lattice constant values resulting from the extra positive charge which results in crystallites size increase. From 5at.% to 9at.% Ti doping concentrations the stress is compressive due to segregation of Ti atoms to the non crystalline region in grain boundaries leading to the shrinkage of the crystallite size.

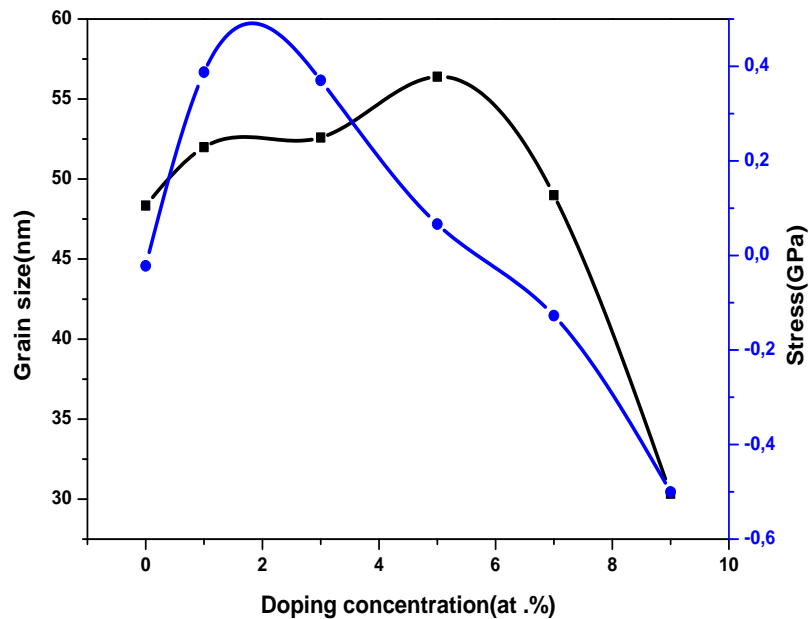


Fig. IV. A. 3. Variation of the calculated values of crystallites size and stress in the films versus Ti doping concentration.

IV.A.2.3. Morphology and chemical analysis

Fig.IV.A.4. Shows SEM images of the ZnO and Ti doped ZnO thin films. It's clear from later images that surface morphology is crack free and considerably affected by the doping concentration. Effectively, all films exhibited granular structures composed of small grains that appear somehow aggregated with porosity around. After, by increasing the doping concentration. From 1% to 3%, films exhibit bigger polygonal grains that are more effectively packed and distributed uniformly, giving denser structures characterized by lower porosity. For 5% and 7% Ti doped ZnO films, samples exhibited random distribution of different sizes of spherical grains, Grains observed at 9% film are dense, polygonal and smaller sized. This clearly shows that the film morphology can be controlled by the concentration of Ti in the film[5].

The composition analysis of Ti doped ZnO thin films performed by energy dispersive X-ray analysis (EDX) are shown in **Fig.IV.A.5**. EDX spectras confirmed the presence of Zn and O and Ti elements in the undoped and doped ZnO films. The weight and atomic percentage compositions of Zn, Ti and O in the thin films are presented in Table IV.2. It is clearly seen from the table that in the range under study, the variation in the final amount of Ti in the thin films of Ti doped ZnO films depends on the starting concentrations of Titania added which supports very well the successful substitution of dopants in the Zn sites, except for the 9 at.% Ti doped ZnO film.

Table.IV.2. Variation of atomic ratios of Zn Ti and Oxygen atoms as a function of Ti doping concentration.

	0 (at. %)	1 (at. %)	3 (at. %)	5 (at. %)	7 (at. %)	9 (at. %)
Zn	59.62	60.64	62.58	61.13	56.95	45.08
O	40.38	39.21	37.16	38.32	41.78	53.73
Ti	0	0.15	0.25	0.55	1.27	1.19

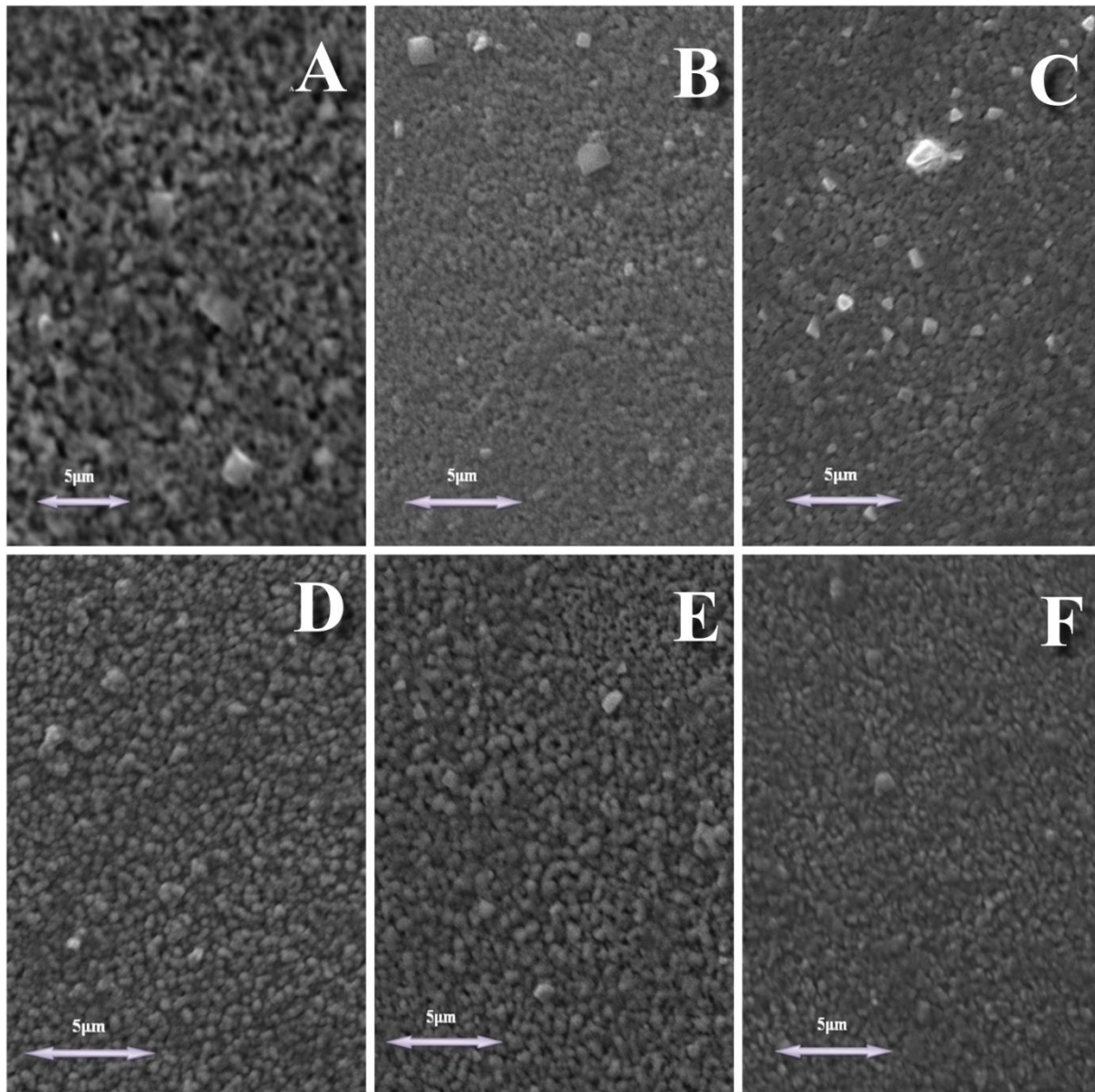


Fig. IV. A. 4. Top view SEM photographs for different Ti doping concentration.

The amount of Zn element decreases with increasing Ti content from 5 at. % to 9 at. %, this is due to the limited solubility of Ti in ZnO matrix to some titanium atoms tend to aggregate near grain boundaries. Chemisorbed oxygen from atmospheric air, which is

extremely prevalent in the spray Pyrolysis process, may be the reason for the increase in oxygen density in this range [6].

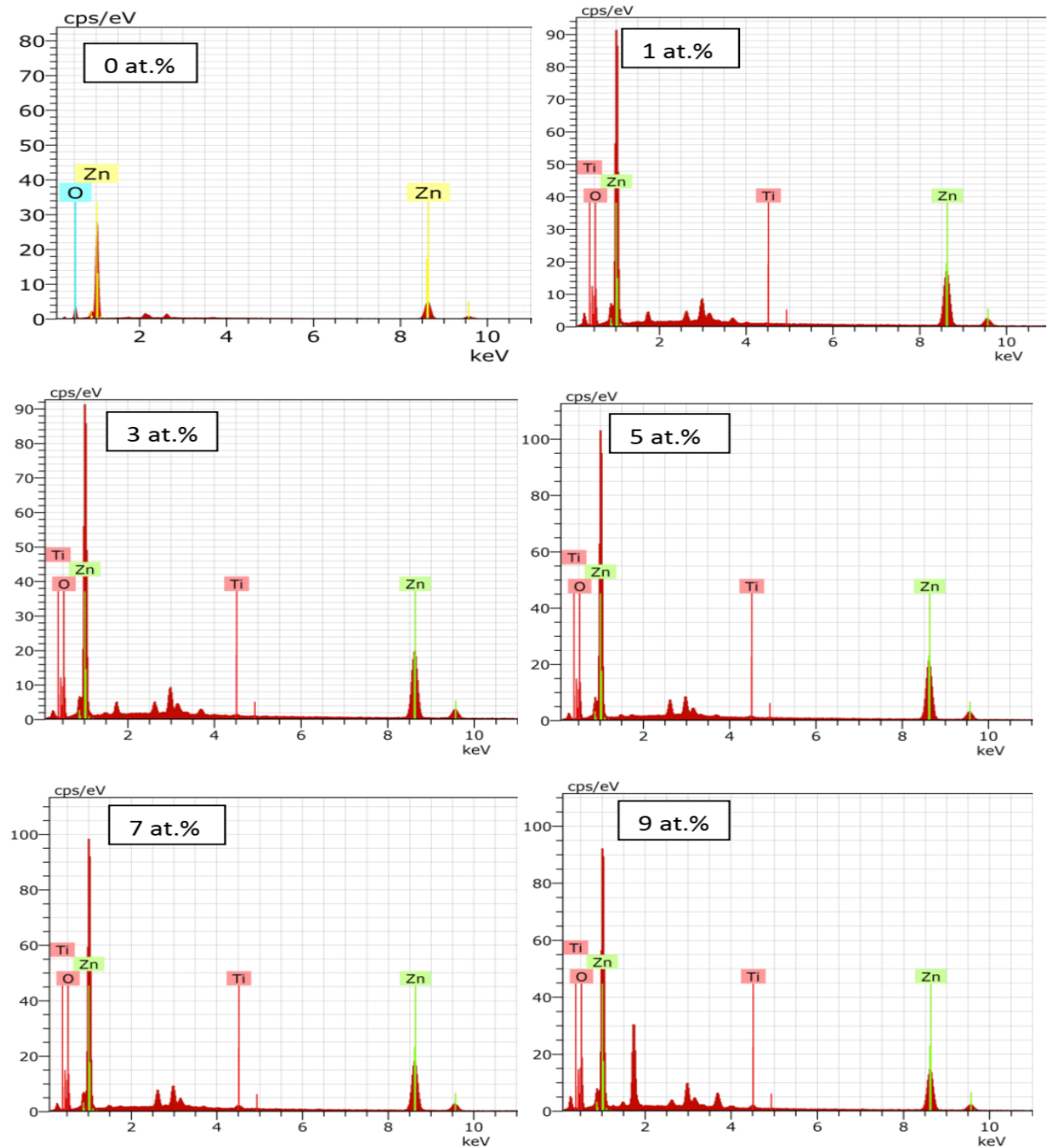


Fig. IV. A. 5.EDX spectra of undoped and Ti-doped ZnO films.

IV.A.2.4. Optical properties

Transparency of the prepared thin films samples, were examined via UV–Vis transmittance spectroscopy, the results are shown in **Fig. IV.A.6**. As shown in this figure, the transparency of ZnO, 1,3,5,7,9 at.% Ti doped ZnO thin films on glass substrate in visible light region (wavelength of 400-800 nm) excluding substrate contribution are about 64,05%, 61,61%, 64,47%, 55,34%, 54,52% and 62,28%, respectively. As it is clear, The transmittances of all the Ti doped ZnO films are lower than that of the pure ZnO layer except for 3 at.%.

as we can see all the transmittance spectres shift to the longer wavelength side (red shifted) with Ti concentration increase except for 3 at.% which shows a blue shift. A blue shift in transmittance spectres means a widening of band gap; this is attributed to the Burstein-Moss band-filling effect[7]. The Ti⁴⁺ ions may substitute Zn²⁺ ions and thus it gives rise to the free carrier concentration which fills the conduction band edge, so the optical band gap is widened. Similar blue shift phenomenon of optical band gaps has been reported previously by Ye et al [2], who fabricated Ti-doped ZnO films by atomic layer deposition.

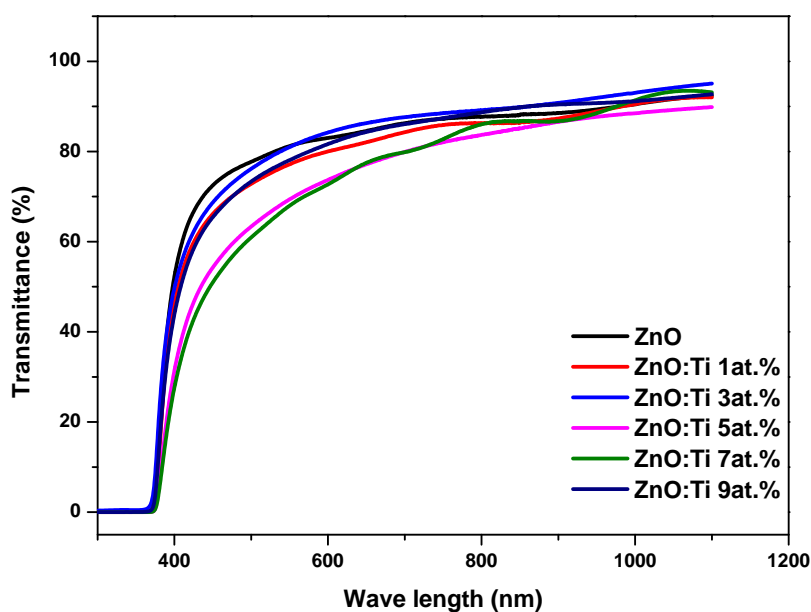


Fig. IV. A. 6. Optical transmittance variation versus Ti doping content.

IV.A.2.5. Electronic Proprieties

The estimation of the optical band gaps of the films is based on Tauc formula for direct band gap semiconductors using the equation (II.5)[8], by the extrapolation of the linear region of the plot $(\alpha h\nu)^2$ versus $(h\nu)$ to intersect at $(h\nu)$ axis, we could determine the values of our optical band gap (E_g). The Urbach energy (E_u) of band tails which characterizes localized states near the bands edges; it is estimated from the inverse slope of the linear plot between $\ln(\alpha)$ versus $(h\nu)$ from equation (II.7)[9].

From **Fig.IV.A.7**, we have found that the calculated optical band gap (E_g) values of the Ti doped ZnO thin films are in the range of 3.06 – 3.15 eV and it has a decreased aspect in general except for 3% where the band gap reaches its maximal value.

We had noticed that all the E_g values are lower than those of the pure ZnO reported by different literature 3.3 eV. Sernelius et al. [10] have discussed the theory of band gap narrowing in Al-doped ZnO. In a polar semiconductor, such as ZnO, there is a displacement of charge from one of the atomic species to the other, and hence the host atoms are charged. A moving charged particle then causes a displacement polarization, which follows the particle in the crystal. An electron attracts the positively charged atoms and repels the negatively charged ones. Effectively, an electron is surrounded by a cloud of positive charge, and the valence band hole is surrounded by a cloud of negative charge. The particle and its charge cloud compose a polaron. The displacement polarization modifies the self-energy shifts caused by the many-body interactions. As a result the conduction band edge shifts towards the valence band and the valence band towards the conduction band leading to the narrowing of the band gap [10].

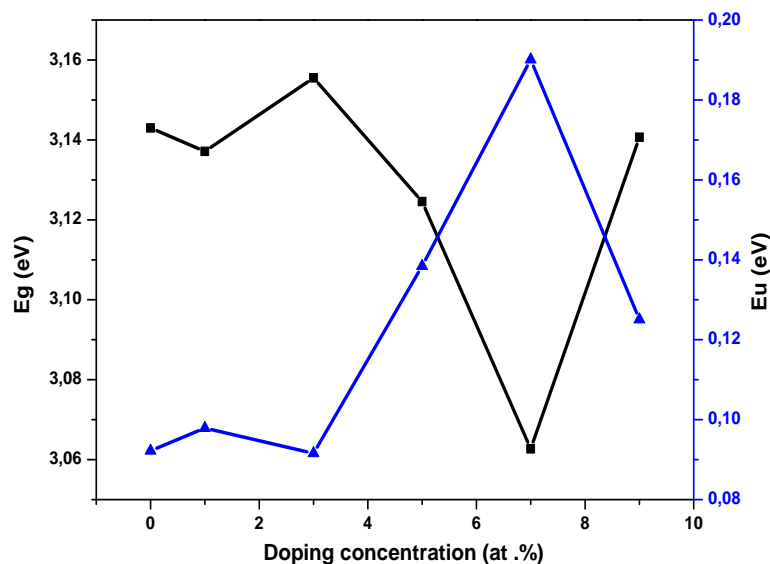


Fig. IV. A. 7. Variation of band gap and band tail width versus doping concentration.

IV.A.2.6. Electrical properties

The dependence of the resistivity on Ti contents in the TZO films is shown in **Fig.IV.A.8**. The resistivity of as-deposited films has been high. This is probably due to the grain boundary effects, since the films are polycrystalline in nature. Also, since air was used as the carrier gas, it is quite likely that a large number of oxygen molecules are chemisorbed in the film both at the grain boundaries and on the surface. The chemisorptions of oxygen will produce potential barrier, which hinders the electrical transport causing a reduction in conductivity[11].

As is displayed, the resistivity for pure ZnO film is 33 Ω .Cm. Then it decreases slightly to a minimum value of 17. Ω .Cm for the sample with 5 at.% it is suggested that is when doping is done in ZnO, the Ti⁴⁺ ions replaces a part of Zn²⁺ ions, and donates two electrons

those later are added to the lattice increasing the carrier concentration and therefore the total resistivity is getting reduced[12],and then goes up with the increase of the Ti contents until it reaches its maximal value for the sample with 9 at.%.

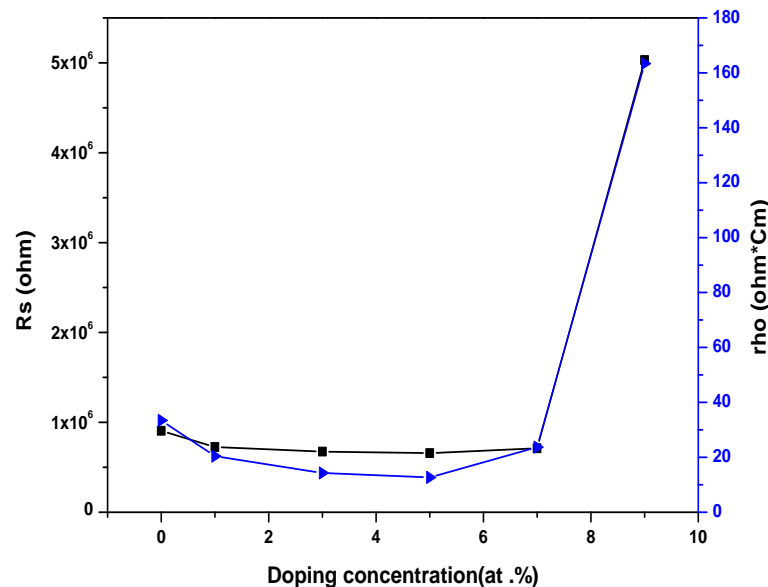


Fig. IV. A. 8. Dependence of electrical resistivity in TiO₂ films on doping concentration.

The increase in the resistivity can be interpreted as follows: As the Ti doping concentration continues to increase, due to limited solubility of Ti in ZnO matrix some titanium atoms tend to aggregate near grain bound arise to form TiO₂ instead of taking the place of Zn²⁺ to generate more free carriers. In addition, the mobility of electrons may be affected by to the deterioration in the crystalline quality, which leads to an increase of carrier scattering. It suggests that the conductivity of ZnO film can be improved significantly with appropriate Ti doping concentration [2].a similar observation was made by Yasemin Caglar et al [13].

IV.A.3. Conclusion

It is clear that, the effect of titanium doping ZnO thin films on the structural, electrical, and optical properties is slightly obvious after our study. Where the TZO films deposited at different percentage of titanium then characterized using a various methods.

Film thickness decreases because of the interference between zinc and titanium spraying particle fluxes reduces the mean free path of both of them and reduces their scattering effect resulting to a lower growth rate

The results of X-ray diffraction showed that TZO thin films have peaks correspond to the hexagonal wurtzite structure of ZnO. Where the intense diffraction peak is around $2\theta=34.42$ with as light shifting of the (002) diffraction peak, also we have found that the lattice constant values slightly differs than the standard values. As the Ti doping content increases from 1 at.% and 5 at.% the films suffers from intensive stress which results in crystallites size increase. From 5 at.% to 9 at.% Ti doping concentrations the stress is compressive due to segregation of Ti atoms to the non-crystalline region in grain boundaries leading to the shrinkage of the crystallite size. SEM images of the ZnO and Ti doped ZnO thin films reveal that surface morphology is crack free, all films exhibited granular structures composed of small grains that appear somehow aggregated with porosity around the morphology of the films considerably affected by the doping concentration. EDX spectras confirmed the presence of Zn and O and Ti elements in the indoped and doped ZnO films. The weight and atomic percentage compositions of Zn, Ti and O in the thin films and the variation in the final amount of Ti in the thin films of Ti doped ZnO films depends on the starting concentrations of Titania added which supports very well the successful substitution of dopants in the Zn sites.

The transparency of ZnO, Ti doped ZnO thin films on glass substrate in visible light region reaches 64,47% for 3 at.%. the calculated band gap (E_g) values of the Ti doped ZnO thin films are in the range of 3, 06 –3, 15 eV and it has a decreased aspect in general except for

3 at.% where the band gap reaches its maximal value. The resistivity for pure ZnO film is 33 Ω.Cm . Then it decreases slightly to a minimum value of 17. Ω.Cm for the sample with 5 at.%.

From all this results we can estimate that the ZnO film of Ti 3at.% doping content has good photocatalytic properties among other samples and as a best one 5 at.% is chosen those films can be used for Dye Sensitized solar cells (DSSC).

- **IV.B. Section two: Effect of Titanium high doping contents (ZnO:TiO₂ composites)**

The effect of high doping concentrations titanium atoms on structural optical electrical and morphological properties of ZnO thin films was studied in this section.

IV.B.1. Experimental details

Titanium doped Zinc oxide thin films with different concentrations were prepared on glass substrates by spray pyrolysis method. The fabrication of the films was carried out using the same parameters such as the first section ,The composite solution was prepared by mixing together the resultant solution of ZnO and TiO₂ with the following ZnO:TiO₂ molar ratios: 1:1 ,1:0,9 ;1:0,7 ;1:0,5;1:0,3 ;1:0 . The prepared solutions were stirred at room temperature and the resultant solutions were sprayed onto glass substrates at 370 °C for 3min to obtain clear thin films with good properties.

IV.B.2.Result and discussion

IV.B.2.1. Film formation mechanism and thickness measurement

The influence of high Titanium concentration on thickness of the ZnO films has been studied, as we can see the thickness is slightly increasing from 300 to 406 nm for pure ZnO to 1:0.5 molar ratio from 1:0.5 to 1:0.7 ZnO: TiO₂ molar ratio the thickness jumps to 1181

nm after that it continues its increasing gradually till it reaches its maximal value for 1:0.9 ZnO: TiO₂ molar ratio this abrupt increasing of thickness could be caused by the appearance of a new compound. The thickness of 1:0.7 ZnO: TiO₂ molar ratio thin film sample is 3 times higher than in the 1:0.5 ZnO:TiO₂ molar ratio which could be interpreted as a new compound is appearing which has a d_{hkl} 3 times greater than that of the (002) in ZnO thin films.

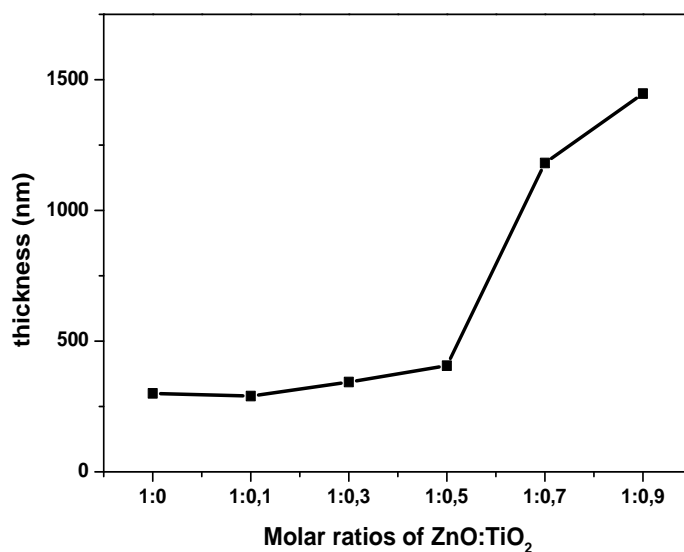


Fig. IV. B. 1. The variation of the thickness of ZnO and ZnO: TiO₂ composite thin films with different molar ratios.

IV.B.2.2. Structural properties

Fig.IV.B.2. shows the diffraction patterns of our samples. For the pure and 0:0.1 to 1:0.5 ZnO:TiO₂ molar ratio films samples, the observed reflections are corresponding to ZnO wurtzite phase (JCPDS data card No: 36-1451) with preferential orientation along the c-axis (002), from the 1:0.3 to 1:0.5 ZnO:TiO₂ molar ratio films samples, small peaks are observed indicating the coexistence of a new phase, spinel Zinc Titanate Zn₂TiO₄ with Tetragonal structure (JCPDS data card No: 018-1487) but the ZnO wurtzite phase is the dominant structure. In the 1:0.7 ZnO:TiO₂ molar ratio film sample with higher Ti content

the ZnO diffraction peaks get reduced even though the film thickness has increased enormously. At the same time a new growth direction appears which correspond to the Ti₅O₉ Magnéli phase with triclinic structure JCPDS data card (No:051-0641).

For the 1:0.9 ZnO:TiO₂ molar ratio film sample the amorphous character cannot be avoided, which means that the substrate temperature is not sufficient .so it could be expected that the TiO₂ crystalline phase is favoured in this case, if the substrate temperature increases above 500 C°. It can be concluded that in addition to correct chemical composition of the sources, temperature is an important factor for the formation and improvement of Zn₂TiO₄ which have excellent photocatalytic properties (especially when it is mixed with ZnO phase) compared with ZnO and TiO₂ separately Khatua et al. Demonstrated that[14], Wan et al. found that ZnO/Zn₂TiO₄ core/shell nanowires exhibited more excellent photovoltaic activity than single ZnO nanowires and the enhanced photocatalytic activity of the ZnO/Zn₂TiO₄ core/shell nanowires was demonstrated by the degradation of acetone under UV light irradiation[15],Khatua et al. also shows that Zn₂TiO₄ nanoparticles can show 6 times higher UV photocatalytic activity than TiO₂ nanoparticles (Degussa P25). They had an extremely good recycling ability which can make the solid state reaction grown Zn₂TiO₄ nanoparticles a better choice for UV photocatalytic dye decomposition application[14],Sandra Andrea Mayén-Hernández et al has found that Ts= 450 °C is good for the preparation of pure Zinc Titanate compound[16].

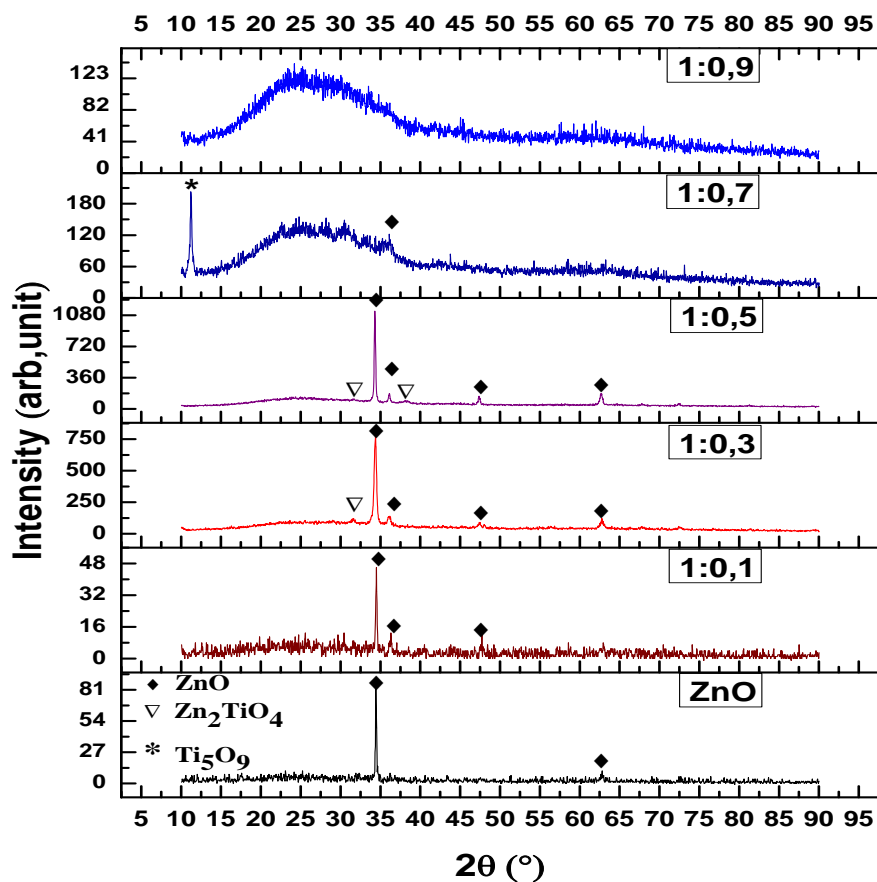


Fig. IV. B. 2. X-ray diffraction spectra of the ZnO and ZnO: TiO₂ composite thin films with different molar ratios.

IV.B.2.3. Morphology and chemical analysis

The morphology of the ZnO and composite ZnO: TiO₂ thin films were determined by using SEM images. **Fig.IV.B.3.** shows the surface morphologies of 6 samples of ZnO thin film (A, B,C, D, E, F) with different molar ratios: (A) pure ZnO, (B) 1:0.1 ZnO:TiO₂ molar ratio, (C) 1:0.3 ZnO:TiO₂ molar ratio, (D) 1:0.5 ZnO:TiO₂ molar ratio (E) 1:0.7 ZnO:TiO₂ molar ratio and (F) 1:0.9 ZnO:TiO₂ molar ratio, deposited by spray pyrolysis technique. From the **Fig.IV.B.3.**, it can be seen that the ZnO thin film have smooth and homogeneous surface morphology with porous, for the sample (B) the film is smoother, homogeneous,

less porous and the particles are well dispersed and becomes more densely pack. The thin film is well adhered to the glass substrate and the particles became densely pack.

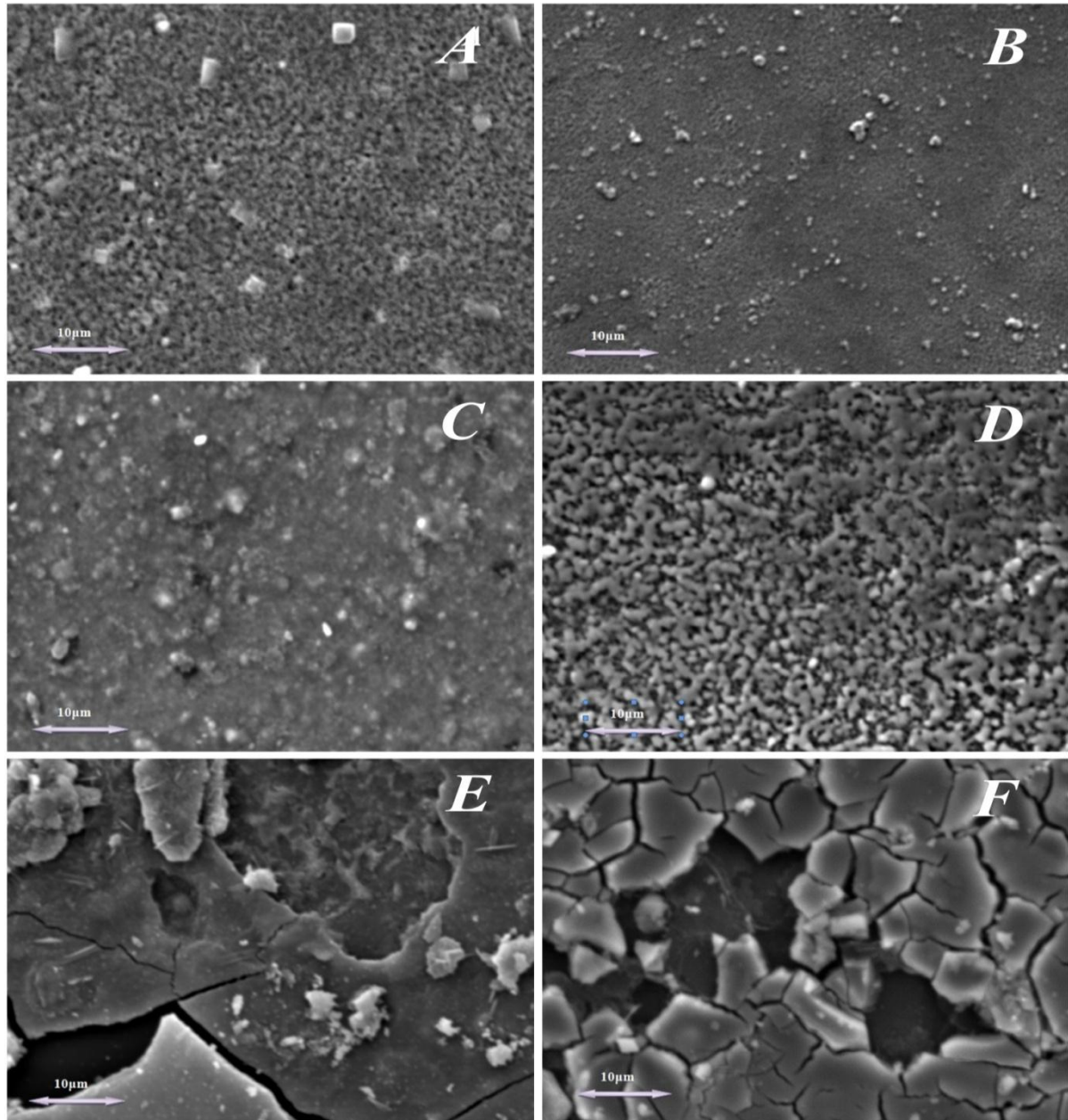


Fig. IV. B. 3. Top view SEM photographs of the ZnO and ZnO: TiO₂ composite thin films with different molar ratios.

For the sample (C) the film starts to become Rough, homogeneous, dense, from this figure, it can be observed that sample (D) with 1:0.5 ZnO:TiO₂ molar ratio was rather rugged it has high surface roughness compared to the other samples, porous with grains coalescing with each other. This would increase the number of grain boundaries and increase the surface area so the surface properties of thin film are improved. Both of the samples (E) and (F) thin films were cracked this is due to the increasing of the thickness of the films so the increasing of growth rate or the substrate temperature is not sufficient for the decomposition of the solution.

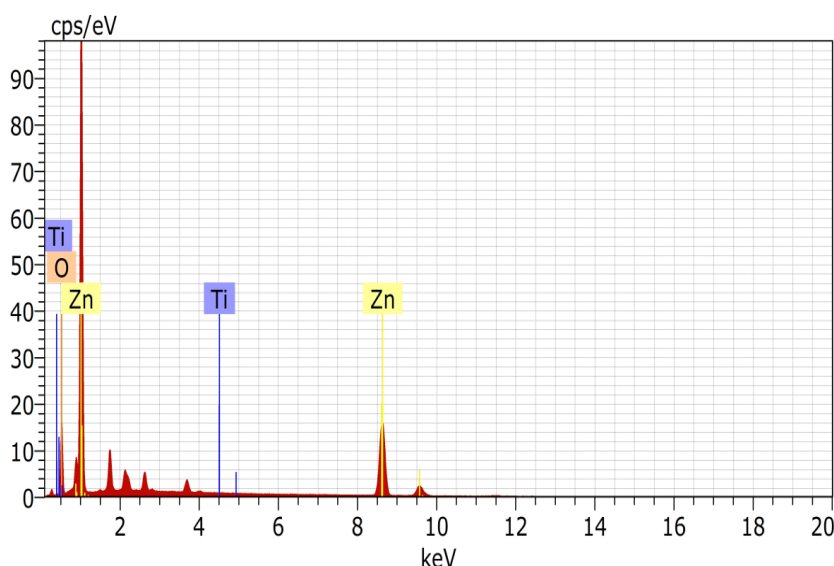


Fig. IV. B. 4. EDAX spectra of the 1:0.5 ZnO:TiO₂ molar ratio thin film.

EDAX results confirmed the presence of Ti, Zn and O elements in the films and from the quantitative analysis it was observed that there was a systematic increase in Ti, O and a decrease in Zn element's amounts in the final product as it was included in the starting solution. The increase in the oxygen amount could be caused by the chemisorptions of oxygen at grain boundaries and also on the surface [17].

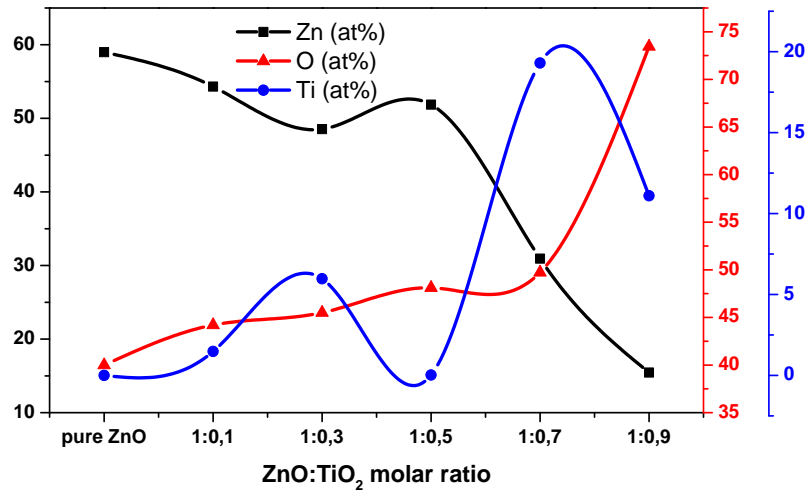


Fig. IV. B. 4. Variation of atomic ratios of Zn , Ti and Oxygen atoms of the ZnO and ZnO:TiO₂ composite thin films with different molar ratios.

IV.B.2.4. Optical properties

Titanium dioxide and zinc oxide both have photocatalytic activity that is initiated by adsorbing the light, so for understanding the optical properties of the prepared composite the UV-Vis spectra are employed. **Fig. IV. B. 5.** Shows the optical transmittances through different ZnO: TiO₂ molar ratios measured in the range of wavelength 250 to 1500 nm. The transmittance spectra revealed that all films had an average transmittance between 9% – 85% within the visible region (400 - 800 nm). The transmission decreases sharply near the ultraviolet region about 380 nm all the samples due to the band gap absorption. From this figure, the transparency of films decreases with the increase of thickness and surface roughness. The low transmittance in visible range might be attributed to the possible light scattering on rough surface (which could be confirmed by the absence of interference fringes for the 1:0.7 and 1:0.9 ZnO:TiO₂ molar ratio samples and high grain boundary that the thin films has, because the particles are less uniform dispersed on the glass substrate and forming large agglomerate particles similar results found by C.M.Firdaus et al.[17]

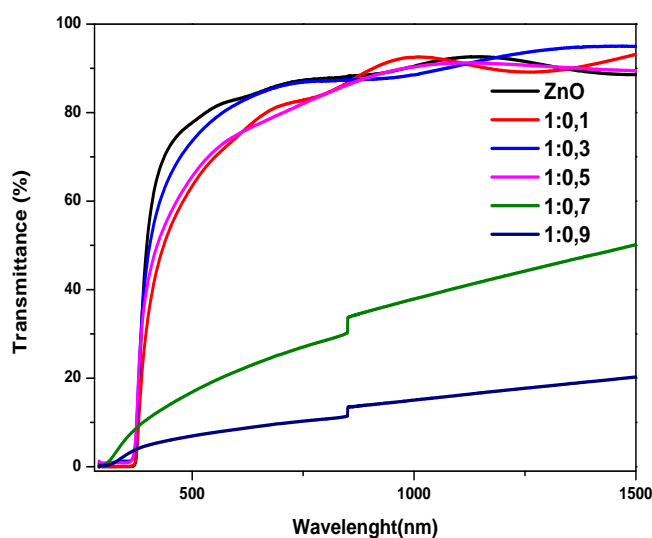


Fig. IV. B. 5. Optical transmittance of the ZnO and ZnO: TiO₂ composite thin films with different molar ratios.

The calculated band gaps of the samples from 0 to 1:0.5 ZnO:TiO₂ molar ratio films are found to be decreased slightly this could be due to the presence of the secondary phase Zn₂TiO₄. To a certain extent, the more Ti atoms in the films, the more Zn₂TiO₄, the narrower the band gap. After 1:0.5 ZnO:TiO₂ molar ratio we can remark that the E_g declines dramatically till it reaches its minimal value (2,3 eV) for 1:0.9 ZnO:TiO₂ molar ratio, this values differs from those of ZnO so it indicates the emergence of a new compound represented in Ti₅O₉.

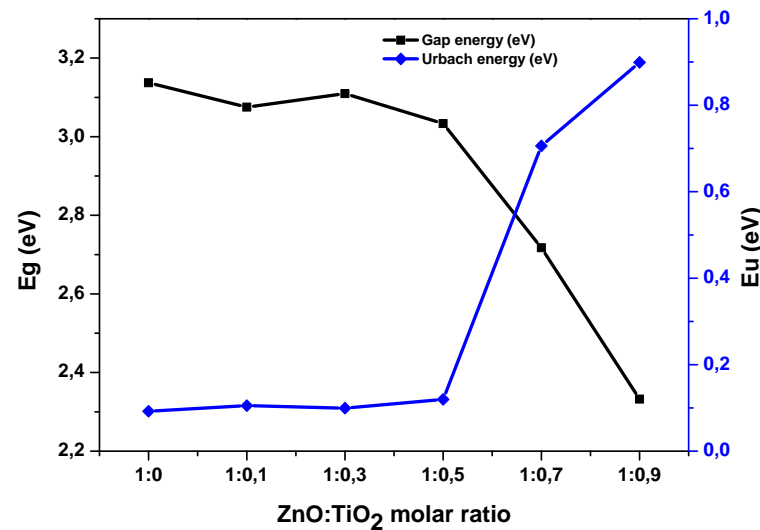


Fig. IV. B. 6. Variation of band gap and band tail width of the ZnO and ZnO: TiO₂ composite thin films with different molar ratios.

So by adding high concentration of Titanium into ZnO material, the band gap of ZnO become reduce and improve the minimum energy required for excitation electron. The electron will become easily excite from the valence band to the conduction band[18].

IV.B.2.5. Electrical properties

From the **Fig.IV.B.7.**, the resistivity of films was increased when the titanium concentration in the ZnO thin films increase might be due to chemisorptions of oxygen at grain boundaries and also on the surface .The increase of resistivity may attributed from the decreases of electron concentration resultant from chemisorptions of oxygen that causes the increasing of hole concentration .The absorbed oxygen may produce potential barrier which hinder the electrical mobility[18].this is confirmed by the EDAX results.

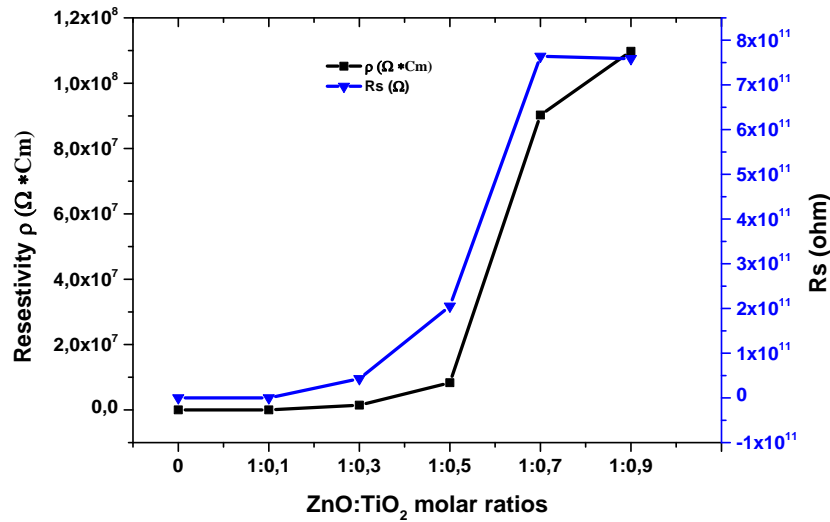


Fig. IV. B. 7. Dependence of electrical resistivity of different ZnO: TiO₂ molar ratios thin film.

IV.B.3.Conclusion

In heterostructures, at least two different materials are combined. In this chapter, we are interested in oxides-based heterostructured of ZnO TiO₂ binary semiconductors because of the new features offered by oxide-based materials [19] .

Highly transparent ZnO: TiO₂ thin films were successfully prepared on glass substrates by the spray pyrolysis technique, with different ZnO: TiO₂ molar ratios. XRD results revealed that, for the pure and 0:0.1 to 1:0.5 ZnO: TiO₂ molar ratio films samples, the observed reflections are corresponding to ZnO wurtzite phase with preferential orientation along the c-axis (002), from the 1:0.3 to 1:0.5 ZnO: TiO₂ molar ratio films samples, small peaks are observed indicating the coexistence of a new phase the spinel Zinc Titanate Zn₂TiO₄ with Tetragonal structure. The ZnO diffraction picks decrease for the 1:0.7 ZnO: TiO₂ molar ratio film sample with greater Ti content, despite the film's large rise in thickness. At the same time, a new growth direction that matches the JCPDS data card (No. 051-0641) for the Ti₅O₉ Magnéli phase with triclinic structure arises. The substrate temperature is

insufficient because the amorphous nature of the film sample with a 1:0.9 ZnO: TiO₂ molar ratio. In conclusion, the production of Zn₂TiO₄, which has outstanding photocatalytic capabilities (particularly when combined with ZnO phase), and its improvement depend significantly on temperature in addition to the sources' suitable chemical composition.

SEM result revealed that when compared to the other samples, the sample with a 1:0.5 ZnO: TiO₂ molar ratio was particularly rough, porous, and had granules that coalesced with each other. This would increase the surface area leading to improvement of the thin film's surface characteristics. The existence of Ti, Zn, and O elements was confirmed by EDAX results, and it was found from the quantitative analysis that there was a consistent increase in Ti, O, and a drop in Zn element amounts in the final product as it had been reported in the initial solution.

Transmittance spectra showed that all films had an average transmittance in the visible range (400–800 nm) of between 9% and 85%. According to the graphs, as thickness and surface roughness rise, films' transparency decreases.

The samples with calculated band gaps between 0 and 1:0.5 ZnO: TiO₂ molar ratio layers were found to have slightly smaller band gaps. This might be due to the presence of the secondary phase Zn₂TiO₄. The quantity of Ti atoms in the films has some effect on the band gap. After 1:0.5 ZnO: TiO₂ molar ratio, the E_g starts to fall significantly and keeps falling until it reaches its lowest value (2, 3 eV) for 1:0.9 ZnO: TiO₂ molar ratio, this means that the minimal energy needed to excite an electron has improved.

The chemisorptions of oxygen on the surface could be the cause of the rise in film resistivity seen when titanium concentration in ZnO thin films increased.

From this study we can conclude that films with 1:0.5 ZnO: TiO₂ molar ratio has good photocatalytic properties among the other samples, due to its high thickness and low gap energy and good structural properties, it is important to study the effect of deposition

temperature on this sample to enhance the growth of spinel Zinc Titanate Zn₂TiO₄ phase which is known as better photocatalysts than ZnO and TiO₂ films separately.

IV.2.Reference

- [1] Lu Y, Tsai S, Chang C. Highly Conductive And Transparent Ti-Doped Zinc Oxide Thin Films. *MRS Online Proc Libr (OPL)*, 769, H1011 2003; 1–9.
 - [2] Ye Z, Lu H, Geng Y, Et Al. Structural , Electrical , And Optical Properties Of Ti-Doped Zno Films Fabricated By Atomic Layer Deposition. *Nanoscale Res Lett* 2013; 8: 1–6.
 - [3] Yilmaz M, Turgut G. Titanium Doping Effect On The Characteristic Properties Of Sol-Gel Deposited Zno Thin Films. *Kov Mater* 2015; 53(5): 333–339.
 - [4] Puchert MK, Timbrell PY, Lamb RN. Postdeposition Annealing Of Radio Frequency Magnetron Sputtered Zno Films. *J Vac Sci Technol A Vacuum, Surfaces, Film* 1996; 14: 2220–2230.
 - [5] Marouf S, Beniaiche A, Guessas H, Et Al. Morphological, Structural And Optical Properties Of Zno Thin Films Deposited By Dip Coating Method. *Mater Res* 2017; 20: 88–95.
 - [6] Dhas CR, Venkatesh R, Sivakumar R, Et Al. Effect Of Solution Molarity On Optical Dispersion Energy Parameters And Electrochromic Performance Of Co₃O₄ Films. *Opt Mater (Amst)* 2017; 72: 717–729.
 - [7] Burstein E. Anomalous Optical Absorption Limit In Insb. *Phys Rev* 1953; 93: 632–633.
 - [8] Tauc, J., Grigorovici, R., & Vancu A. Optical Properties And Electronic Structure Of Amorphous Germanium. *Phys Status Solidi* 1966; 15: 627–637.
-

- [9] Meulenkamp EA. Size Dependence Of The Dissolution Of Zno Nanoparticles. *J Phys Chem B* 1998; 102: 7764–7769.
- [10] Sernelius BE, Berggren KF, Jin ZC, Et Al. Band-Gap Tailoring Of Zno By Means Of Heavy Al Doping. *Phys Rev B* 1988; 37: 10244–10248.
- [11] Joseph B, Manoj PK, Vaidyan VK. Studies On Preparation And Characterization Of Indium Doped Zinc Oxide Films By Chemical Spray Deposition. *Bull Mater Sci* 2005; 28: 487–493.
- [12] Rajasekaran M, Arunachalam A, Kumaresan P. Structural, Morphological And Optical Characterization Of Ti-Doped Zno Nanorod Thin Film Synthesized By Spray Pyrolysis Technique. *Mater Res Express*; 7. Epub Ahead Of Print 2020. DOI: 10.1088/2053-1591/Ab815d.
- [13] Caglar Y. Sol-Gel Derived Nanostructure Undoped And Cobalt Doped Zno: Structural, Optical And Electrical Studies. *J Alloys Compd* 2013; 560: 181–188.
- [14] Khatua L, Panda R, Nayak AK, Et Al. Efficient UV Photocatalytic Dye Decomposition Activity With Cost Effective Solid State Reaction Grown Zinc Orthotitanate (Zn₂TiO₄) Nanoparticles. *J Alloys Compd* 2018; 764: 895–900.
- [15] Wan L, Li X, Qu Z, Et Al. Facile Synthesis Of Zno/Zn₂TiO₄ Core/Shell Nanowires For Photocatalytic Oxidation Of Acetone. *J Hazard Mater* 2010; 184: 864–868.
- [16] Mayén-Hernández SA, Torres-Delgado G, Castanedo-Pérez R, Et Al. Photocatalytic Activity In Zn₂TiO₄ + Zno Thin Films Obtained By The Sol-Gel Process. *J Adv Oxid Technol* 2007; 10: 90–93.
- [17] Firdaus CM, Rizam MSBS, Rusop M, Et Al. Characterization Of Zno And Zno : Tio₂ Thin Films Prepared By Sol-Gel Spray-Spin Coating Technique. *Procedia Eng* 2012; 41: 1367–1373.
-

- [18] Firdaus CM, Rusop M, Baki SRMS, Et Al. Optical And Electrical Properties Of ZnO And ZnO : TiO₂ Thin Films Prepared By Sol-Gel Spray-Spin Coating Technique. 2012 10th IEEE Int Conf Semicond Electron ICSE 2012 - Proc 2012; 158–162.
- [19] Abdeouahab N. Preparation And Characterization Of Thin Films Nanostructures Based On ZnO And Other Oxides. Larbi Ben M'hidi University, 2019.

General conclusion and future prospects

The described research in this thesis focused on the synthesis and characterization of two transparent conducting oxides, which are Titanium dioxide and Zinc oxide, and their composite via spray pyrolysis depositing technique to investigate the effect of preparation parameters such as the nature of precursors used for the starting solution, molarities, on each oxide then doping and high doping concentrations of titanium species in ZnO films on the structural, optical and electrical properties of these thin films aims to use it in photocatalytic and photovoltaic applications.

As a starting point, we can summarize that the spray pyrolysis technique can be utilized to successfully deposit thin layers of semiconductor oxides with an appropriate and suitable microstructure for a specific application. Furthermore, it was found that the influence of the deposition parameters and operating conditions is dependent on the material deposited, and each oxide has its own characteristics in response to changes in these parameters. The conclusions connected to each oxide are presented in this second section:

From the experimental results, starting by the study of precursor nature and molarities in TiO₂ films and by comparing the properties of TiO₂ thin films deposited from two precursor solutions with different concentrations. We have found that films made from TiCl₃ were thicker than those made from TTIP, which is related to the way that every precursor's characteristics affected the growth velocity.

The films of both show poor crystallinity in the XRD patterns, with the characteristic anatase peaks. The analysis of the SEM micrographs reveals that the films made from TTIP were well adherent, uniform, pore-free, dense, and crack-free with nano-scale grains, while the films made from TiCl₃ were rough, comprised nano or micropores in an irregular shape with splashes distributed randomly, and did not show any grain or grain boundaries, confirming their amorphous structure. The nature of the initial solution also had a significant impact on the optical properties; interference fringes were observed in thin films of type TTIP while they were absent in those of type TiCl₃, and transmittance decreased as solution concentration increased. The increase in film thickness actually causes the transmittance to decrease at higher molar concentrations. Additionally, we observed that the predicted optical band gap (E_g) appeared decreased for both TTIP and TiCl₃ films and was bigger in TTIP films. This drop is supported by an increase in band tail

width (Urbach energy) as solution concentration rises. For the two precursors, the relationship between the resistivity of the TiO₂ films and a rise in precursor concentration is inverse, while the values are close to one another.

The variation in resistivity is attributable to varying carrier concentration and/or mobility. Because of its porous shape and anatase crystallographic phase, which is well known as the most suited structure for photocatalytic application, the thin film produced by TiCl₃ at 0.175M may have high photocatalytic capabilities.

The effects molarities and starting solution sources were either studied for ZnO films, structural, optical and electrical properties were affected by varying those parameters. The produced ZnO thin films feature a high-quality Wurtzite hexagonal structure with the favored orientation (002) direction, according to XRD examination for both sources. The effect of molarity has an impact on all structural characteristics. With zinc acetate as the source, the films' crystallinity improved as the molar concentration increased, and while with zinc chloride at high concentrations, the crystallinity degraded as the molar concentration rose. The ZnO film with a molarity of 0.4M for the zinc acetate source and with 0.05M for zinc chloride exhibits the highest transmittance. According to the change in molarity, the optical energy gap for zinc acetate rises from 3, 09 to 3, 16 eV, for zinc chloride, it reduced from 3, 13 to 2,9 eV. ZnO films produced from both sources exhibit resistivity on average at 10¹ Ω.cm. We, therefore, concluded that the manufactured zinc oxide thin films need sufficient molarity, such as 0.05 M for the zinc chloride starting solution source, to have good crystallite size, transmittance, band gap energy, and conductivity.

It is clear that, the effect of titanium doping ZnO thin films on the structural, electrical, and optical properties is slightly obvious after our study. Where the TZO films deposited at different percentage of titanium then characterized using a various methods.

Film thickness decreases because of the interference between zinc and titanium spraying particle fluxes reduces resulting to a lower growth rate. The X-ray diffraction data demonstrated that the peaks of TZO thin films conform to the hexagonal wurtzite structure of ZnO. Additionally, we have discovered that the lattice constant values significantly deviate from the standard values where the intensity diffraction peak is located around $2\theta = 34.42$ with a minor movement of the (002) diffraction peak. The films experience intense stress when the Ti doping level rises between 1 at.% and 5 at.%, which causes crystallite

size to increase. The stress is compressive between the concentrations of 5 at.% and 9 at.% Ti doping because the segregation of Ti atoms to the non-crystalline area in grain boundaries causes the size of the crystallite to shrink. The surface morphology of the ZnO and Ti doped ZnO thin films can be shown in SEM pictures to be free of cracks. All films also showed porosity with granular structures made up of small grains that appeared to be aggregated. The Zn, O, and Ti elements were present in both the undoped and doped ZnO films, according to EDAX spectra. The starting concentrations of Titania added determine the weight and atomic percentage compositions of Zn, Ti, and O in the thin films as well as the variation in the final amount of Ti in the thin films of Ti doped ZnO films. This strongly supports the successful replacement of dopants in the Zn sites.

In the visible light region, the transparency of ZnO, Ti doped ZnO thin films on glass substrate reaches 64,47% for 3 at.%. The computed band gap (E_g) values of the Ti doped ZnO thin films are in the range of 3, 06–3, 15 eV. The resistivity for pure ZnO film, is 33 Ω .cm. After that, it gradually drops until it reaches a minimum value of 17. Ω .Cm for the sample with Ti= 5 at.%. The ZnO film with a Ti 3 at.% doping concentration has good photocatalytic properties compared to other samples, and 5 at.% is selected as the best one based on all of these data.

With various ZnO: TiO₂ molar ratios, very transparent ZnO: TiO₂ thin films were successfully prepared on glass substrates using the spray pyrolysis technique. The ZnO wurtzite phase with preferential orientation along the c-axis (002) corresponds to what the XRD results showed for pure and the samples with 0:0.1 to 1:0.5 ZnO: TiO₂ molar ratio. However, from the samples with 1:0.3 to 1:0.5 ZnO: TiO₂ molar ratio, small peaks are seen, indicating the coexistence of a new phase, the spinel Zinc Titanate with Tetragonal structure. The ZnO diffraction peaks for the 1:0.7 ZnO: TiO₂ molar ratio diminished. At the same time, a new growth direction emerges that is consistent with the triclinic structure of the Ti₅O₉ Magnéli phase. According to the SEM results, The sample with a 1:0.5 ZnO: TiO₂ molar ratio was notably rough, porous, and contained granules that coalesced with each other,. This would increase the surface area, improving the surface properties of the thin film. EDAX results validated the existence of Ti, Zn, and O elements, and it was found that there was a constant increase in Ti, O, and a decrease in Zn element amounts in the final product as it had been reported in the initial solution. Transmittance spectra showed that all films had an average transmittance in the visible range of between 9% and

85%. According to the graphs, as thickness and surface roughness rise, films' transparency decreases. It was found that the band gaps were a little bit reduced in the sample with a 1:0.5 ZnO: TiO₂ molar ratio. The secondary phase Zn₂TiO₄ may be the cause of this. The band gap is somewhat influenced by how many Ti atoms are present in the films. The E_g begins to dramatically decline after the 1:0.5 ZnO: TiO₂ molar ratio and continues to decline until it reaches its lowest value (2, 3 eV) for 1:0.9 ZnO: TiO₂ molar ratio, indicating an improvement in the minimum energy required to excite an electron. The chemisorptions of oxygen on the surface could be the cause of the rise in film resistivity seen when titanium concentration in ZnO thin films increased.

“Do the best you can until you know better. Then when you know better, do better.”

This Maya Angelou quotation is relevant now since it is towards the finish of a work that we see what truly needs to be done. Thus, after finishing this job, we can think about many angles:

- Investigating the impact of temperature on ZnO: TiO₂ composites to determine the ideal temperature for producing pure zinc titanate compound and promoting the crystal development of that compound.
- Analyzing the deposited films' photocatalytic characteristics to verify the findings of this research

Abstract

Our study focused on the deposition and characterization of thin films based on zinc and titanium by pneumatic spray technique in order to obtain materials of good properties required for their use in the photovoltaic and photocatalytic applications.

In the first part of our work, we have developed thin films of titanium oxide and zinc oxide to study the effect of molarity and precursor's nature on the properties of these materials. The second part concerns the study of Ti doped ZnO and ZnO: TiO₂ films. For this we analyzed our films by various techniques: DRX, SEM, EDS, UV-VIS-NIR and four probes technique.

The main results of this work are the synthesized of Titanium oxide and zinc oxide thin films with good crystallite size, transmittance, band gap energy and conductivity requires adequate molarities such as 0.175M for TiCl₃ and 0.05 M for Zinc chloride starting solutions sources. Films with 1:0.5 ZnO: TiO₂ molar ratio could have good photocatalytic properties among the other samples, due to its high thickness 406 (nm) and low gap energy 3.03 eV and good structural properties including the growth of spinel Zinc Titanate Zn₂TiO₄ phase which is known as better photocatalysts than ZnO and TiO₂ films separately.

Keywords: Thin films, pneumatic spray, TiO₂, ZnO, photocatalytic properties.

ملخص

تتمحور دراستنا حول ترسيب وتشخيص الطبقات الرقيقة التي تعتمد على الزنك والتيتان بواسطة تقنية الرش البيروليزي من أجل الحصول على طبقات ذات خصائص جيدة لاستخدامها في التطبيقات الكهروضوئية و تطبيق التحفيز الضوئي.

في الجزء الأول من عملنا، قمنا بتحضير طبقات رقيقة من أكسيد التيتان وأكسيد الزنك وذلك بدراسة تأثير تركيز المحلول وطبيعة المحلول الابتدائي على خصائص هذه الطبقات. الجزء الثاني مخصص لدراسة شرائح أكسيد الزنك المطعمة بالتيتان Ti:ZnO وشرائح ZnO: TiO₂. لهذا قمنا بتشخيص طبقاتنا بواسطة تقنيات مختلفة: انعراج الأشعة السينية، المجهر الإلكتروني الماسح، التحليل الكيميائي، المطيافية فوق البنفسجية و المرئية وتقنية أربع نقاط. واهم النتائج المتحصل عليها : يتطلب تصنيع الأغشية الرقيقة من أكاسيد التيتان و الزنك ذات الحجم البلوري الجيد ، والنفاذية ، وطاقة فجوة النطاق والتوصيل تركيز مولي مناسب مثل 0.175م لكلوريد التيتانيوم و 0.05م لكلوريد الزنك كمصدر لمحلول ابتدائي. الأغشية ذات النسبة المولية 1:0.5 ل ZnO: TiO₂ لها خصائص تحفيز ضوئي جيدة بين العينات الأخرى ، نظراً لسمكها العالي 406 نانومتر وطاقة فجوة منخفضة (3.03 eV) وخصائص بنيوية جيدة تتضمن نمو تيتانات الزنك Zn₂TiO₄ طور السبينال والذي يُعرف كمحفز ضوئي أفضل من شرائح ZnO و TiO₂ بشكل منفصل.

الكلمات المفتاحية: الشرائح الرقيقة ، تقنية الرش البيروليزي ، تطبيق التحفيز الضوئي، ZnO، TiO₂.